Punching Shear Behaviour of GFRP-RC Slab-Column Edge Connections with High Strength Concrete and Shear Reinforcement

by

AHMED MAHMOUD MOHAMED MOSTAFA

A Thesis submitted to the Faculty of Graduate Studies of

The University of Manitoba

in partial fulfillment of the requirements of the degree of

MASTER OF SCIENCE

Department of Civil Engineering

University of Manitoba

Winnipeg, MB, Canada

ABSTRACT

Reinforced concrete (RC) flat plate systems are commonly used in parking garages, allowing for more clearance height for vehicles due to the absence of beams. However, flat plates are susceptible to punching shear failure. This type of failure is very dangerous due to its brittle nature, where the column along with a part of the slab suddenly penetrates through the slab giving no warning before it occurs. In North America, parking garages are vulnerable to the corrosion of steel reinforcement since they are exposed to harsh conditions such as wet-dry cycles, freeze-thaw cycles, and de-icing salts. To overcome the problems associated with steel corrosion, fibre-reinforced polymer (FRP) reinforcement is used in RC structures; thanks to its superior performance in corrosive environments and its durable nature. However, FRP-RC structures are expected to have lower shear capacity than steel-RC ones due to the lower modulus of elasticity and transverse stiffness of FRP bars than steel ones. Therefore, it deems necessary to investigate the shear behaviour of such FRP-RC slab-column connections.

An experimental study was conducted at the University of Manitoba in the W. R. McQuade structures laboratory to investigate the effect of different parameters on the punching shear behaviour of slab-column edge connections. Seven full-scale Glass (G) FRP-RC slab-column edge connections were constructed and tested to failure. The test connections were divided into two series. Series I included three connections to investigate the effect of flexural reinforcement ratio (0.90, 1.35 and 1.80%) on the punching shear strength of high strength concrete (HSC) connections, while Series II included four connections to examine the effect of GFRP shear reinforcement type (GFRP headed studs or corrugated bars) and pattern (six or eight lines of shear reinforcement) on the behaviour of normal strength concrete (NSC) connections. Test results

showed that increasing the reinforcement ratio increased the punching capacity and the post-cracking stiffness of the HSC connections. Also, the use of headed studs and corrugated bars increased the punching capacity and the deformability of the NSC connections. In addition, test results were compared to the predictions of the Canadian and American design provisions for FRP-RC structures. Generally, the capacity predictions of the Canadian standards were in good agreement with the experimental results, while the American guidelines highly underestimated the capacities of the connections.

ACKNOWLEDGMENTS

First and foremost, the author is so thankful to God for providing him with the strength and knowledge required to successfully do this work. The author hope that this work be for God sake and for the sake of useful knowledge and, thus, he will be rewarded.

{And it is He who spread the earth and placed therein firmly set mountains and rivers; and from all of the fruits He made therein two mates; He causes the night to cover the day. Indeed in that are signs for a people who give thought} Quran - ar-Ra'd (The Thunder) - Verse 3.

The author would like to express his sincere gratitude and appreciation to his supervisor Dr. Ehab El-Salakawy, P. Eng, Professor and Canada Research Chair in Durability and Modernization of Civil Structures in the Department of Civil Engineering at the University of Manitoba for his guidance, support and precious advices and experiences he shared with him.

In addition, the author would like to thank all his colleagues in the research group especially Mr. Mohamed El-Gendy for his help and support.

The financial support provided by the Natural Science and Engineering Research Council of Canada (NSERC) through Discovery and Canada Research Chair programs is gratefully acknowledged. Many thanks to the W. R. McQuade structures laboratory technical staff for their technical assistance during the construction and testing of the specimens.

Finally, I would like to express my sincere gratitude to my family for their invaluable effort and support not only during the course of this study, but throughout all my life.

Ahmed Mahmoud Mostafa, October 2016

TABLE OF CONTENTS

LIST OF TABLES

LIST OF FIGURES

CHAPTER 1

INTRODUCTION

1.1. BACKGROUND

The corrosion of steel reinforcement leads to an increase in maintenance cost and a decrease in the life span of the structure. Although many techniques are used to protect steel reinforcement from the corrosion, such as increasing concrete cover, the use of galvanized or stainless steel bars, epoxy coating and cathodic protection, none of them provide a long-term solution for the steel corrosion problem and they are cost-ineffective. The use of fiber reinforced polymers (FRPs) in reinforced concrete (RC) structures instead of conventional steel reinforcement has been widely increased during the last two decades. This is attributed to the superior performance of FRPs in corrosive environments and its durable nature. The FRP bars have high tensile strength, no magnetic conductivity, low electrical and thermal conductivity, and light weight. However, FRP bars have different characteristics from those of conventional steel such as low modulus of elasticity, linear stress-strain relationship until failure, small resistance in the transverse direction, different bond characteristics and low compressive strength.

Extensive research has been carried out to investigate the feasibility of using FRP bars as reinforcement in new structures as well as strengthening and retrofitting of existing ones. Most of the research studies focused on investigating the flexural behaviour of FRP-RC members. However, less research has been done to study the shear behaviour of FRP-RC members and particularly the punching shear behaviour of flat plates. This lack of research limits the understanding of the behaviour of FRP-RC flat plates.

1.2. PROBLEM DEFINITION

In North America, the majority of parking garage structures are constructed using reinforced concrete flat plate systems. The flat plate systems have many advantages such as, reduced storey heights, simplified formwork and ability to sustain heavy loads. Corrosion of steel reinforcement is a very common problem in those structures as a result of exposure to harsh environment such as freeze-thaw and wet-dry cycles as well as de-icing salts. Therefore, using FRP reinforcement, instead of conventional steel reinforcement, is a viable solution to overcome the steel corrosion-related problems in such structures.

Punching shear failure in the flat plate system is the most dangerous type of failure since it is brittle and sudden. Also, the failure of one joint in the system may lead to a progressive collapse of the whole building. Punching shear failure occurs due to high shear stresses and unbalanced bending moment transfer from the slab to the column. Unfortunately, this combination of shear and unbalanced bending moment is inevitable at slab-column connections as a result of unequal spans and unsymmetrical loading. Consequently, accurate calculations of the shear stresses and the unbalanced bending moment transferred to the columns are required to prevent such failure.

Due to the differences in mechanical characteristics between steel and FRP bars, FRP-RC members are expected to behave differently. The relatively lower modulus of elasticity of FRP bars results in wider cracks and consequently less depth to the neutral axis in FRP-RC members. This results in smaller shear strength due to less contribution of the aggregate interlock and un-cracked concrete components to the shear strength. Also, further reduction in the shear strength is expected due to the smaller dowel action of FRP bars because of their low transverse stiffness. As a result, FRP-RC slab column connections are expected to have less punching shear capacity than that of steel-RC ones. Consequently, code provisions derived for slabs reinforced with steel cannot

be applicable for FRP-RC slabs. Experimental investigations are required to study the punching shear behaviour of flat plate system reinforced with FRP bars for better understanding of the behaviour and to provide design recommendation for such slabs.

Many researchers have investigated the effect of several parameters on the punching shear behaviour of steel-RC slab-column connections (Richart 1948; Vanderbilt 1972; Dilger and Ghali 1981; Swamy and Ali 1982; Mokhtar et al. 1985; Elgabry and Ghali 1987; Hawkins et al. 1989; Gardner 1990; Marzouk and Hussein 1991; Alexander and Simmonds 1992; Marzouk et al. 1996, 1998, 2000; El-Salakawy et al. 1998, 2000; Ghannoum 1998; Osman et al. 2000; Dilger et al. 2005; Ozden et al. 2006; Rizk et al. 2011). On the other hand, few studies have been conducted to investigate the punching shear behaviour of FRP-RC slab-column connections (Banthia et al. 1995; El-Ghandour et al. 1999, 2003; Matthys and Taerwe 2000; Ospina et al. 2003; Zaghloul 2002, 2007; Zaghloul and Razaqpur 2004; El-Gamal et al. 2005; Dulude et al. 2013; Hassan et al. 2013; El-Gendy and El-Salakawy 2016a; Gouda and El-Salakawy 2016). To the author's best knowledge, only two research studies have been done to study the punching shear behaviour of FRP-RC slab-column edge connections constructed with normal strength concrete (Zaghloul 2007; El-Gendy and El-Salakawy 2016a). As a result, there is a need for more research to better understand the behaviour of such slabs.

1.3. SCOPE OF WORK

Slab-column connections can be classified into three types depending on their location; interior, edge, and corner connection (Fig. 1.1). Among those three connections, edge and corner connections are more critical to punching shear failure than interior ones due to the relatively higher moments transferred between the slab and the column at this location and the probable lack of slab reinforcement anchorage due to small column cross-sections and the discontinuity of the

slab. This experimental study focuses on studying the punching shear behaviour of isolated full scale slab-column edge connections. The test specimens represent the zone of negative moment around the columns. This negative moment zone is bounded by the lines of contra-flexure around the edge columns. All slabs are totally reinforced with glass (G) FRP longitudinal bars with or without GFRP shear reinforcement. The GFRP bars have become of much interest in the construction industry due to their lower prices compared to other FRP bars types (i.e. carbon, aramid and basalt FRP bars). The columns are of square cross section and are adequately reinforced with steel bars and stirrups to prevent any premature failure. Moreover, all test connections are subjected to a moment-to-shear ratio of 0.4 m during testing.

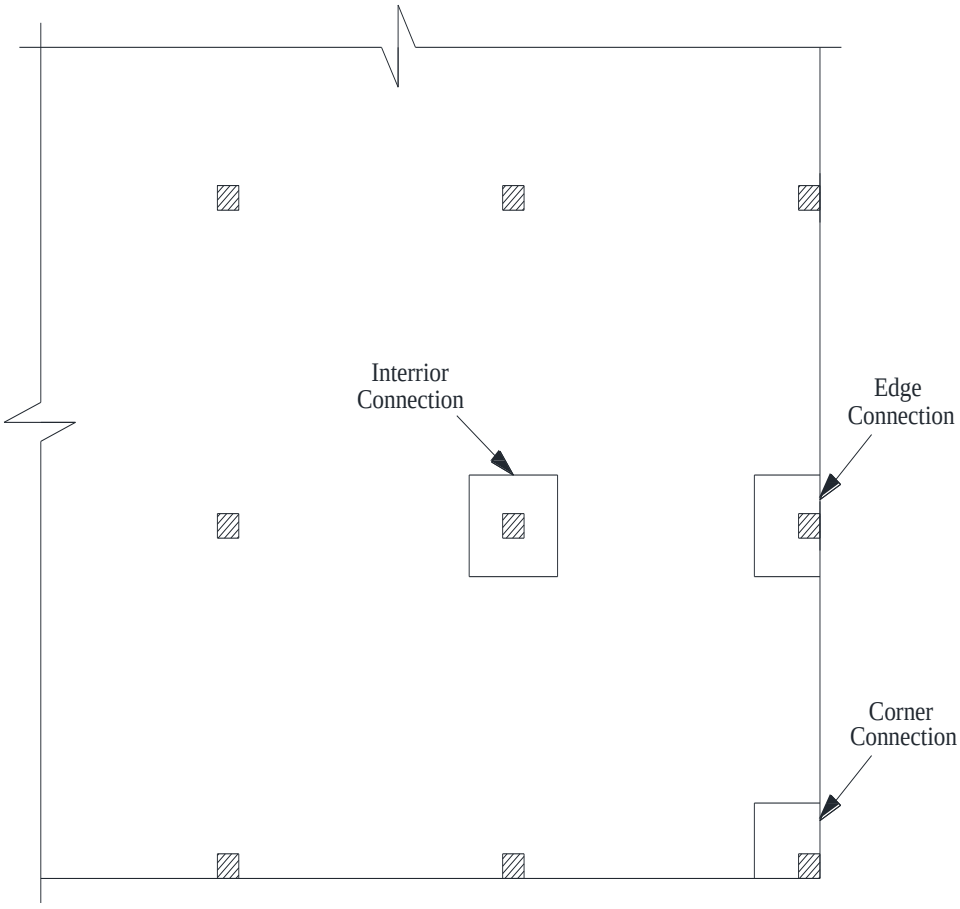

Figure 1.1: Types of slab-column connections

1.4. OBJECTIVES

The main objectives of this study are to:

- Investigate the punching shear behaviour of GFRP-RC slab-column edge connections with and without shear reinforcement subjected to unbalanced moment.
- Investigate and verify the punching shear provisions of the Canadian standards, CSA/S806-12 (CSA 2012) and the American guidelines ACI 440.1R-15 (ACI Committee 440 2015).
- Provide recommendations for designers and researchers regarding the analysis and the design of GFRP-RC slab-column edge connections.

To achieve these objectives, the effects of the following specific parameters on the punching shear behaviour of GFRP-RC slab-column edge connections are studied:

- Flexural reinforcement ratio on high strength concrete (HSC) connections.
- Shear reinforcement type.
- Shear reinforcement pattern.

1.5. METHODOLOGY

The aforementioned objectives were achieved by conducting an experimental investigation, in the W. R. McQuade Heavy Structures Laboratory at the University of Manitoba, on a total of seven isolated full-scale slab-column edge connections reinforced with GFRP bars. Each connection simulates a portion of a slab in a parking garage building consisting of three 6.5 m-long bays in both directions bounded by the slab free edge and the lines of contra-flexure.

1.6. THESIS ORGANIZATION

The thesis consists of five chapters as follows:

- Chapter 1 presents a brief background, problem definition, scope of work, objectives of the research and the methodology followed to achieve these objectives.
- Chapter 2 includes information about FRP materials and their constituent materials, an overview of the existing design provisions regarding punching shear in different codes and guidelines for both steel-RC and FRP-RC slab-column connections and a review of previous research related to punching shear behaviour of slab-column connections reinforced with both steel and FRP bars.
- Chapter 3 provides description of the experimental program. The details of the test connections in terms of dimensions, material properties and reinforcement details are presented. Also, the details and layout of instrumentation used to monitor the behaviour of the connections during testing (LVDTs, strain gauges and PI gauges), in addition to the details of the test setup and testing procedure are explained.
- Chapter 4 presents the analysis and discussion of the experimental test results in terms of cracking pattern, mode of failure, deflection, strains in the reinforcement and concrete, ultimate strength of the test connections. Also, this chapter includes a comparison between the experimental punching shear strength and those predicted by available code provisions.
- Chapter 5 presents the conclusions drawn from the experimental investigation as well as recommendations for future work.

CHAPTER 2

LITERATURE REVIEW

2.1. INTRODUCTION

During the last decades, extensive research has been conducted to investigate the punching shear behaviour of steel-reinforced concrete (RC) slabs. The behaviour of the steel-RC slabs is well-established and thus many codes have design provisions for such slabs. Recently, FRP reinforcement is being widely used in construction industry as a viable alternate to the conventional steel reinforcement to solve the corrosion-related problems in structures exposed to corrosive environments. However, there are few research studies on the punching shear behaviour of FRP-RC slabs. As a result, there is a lack of provisions regarding the punching shear in the available codes and guidelines for FRP-RC structures. Due to the difference in properties between FRP and steel reinforcement, the design provisions and guidelines for steel-RC could not be applied to those reinforced with FRP bars.

In this chapter, a brief overview of the material properties and the main characteristics of FRP bars are presented followed by a discussion of the two general types of failure associated with flat plates and a summary of the available codes and guidelines regarding punching shear in both steel and FRP-RC flat slabs. At last, previous research available on punching shear behaviour of both steel and FRP-RC flat slabs are presented.

2.2. PROPERTIES OF FRP REINFORCEMENT

2.2.1. Composition

Fibre reinforced polymers are composite materials consisting of fibers and a matrix (resin). The properties of the final FRP product depend on the properties of each constituent in addition to the

manufacturing process. The fibres are brittle and have high strength and are responsible for carrying the load and providing the strength. While the resin is responsible for providing a cohesive environment to transfer stresses between fibres, lateral support for the fibres against buckling, and keeping the fibres together.

2.2.1.1. Fibers

The performance of fibres is affected by many factors such as their length, cross-sectional shape and chemical composition. The most commonly fibers used to produce FRPs are glass, carbon and aramid fibres. Among these three types, glass fibres are the most commonly used in structural engineering applications due to their relatively cheaper production cost compared to the other two types. Glass fibres have other advantages such as high tensile strength, high chemical resistance, high insulating properties and Low thermal conductivity. On the other hand, they have some disadvantages such as low tensile modulus, low fatigue resistance and high density. There are four common types of glass fibres which are:

- S-glass: has high strength
- E-glass: has high electrical resistance
- C-glass: has high chemical resistance
- A-glass: has high alkali resistance

Carbon fibres have the highest tensile strength and stiffness among the three types of fibres. They have high resistance to chemicals, high fatigue resistance and excellent performance in high temperatures. Despite their better properties compared to glass fibres, they are not widely used as they are very expensive. They also have some disadvantages; they are sensitive to the processing conditions during manufacturing, have low strain capacity, and high electrical conductivity.

Carbon fibres are classified into two main types, polyacrylonitrile fibres (PAN) and Pitch-based fibres. PAN fibres are synthetic fibres with very high strength (up to 40000 MPa). There are three types of PAN fibers; high tensile strength (HT), high modulus (HM), and ultrahigh modulus (UHM). The high tensile strength fibers have the lowest modulus, while the ultrahigh-modulus fibers have the lowest tensile strength and strain. Pitch-based fibres are cheaper than PAN fibres but they have lower strength and modulus. There are two types of pitch-based fibres; ordinary and high modulus.

Aramid fibers have excellent impact resistance, high damping coefficient and low thermal conductivity. They have good resistant to organic solvents and fuels. However, aramid fibres have some disadvantages such as, low compressive strength, sensitivity to ultraviolet light, low resistance to high temperatures and difficulty in cutting or machining.

2.2.1.2. Resin

The physical and thermal properties of the resin have a big influence on the mechanical properties and the manufacturing process of the composite. Thus, the resin has to be selected properly. FRP composites are generally made of two types of resins which are; thermosetting or thermoplastic. Once formed, thermosetting resins cannot be reshaped, while thermoplastic resins can be liquefied by heat and solidified by cooling. Thermosetting resins are more frequently used in the manufacturing of FRP composites than thermoplastic resins. Polyester, vinyl ester and epoxy are the most common types of thermosetting resins.

2.2.2. Manufacturing Process

FRP composites are made through three manufacturing process which are; pultrusion, braiding, and filament winding:

1- Pultrusion: It is a technique used to produce continuous lengths of FRP bars with a constant profile. The process is done by pulling the reinforcing material through a resin impregnation bath then through a shaping die to cure the resin. Reinforcing bars and standard sections are made through this process.

2- Braiding: It is a process in which two or more yarns are interlocked to form an integrated structure.

3- Filament winding: It is a process in which continuous fibres are impregnated with resin and then wrapped around a mandrel. After that, the product is cured using heat lamps. This process creates a controlled thickness, wind angle, and fibre-volume fraction product. Pipes, tubes, and storage tanks are the most common products that can be manufactured by this process.

2.2.3. Physical Properties

2.2.3.1. Density

The density of the FRP material is about one-sixth to one-fourth that of steel density. Thus, FRP reinforcement bars are much lighter than steel bars. This leads to a reduced transportation cost and easier handling for FRP bars. Table 2.1 shows the densities of different types of reinforcing bars.

Table 2.1: Typical densities of reinforcing bars (ACI Committee 440 2015)

Reinforcement type	Steel	GFRP	CFRP	AFRP
Density (gm/cm^3)	7.9	1.25-2.1	1.5-1.6	1.25-1.4

2.2.3.2. Coefficient of thermal expansion

The coefficients of thermal expansion of FRP bars are different in the longitudinal and transverse directions depending on the types of the constituents (fibers and resin). The longitudinal coefficient of thermal expansion depends on the properties of the fibres, while the transverse coefficient depends on the properties of the resin. Table 2.2 shows the coefficients of thermal expansion of different types of reinforcing bars. Since the coefficient of thermal expansion for CFRP in the longitudinal direction is close to zero, it is not affected by temperature variation. The negative coefficient of thermal expansion for AFRP in the longitudinal direction indicates that AFRP contracts when increasing temperature and expands when temperature is decreased.

Table 2.2: Typical coefficient of thermal expansion for reinforcing bars (ACI Committee 440 2015)

	CTE, $\times 10^{-6}/^{o}C$			
Direction	Steel	GFRP	CFRP	AFRP
Longitudinal, α_L	11.7	6 to 10	-9 to 0	-6 to -2
Transverse, α_T	11.7	21 to 23	74 to 104	60 to 80

2.2.4. Mechanical Properties

2.2.4.1. Tensile behaviour

Fibre Reinforced Polymers bars are brittle materials which characterized by a linear elastic stress-strain relationship up to failure when subjected to tensile stress. Figure 2.1 shows that they do not exhibit any yielding behaviour before rupture unlike steel reinforcement.

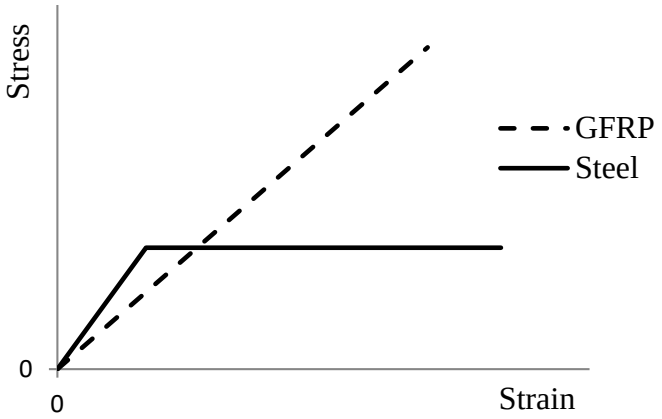

Figure 2.1: Typical stress-strain relations for reinforcing bars

The tensile strength of the FRP bars is much higher than that of the steel bars. However, the stiffness of FRP bars is lower than that of the steel bars as shown in Table 2.3. The stiffness of FRP bars depends on its consistent materials. FRP bars made of thermosetting resin cannot be bent after manufactured as thermosetting resin cannot be reshaped after curing. In case of FRP bars made of thermoplastic resin it can produced with bends, however, it is not recommended to use bent bars due to the strength reduction of 40% to 50% in the bent portion compared with the strength of a straight bar due to stress concentrations (ACI Committee 440 2015).

Table 2.3: Typical tensile properties of reinforcing bars (ACI Committee 440 2015, Pultrall Inc. 2015)

	Steel	GFRP (V-ROD) (HM)	CFRP	AFRP
Yield Stresses (MPa)	276 to 517	N / A	N / A	N / A
Tensile Strength (MPa)	483 to 690	1000 to 1370	1518 to 1899	1720 to 2540
Elastic Modulus (GPa)	200	62.6 to 65.6	127 to 144	41 to 125
Yield Strain	0.14 to 0.25%	N / A	N / A	N / A
Rupture Strain	6% to 12%	1.68 to 2.1%	1.18 to 1.3%	1.9 to 4.4%

2.2.4.2. Compressive behaviour

The compressive strength and modulus of elasticity of FRP bars is smaller than its tensile ones. However, some research indicated that the compressive modulus of elasticity is approximately 80% for GFRP, 85% for CFRP and 100% for AFRP of the tensile modulus of elasticity for the same product (ACI committee 440 2015).

2.2.4.3. Shear behaviour

FRP bars may fail when its resins are subjected to inter-laminar shear as the resin is usually unreinforced in the transverse direction of the bar. The solution for this problem is to increase the shear resistance by orienting fibers in an off-axis direction across the layers of longitudinal fibers.

2.2.4.4. Bond behaviour

The bond behaviour of FRP bars depends on many factors such as; the surface condition of the bar (sand-coated or ribbed), the mechanical properties of the bar and the environmental conditions. The bond force between the FRP bar and the surrounding concrete can be produced by adhesion, friction and mechanical interlock.

2.3. TYPES OF FAILURE OF CONCRETE FLAT PLATES

Reinforced concrete flat plates can fail due to two types of failure; flexural failure and shear failure.

2.3.1. Flexural Failure

Flexural failure occurs under the effect of bending moments, which induce compressive stresses in one side of the slab and tensile stresses in the other side. The failure occurs when the flexural capacity of the slab-column connection (V_{flex}) is less than its punching shear capacity (V_c). For

the design purpose, it is usually assumed that the tensile reinforcement (flexural reinforcement) resist all the tensile stresses while the concrete resists all the compressive ones.

There are three modes of flexural failure depending on the amount of flexural reinforcement:

1- **Tension failure:** It occurs when the flexural reinforcement reaches its design failure strain before concrete reaches its ultimate compressive strain. Sections subjected to this type of failure are considered as under-reinforced sections. In case of steel-RC members, this type of failure is preferred as it gives ample warning before it takes place. In contrast, this type of failure is avoided in case of FRP-RC members as it characterized by its sudden and violent behaviour.

2- **Balanced failure:** It occurs when the flexural reinforcement reaches its design failure strain at the same time the concrete reaches its ultimate compressive strain. This kind of failure is hypothetical and does not occur in real life.

3- **Compression failure:** It occurs when the concrete crushes under compression while the strain in the flexural reinforcement is smaller than the design failure strain. Sections subjected to this type of failure are considered as over-reinforced sections. In case of steel-RC members, this type of failure is avoided as it takes place without much warning. For FRP-RC members, this type of failure is desirable as it is less violent than tension failure.

2.3.2. Shear Failure

Flat slabs can encounter two types of shear failure:

1- **One-way shear:** This type of failure is similar to the mechanism of beam shear failure. An inclined crack is developed across the entire width of the structure causing failure. This type of shear failure is usually not critical and rarely happens in flat slab systems.

2- **Two-way shear (punching shear):** This type of failure is usually encountered in flat slabs and footings. It occurs due to the transfer of shear force with or without moment between the slab and column. The combination of shear and unbalanced moment is unavoidable because of unsymmetrical loading. The stresses resulting from the two-way shear are much higher than those resulting from the one-way shear. The failure begins with the formation of tangential cracks around the vicinity of the column followed by radial cracks extending from the column. With increasing the load, circumferential cracks form and connect the radial cracks together. When the failure occurs, the column with a conical portion of the slab punch through the floor. Generally, punching shear failure in flat slabs is sudden and brittle and may lead to the collapse of the whole building.

2.4. BUILDING CODES PROVISIONS FOR PUNCHING SHEAR

The design provisions for punching shear, adopted in different codes and guidelines, are empirically derived based on the test results of extensive experimental programs carried out to investigate the punching shear behaviour of flat slabs. As a result, different codes provide different methods to evaluate the punching shear capacity of either steel- or FRP-RC flat slabs.

In the following sections, the punching shear provisions in the North American, European and Japanese codes and guidelines will be discussed.

2.4.1. Provisions for Steel-RC Slab-Column Connections

The discussion will be limited to the case of slab-column edge connections without shear reinforcement and with stud shear reinforcement.

2.4.1.1. Canadian code CSA/A23.3-14

The CSA/A23.3-14 (CSA 2014) considers the critical punching shear perimeter to be at *d*/2 from the face of the column and to have three straight sides in case of edge connections. The code requires the maximum factored shear stress, v_f, due to the factored shear force and unbalanced moments to be less than the factored shear stress resistance, v_r.

Factored Shear Stress

The CSA/A23.3-14 (CSA 2014) resolves the shear forces and unbalanced moments transferred to the column into a single shear force acting at the centroid of the critical section and a single moment about the centroidal axes of the critical section. The shear stress is assumed to vary linearly around the centroid of the critical section (Fig. 2.2).

The factored shear stress, v_f, is calculated from the following equation:

$$v_f = \frac{V_f}{b_o d} + \frac{\gamma_v M_f e}{J} \tag{2.1}$$

Where;

V_f = factored shear force

b_o = perimeter of the critical section

d = slab average effective depth

γ_v = fraction of the unbalanced moment transferred by eccentricity of shear and can be calculated as:

$$\gamma_v = 1 - \frac{1}{1+\frac{2}{3}\sqrt{\frac{b_1}{b_2}}} \tag{2.2}$$

b_1 = width of the critical section for shear measured in the direction of the span for which moments are determined

b_2 = width of the critical section for shear measured in the direction perpendicular to b_1

M_f = factored moment transferred between slab and column

e = distance from the centroid of the critical shear section to the point where shear stress is being calculated

J = a property of the critical shear section similar to the polar moment of inertia

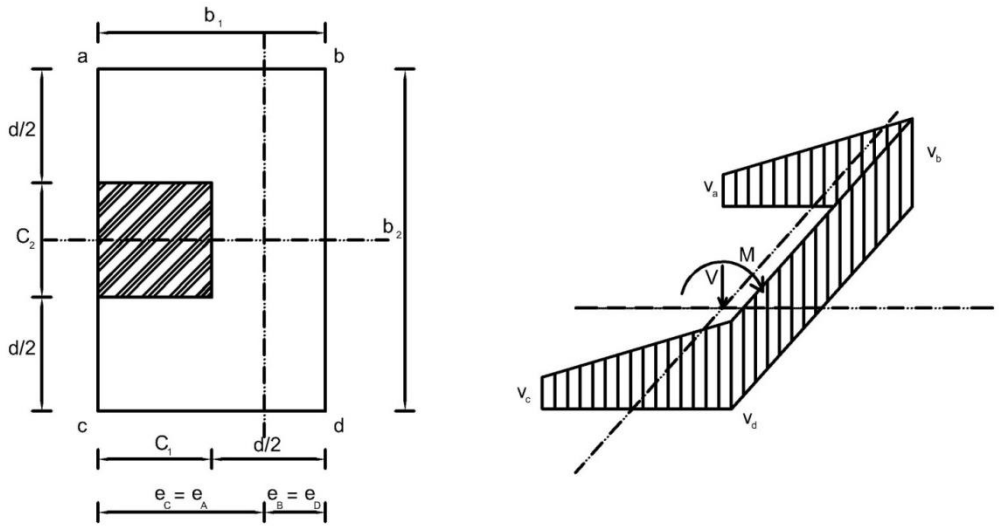

Figure 2.2: Shear stress distribution and critical shear perimeter (CSA/A23.3-14)

Shear Stress Resistance without Shear Reinforcement

The factored shear stress resistance, v_r, shall be the smallest of:

$$v_r = v_c = 0.19\left(1 + \frac{2}{\beta_c}\right)\lambda\,\varphi_c\,\sqrt{f_c'} \tag{2.3}$$

$$v_r = v_c = \left(0.19 + \alpha_s\frac{d}{b_o}\right)\lambda\,\varphi_c\,\sqrt{f_c'} \tag{2.4}$$

$$v_r = v_c = 0.38\,\lambda\,\varphi_c\,\sqrt{f_c'} \tag{2.5}$$

Where;

v_c = factored shear stress resistance for concrete

β_c = the ratio of longer to shorter side of the column

λ = factor takes into account the concrete density (1.0 for normal density concrete)

φ_c = resistance factor for concrete (0.65)

f_c' = compressive strength of concrete (MPa)

α_s = 3.0 for edge columns

When the effective depth exceeds 300 mm, v_c obtained from the above equations have to be multiplied by 1300/ (1300 + *d*).

Shear Stress Resistance with Stud Shear Reinforcement

The code requires the shear reinforcement to be extended to a distance 2*d* from the face of the column or to the section where v_f is not greater than the value specified in Equation 2.6, whichever longer, where v_f is the factored shear stress resistance outside the shear reinforced zone.

$$v_f = 0.19\,\lambda\,\varphi_c\,\sqrt{f_c'} \tag{2.6}$$

In case of using headed shear reinforcement, v_f shall not be greater than $0.75\,\lambda\,\varphi_c\,\sqrt{f_c'}$. The factored shear stress resistance within the shear reinforced zone, v_r, is the summation of the factored shear resistance provided by the concrete, v_c, and the factored shear resistance provided by the stud shear reinforcement, v_s, where;

$$v_c = 0.28\,\lambda\,\varphi_c\,\sqrt{f_c'} \tag{2.7}$$

$$v_s = \frac{\varphi_s A_{vs} f_{yv}}{b_o s} \tag{2.8}$$

Where;

φ_s = resistance factor for steel (0.85)

A_{vs} = the cross-sectional area of the headed shear reinforcement on a concentric line parallel to the perimeter of the column

f_{yv} = the specified yield strength of the headed shear reinforcement

s = radial spacing between the parallel lines of studs

The distance between the first line of studs and the column face shall be taken as $0.4d$ while s is determined according to v_f value as follows:

When $v_f \leq 0.56\lambda\varphi_c\sqrt{f_c'}$, $s \leq 0.75d$ When $v_f > 0.56\lambda\varphi_c\sqrt{f_c'}$, $s \leq 0.5d$

2.4.1.2. American code ACI 318-14

As the CSA/A23.3-14 (CSA 2014), the ACI 318-14 (ACI Committee 318 2014) considers the critical punching shear perimeter to be at $d/2$ from the face of the column and to have three straight sides in case of edge connections.

The code requires the factored shear stress, v_u, resulting from the factored shear force, V_u, and the factored unbalanced moment, M_u, to be less than the reduced nominal shear strength, φv_n.

Factored Shear Stress

The factored shear stress, v_u, is calculated using the same provisions provided by the CSA/A23.3-14 (CSA 2014).

Shear Stress Resistance without Shear Reinforcement

The nominal shear stress resistance, V_n, shall be the smallest of:

$$V_n = V_c = 0.083\left(2 + \frac{4}{\beta_c}\right)\lambda\sqrt{f_c'}b_o d \tag{2.9}$$

$$V_n = V_c = 0.083\left(2 + \alpha_s\frac{d}{b_o}\right)\lambda\sqrt{f_c'}b_o d \tag{2.10}$$

$$V_n = V_c = 0.33\lambda\sqrt{f_c'}b_o d \tag{2.11}$$

Where;

V_c = nominal shear strength provided by concrete

β_c = the ratio of longer to shorter side of the column

λ = factor takes into account the concrete density (1.0 for normal density concrete)

f_c' = compressive strength of concrete

b_o = perimeter of critical section

d = average slab effective depth

α_s = 3 for edge columns

Shear Stress Resistance with Stud Shear Reinforcement

The code requires the shear reinforcement to be extended to the section where v_f is not greater than the value specified in Equation 2.12

$$v_f = 0.17\lambda\varphi\sqrt{f_c'} \tag{2.12}$$

In case of using headed shear reinforcement, V_c and V_n shall not be greater than the values specified in Equations 2.13 and 2.14, respectively.

$$V_c = 0.25\,\lambda\sqrt{f_c'}b_o d \tag{2.13}$$

$$V_n = 0.66\,\lambda\sqrt{f_c'}b_o d \tag{2.14}$$

The nominal shear stress resistance provided by the stud shear reinforcement, v_s, can be calculated from the following equation:

$$v_s = \frac{A_v f_{yv}}{b_o s} \geq 0.17\lambda \sqrt{f_c'} \tag{2.15}$$

Where;

A_{vs} = cross-sectional area of the headed shear reinforcement on a concentric line parallel to the perimeter of the column

f_{yv} = the specified yield strength of the headed shear reinforcement

The distance between the first line of studs and the column face shall be taken as 0.4*d* while *s* is determined according to v_f value as follows:

When $v_f \leq 0.50\lambda\varphi_c\sqrt{f_c'}$, $s \leq 0.75d$

When $v_f > 0.50\lambda\varphi_c\sqrt{f_c'}$, $s \leq 0.5d$

2.4.1.3. European code EN 1992-1-1:2004

The Euro code considers the critical punching shear perimeter to be at distance equal to 2*d* from the face of the column whether the column section is rectangular or circular as shown in the following figure.

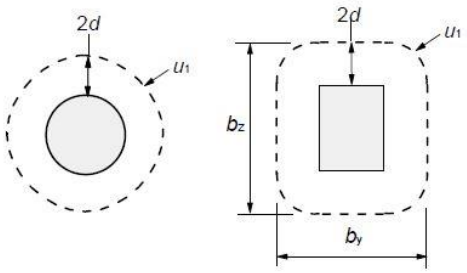

Fig 2.3: Critical punching shear perimeter

Punching Shear Stresses Calculations

The code calculates the punching shear stresses, regardless the type of the connection, from the following equation:

$$V_{ED} = \frac{\beta V}{dU_i} \tag{2.16}$$

Where;

V_{ED} = punching shear stresses (MPa)

V = factored shear force (N)

U_i = the length of the control perimeter being considered

d = the mean effective depth of the slab (mm), which may be taken as (d_y + d_z)/2

Where;

d_y, d_z = the effective depths in the y- and z- directions of the control section, respectively

β is calculated as:

$$\beta = 1 + \frac{KMU_1}{VW_1} \tag{2.17}$$

Where;

U_1 = the length of the basic control perimeter (2d from the column face)

k = coefficient depends on the ratio between the column dimensions C_1 and C_2 as shown in table 2.4

Table 2.4: Values of k for rectangular loaded areas (EN 1992-1-1:2004)

C_1/C_2	$\ll 0.5$	1.0	2.0	$\gg 3.0$
k	0.45	0.6	0.7	0.8

W_1 = function of the perimeter, $U_{i,}$ as follows:

$$W_1 = \int_0^{U_i} |e| \, dl \tag{2.18}$$

Where;

dl = a length increment of the perimeter

e = the distance of dl from the axis about which the moment M acts

For a rectangular column:

$$W_1 = \frac{C_1^2}{2} + C_1C_2 + 4C_2d + 16d^2 + 2\pi dC_1 \tag{2.19}$$

Where;

C_1 = the column dimension parallel to the eccentricity of the load

C_2 = the column dimension perpendicular to the eccentricity of the load

For edge column connections, where the eccentricity is perpendicular to the slab edge, the punching force may be considered to be uniformly distributed along the control perimeter U_{1*} as shown in Figure 2.4. If there are eccentricities in both orthogonal directions, β may be determined using the following equation:

$$\beta = \frac{U_1}{U_{1*}} + k \frac{U_1}{W_1} e_{par} \tag{2.20}$$

Where;

e_{par} = the eccentricity parallel to the slab edge resulting from a moment about an axis perpendicular to the slab edge

k can be determined from Table 2.4 with the ratio C_1/C_2 replaced by $C_1/2C_2$

W_1 is calculated for the basic control perimeter U_1.

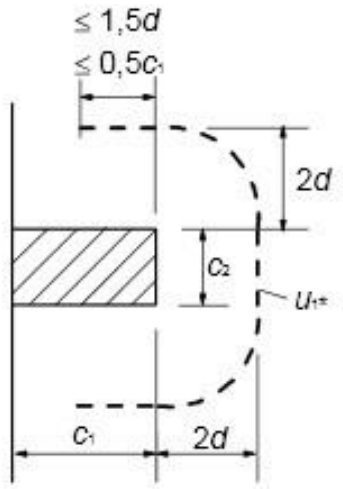

Figure 2.4: Reduced basic control perimeter U_{1*}

For a rectangular column:

$$W_1 = \frac{c_2^2}{2} + C_1C_2 + 4C_1d + 8d^2 + 2\pi dC_2 \quad (2.21)$$

Shear Stress Resistance without Shear Reinforcement

The punching shear strength ($V_{Rd,C}$) is calculated by the following equation:

$$V_{Rd,C} = C_{Rd,C}\, K(100\, \rho_1\, f_{ck})^{1/3} + k_1\, \sigma_{cp} \geq (V_{min} + k_1\, \sigma_{cp}) \quad (2.22)$$

$$V_{min} = 0.035\, K^{3/2}\, f_{ck}^{1/2} \quad (2.23)$$

Where;

$V_{Rd,C}$ = the shear resistance of concrete (MPa)

f_{ck} = the characteristic concrete cylinder strength (MPa)

$$K = 1 + \sqrt{\frac{200}{d}} \leq 2.0 \quad d \text{ in mm} \quad (2.24)$$

$$\rho_1 = \sqrt{\rho_{1y} + \rho_{1z}} \leq 0.02 \quad (2.25)$$

$\rho_{1y}+\rho_{1z}$ relate to the bonded tension steel in *y*- and *z*- directions respectively. The values ρ_{1y} and ρ_{1z} should be calculated as mean values taking into account a slab width equal to the column width plus 3*d* each side.

$$\sigma_{cp}=(\sigma_{cy}+\sigma_{cz})/2 \tag{2.26}$$

$$\sigma_{cy}=\frac{N_{Ed,y}}{A_{cy}} \tag{2.27}$$

$$\sigma_{cz}=\frac{N_{Ed,z}}{A_{cz}} \tag{2.28}$$

Where;

σ_{cy}, σ_{cz} = the normal concrete stresses in the critical section in y- and z directions, respectively (MPa, positive if compression)

$N_{Ed,y}$, $N_{Ed,z}$= the longitudinal forces across the full bay for internal columns and the longitudinal force across the control section for edge columns.

A_c = the area of concrete

The recommended value for $C_{Rd,C}$ is $0.18/\gamma_c$ and that for $k_1$equals 0.1

Shear Stress Resistance with Stud Shear Reinforcement

The punching shear strength ($V_{Rd,Cs}$) is calculated by the following equation:

$$V_{Rd,Cs}=0.75\,V_{Rd,C}+1.5(d/s_r)\,A_{sw}f_{ywd,ef}(1/(u_1 d))\,\sin\alpha \tag{2.29}$$

Where;

A_{sw} = area of one perimeter of shear reinforcement around the column (mm^2)

s_r = the radial spacing of perimeters of shear reinforcement (mm)

α = the angle between the shear reinforcement and the plane of the slab

$f_{ywd,ef}$ = the effective design strength of the punching shear reinforcement, and it can be calculated as:

$$f_{ywd,ef} = 250 + 0.25\ d \leq f_{ywd} \tag{2.30}$$

Where;

d = mean of the effective depths in the orthogonal directions (mm)

If a single line of bent-down bars is provided, then the ratio d/s_r in Equation 2.30 may be taken as 0.67.

2.4.2. Provisions for FRP-RC Slab-Column Connections

The discussion will be limited to the case of slab-column edge connections without shear reinforcement only as no design provisions regarding the design of FRP-RC slab-column connections with shear reinforcement exists. This indicates the necessity for more research in this topic.

2.4.2.1. Canadian standard CSA/S806-12

The CSA/S806-12 (CSA 2012) considers the critical punching shear perimeter to be at $d/2$ from the face of the column. The code accounts for the difference in mechanical properties between steel and FRP reinforcement as well as the effect of flexural reinforcement.

Shear Stress Resistance without Shear Reinforcement

The factored shear stress resistance, v_r , shall not exceed the limits specified in CSA/A23.3-14 (CSA 2014) and the smallest of the following values:

$$v_r = v_c = 0.028 \left(1 + \frac{2}{\beta_c}\right) \lambda\ \varphi_c (E_F \rho_F f_c')^{\frac{1}{3}} \tag{2.31}$$

$$v_r = v_c = 0.147\left(0.19 + \alpha_s \frac{d}{b_o}\right) \lambda\, \varphi_c (E_F \rho_F f_c')^{\frac{1}{3}} \quad (2.32)$$

$$v_r = v_c = 0.056\lambda\, \varphi_c (E_F \rho_F f_c')^{\frac{1}{3}} \quad (2.33)$$

Where;

v_c = factored shear stress resistance for concrete

β_c = the ratio of longer to shorter side of the column

λ = factor takes into account the concrete density (1.0 for normal density concrete)

φ_c = resistance factor for concrete (0.85)

E_F = elastic modulus for FRP flexural reinforcement

ρ_F = FRP flexural reinforcement ratio

f_c' = compressive strength of concrete (MPa)

α_s = 3 for edge columns

d = slab average effective depth

b_o = perimeter of critical section

When the effective depth exceeds 300 mm, v_c obtained from the above equations have to be multiplied by $\left(300/_d\right)^{0.25}$.

2.4.2.2. American guideline ACI 440.1R-15

The ACI 440.1R-15 (ACI 2015) considers the critical punching shear perimeter to be at *d*/2 from the face of the column and to have three straight sides in case of edge connections.

Shear Stress Resistance without Shear Reinforcement

The nominal shear stress resistance V_n is calculated as:

$$V_n = V_c = 0.8\sqrt{f_c'}b_o c \tag{2.34}$$

Where;

V_c = nominal shear strength provided by concrete

f_c' = compressive strength of concrete (MPa)

b_o = perimeter of critical section

c = cracked transformed section neutral axis depth

Where;

$$c = kd \tag{2.35}$$

$$k = \sqrt{2\rho_f n_f + (\rho_f n_f)^2} - \rho_f n_f \tag{2.36}$$

Where;

n_f = modular ratio

ρ_F = FRP flexural reinforcement ratio

Thus, Equation 2.34 can be rewritten as:

$$V_n = V_c = (2.5k)0.32\sqrt{f_c'}b_o d \tag{2.37}$$

2.4.2.3. JSCE 1997 (Japan Society of Civil Engineering 1997)

Shear Stress Resistance without Shear Reinforcement

The design punching shear capacity, V_{pcd}, can be calculated by applying the following equations:

$$V_{pcd} = \beta_d \beta_p \beta_r \frac{f_{pcd} u_p d}{\gamma_b} * \frac{1}{\alpha} \tag{2.38}$$

$$\beta_d = \sqrt[4]{\frac{1000}{d}} \leq 1.5 \tag{2.39}$$

$$\beta_p = \sqrt[3]{100\rho \frac{E_f}{E_s}} \leq 1.5 \tag{2.40}$$

$$\beta_r = 1 + \frac{1}{1 + 0.25\,{}^{u}/_{d}} \tag{2.41}$$

$$f_{pcd} = 0.2\sqrt{f'_{cd}} \leq 1.2 \tag{2.42}$$

$$\alpha = 1 + 1.5 * \frac{e_x + e_y}{\sqrt{b_x b_y}} \tag{2.43}$$

Where;

f_{pcd} = design compressive strength of concrete

u_p = peripheral length of the design cross-section at $d/2$ from the column face

d = average effective depth of both orthogonal directions

γ_b = partial safety factor

α = a factor takes into account the eccentricity of the shearing force

ρ = average flexural reinforcement ratio in both orthogonal direction

u = the peripheral length of the column

e_x, e_y = the load eccentricity in the two orthogonal directions

b_x, b_y = the dimensions of the critical section in the two orthogonal directions

E_f, E_s = the elastic modulus for the FRP and steel reinforcement, respectively

2.5. YIELD LINE THEORY

The yield line theory is used to calculate the values of the vertical shear force, V_{flex}, and the unbalanced moment, M_{flex}, which produce flexural failure in slab-column connections in terms of the bending moment per unit width of the slab at yielding of the flexural reinforcement. These calculated values are the upper bound of the shear force and the unbalanced moment transferred between the slab and the column at slab-column connections. The values can be calculated by assuming a failure pattern compatible with the boundary conditions of the tested slab. This failure pattern consists of the cracking lines in which the tension steel has yielded forming plastic hinges. The failure pattern is formed by dividing the slab into segments by these cracking lines. All the possible failure patterns should be examined (Park and Gamble 2000) as the resulting ultimate capacity may be overestimated if an incorrect pattern was used. Many researchers have used the theory to efficiently estimate the ultimate flexural capacities of the steel-RC slab-column connections (Mortin 1989; El-Salakawy et al. 2000; Ritchie et al. 2006; Stein et al. 2007). Figure 2.5 shows different suggested failure patterns.

In case of FRP reinforcement, there is no yielding point that identifies the formation of plastic hinges as the behaviour is linear elastic up to failure. However, FRP-RC slab-column connections develop large post-cracking deformations prior to flexural failure due to the relatively low modulus of elasticity of the FRP reinforcement. Gar et al. (2014) introduced an equivalent plastic moment capacity for FRP-RC slabs, M_p, corresponding to the yielding moment capacity of the steel-RC slabs. The flexural behaviour of FRP-RC sections was idealized into a trilinear behaviour as shown in Figure 2.6. To obtain the equivalent plastic moment, the idealized trilinear behaviour was simplified into an energy-equivalent bilinear behaviour similar to that of the steel-RC elements with the same area under the response.

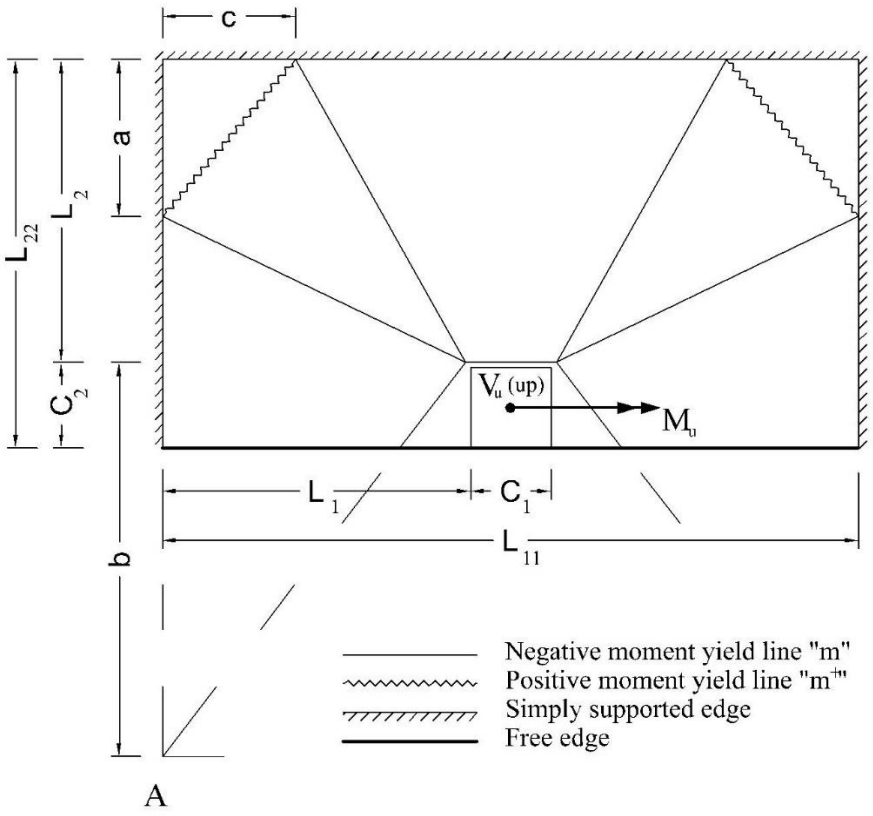

(a) Mortin (1989)

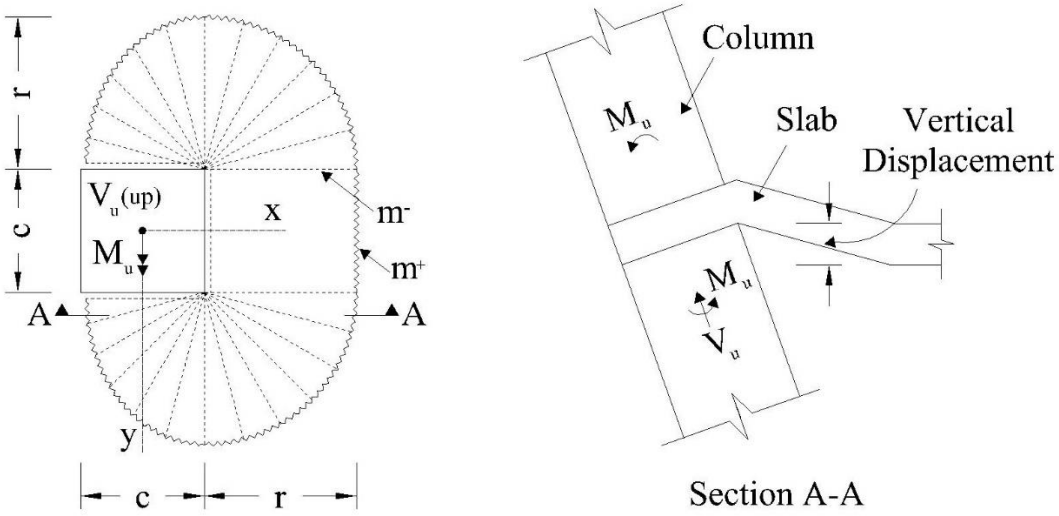

(b) Ritchi et al. (2006) and Stein et al. (2007)

Figure 2.5: Different yield line patterns for steel-RC slab-column edge connections

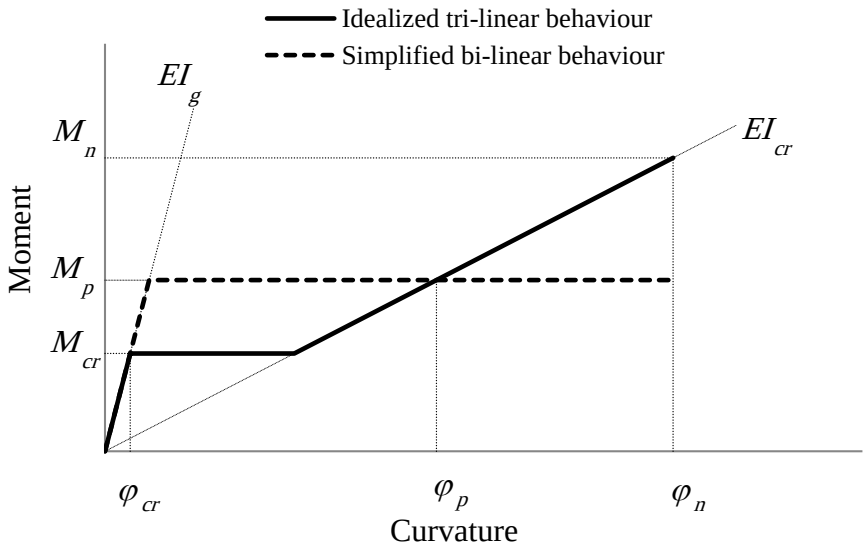

Figure 2.6: Moment-curvature response for FRP-RC sections (Gar et al. 2014)

Equation 2.44 shows the resulted formula for the plastic moment capacity, M_p:

$$M_p = 0.5M_n + 0.5\left(1 - \frac{I_{cr}}{2I_g}\right)\left(\frac{M_{cr}}{M_n}\right)M_{cr} \quad (2.44)$$

Where;

M_n = nominal moment capacity of the section

M_{cr} = cracking moment capacity of the section

I_g = gross moment of inertia of the section

I_{cr} = cracked moment of inertia of the section

El-Gendy and El-Salakawy (2016a) and Gouda and El-Salakawy (2016) have used the previous equation to effectively calculate the flexural capacities of GFRP-RC slab-column edge and interior connections, respectively, using the patterns shown in Fig. 2.7.

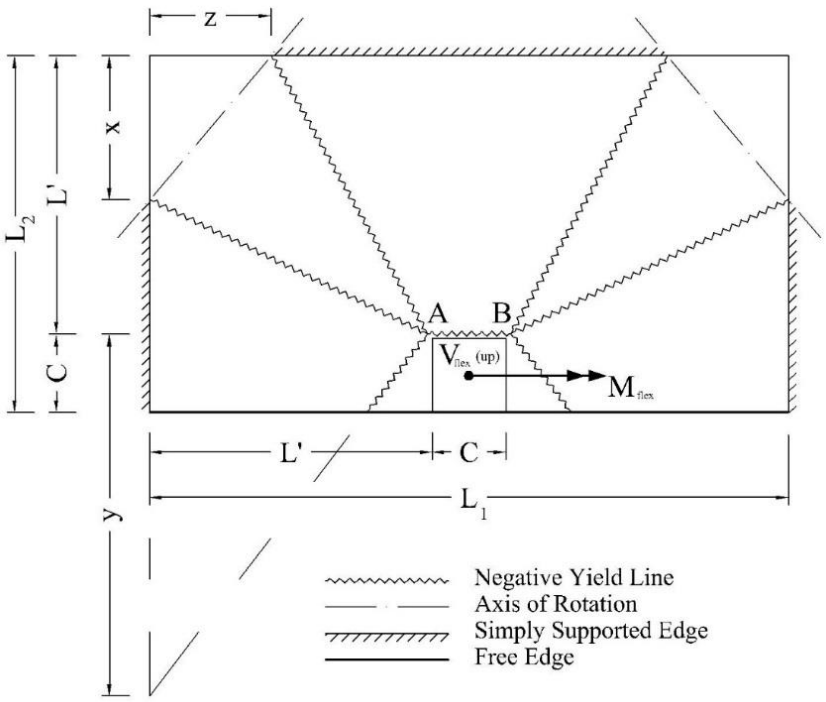

(a) El-Gendy and El-Salakawy (2016a)

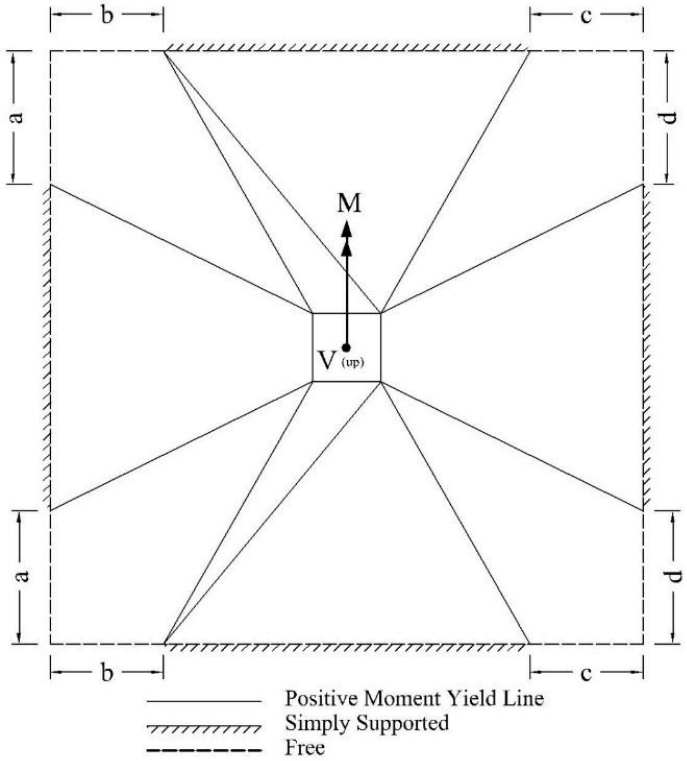

(b) Gouda and El-Salakawy (2016)

Figure 2.7: Different yield line patterns for FRP-RC slab-column connections

2.6. RESEARCH ON STEEL-RC SLAB-COLUMN CONNECTIONS

2.6.1. Effect of Flexural Reinforcement Ratio

The effect of flexural reinforcement ratio on the punching shear behaviour of slab-column connections have been extensively studied by many researchers (Gardner 1990; Marzouk et al. 1998, 2000; Osman et al. 2000; Ozden et al. 2006; Stein et al. 2007; Widianto et al. 2009; Rizk et al. 2011). Dilger et al. (2005) performed a review study of the major international codes with regard to the effect of the flexural reinforcement on the design equations for punching shear of two-way slabs compared to available experimental data. It was stated that, with the exception of codes based on the ACI 318-05 code (ACI Committee 318 2005) including CSA/A23.3-04 code (CSA 2004); all other major international codes such as the European standard EN 1992-1-1:2004 and the British standard BS 8110-97 (British Standard 1997) reflect the effect of flexural reinforcement ratio in the design equations for punching shear. The authors also concluded that, in most cases the punching shear strength is increased in proportion to the cubic root of the flexural reinforcement ratio.

Marzouk and Hussein (1991) investigated the punching shear behaviour of high-strength concrete slabs by testing 17 full-scale slab-column interior connections to study the effect of reinforcement ratio, concrete strength, slab depth, and column dimensions on the punching shear capacity of these connections. The slab thickness was either 150 or 120 mm using a concrete strength of 75 MPa. It was found that increasing the flexural reinforcement ratio increases the flexural capacity and stiffness of the connection; however, increasing the flexural reinforcement ratio decreases the ductility. For the 150-mm thick slab, an increase in the punching capacity of 63% was reported when the reinforcement ratio was increased from 0.6 to 2.4%. For the 120-mm thick slab, an increase of 78% was reported when the reinforcement ratio was increased from 0.9 to 2.3%.

Vanderbilt (1972) tested 15 slabs having a slab thickness of 50 mm to investigate the influence of the reinforcement ratio, column size and shape on the punching shear capacity of slab-column interior connections. It was reported that, no matter what column size and shape are, punching capacity increases with increasing the reinforcement ratio. An increase of 22% in the punching shear strength resulted from doubling the reinforcement ratio from 1.3 to 2.6%.

Osman et al. (2000) tested six slab-column interior connections under concentric load to study the effect of concrete strength, aggregate type, and flexural reinforcement ratio on the punching shear capacity of these connections. It was found that increasing the reinforcement ratio from 0.5 to 1.0% changed the mode of failure from a ductile flexure failure to punching shear failure with some ductility. However, further increase in the reinforcement ratio caused a brittle punching failure. They also found that doubling the reinforcement ratio from 1.0 to 2.0% caused a 30% increase in the punching capacity. On the other hand, the ductility decreased as the reinforcement ratio increased. Doubling the reinforcement ratio from 0.5 to 1.0% decreased the ductility by 23%, while increasing the ratio from 0.5 to 2.0% decreased the ductility by 48%.

From the previous different test results, it can be concluded that increasing the flexural reinforcement ratio has a significant effect on increasing the load carrying capacity of slab-column connections. An explanation for this behaviour is given by Richart (1948) where it was stated that significant yielding of the flexural reinforcement results in large and wide cracks which, in turn, decreased the contribution of the aggregate interlock component to the shear strength of the section. Also, larger cracks decrease the area of un-cracked concrete which is the effective area resisting shear stresses. Therefore, it can be concluded that the amount of flexural reinforcement has a significant influence on the punching capacity of slab-column connections.

2.6.2. Effect of Concrete Compressive Strength

Hawkins et al (1989) tested 36 slab-column interior connections to study the effect of concrete compressive strength along with other parameters on the punching shear behaviour. The concrete strength varied from 18 to 57 MPa. It was reported that the connection stiffness increased with increasing the concrete strength but at a rate less than the ratio of the $\sqrt{f_c'}$ values. Also, a slight increase in the ductility was found with increasing the concrete strength. Gardner (1990) and Marzouk and Hussein (1992) supported the previous findings where the use of the cubic root function of the concrete compressive strength was suggested instead of the square root function.

Marzouk and Hussein (1991) tested 17 full-scale interior slab-column connections subjected to gravity loads only to study the effect of concrete compressive strength and other parameters on the punching shear capacity of these connections. The compressive strength of the used concrete ranged from 40 MPa to 70 MPa. It was found that the high strength concrete (HSC) slabs exhibited a more brittle failure mode than the normal strength concrete (NSC) slabs. In addition, the angle of failure surface was found to be steeper in the case of HSC ranging from 32^o to 38^o, while it ranged from 26^o to 30^o in case of NSC.

Ghannoum (1998) tested six full-scale slab-column interior connections having the concrete compressive strength as one of the parameters. The author found that the punching shear resistance increased by 47and 53 % when increasing the concrete compressive strength from 37 MPa to 57 and 67 MPa, respectively. In addition, increasing the concrete compressive strength of slabs improved their performance in terms of higher post-cracking stiffness, greater ductility, and smaller crack widths.

Marzouk et al. (1998) tested six full-scale slab-column interior connections subjected to a combination of gravity and lateral loads. Three connections were made of HSC (75 MPa) and the other three with NSC (35 MPa). Two of the test specimens were tested under gravity loads only (one with NSC and one with HSC) while the other four were tested under a combination of gravity and lateral loads. It was found that increasing the concrete compressive strength results in an increase in the ultimate deflection by 91 and 74%, in displacement ductility by 87 and 68%, and in energy absorbed by 197 and 89% for specimens with steel reinforcement ratios of 0.5 and 1.0% respectively. Also, increasing the concrete compressive strength of the slab from 35 to 75 MPa increased the shear strength by 22 and 5% for specimens with reinforcement ratio of 0.5 and 1.0%, respectively. This ratio should be 45% according to ACI 318-95 code (ACI Committee 318 1995); therefore, it was concluded that, the code provisions should be modified to adequately predict the shear strength of HSC slab. For HSC connections, very few and very narrow cracks were observed until ultimate loads; however, considerable spalling of concrete cover was observed once failure occurred.

2.6.3. Effect of Shear Reinforcement

Shear reinforcement is used when the shear capacity provided by concrete in a slab-column connection is not adequate to resist the applied shear stress. Providing shear reinforcement to the slab column connections can effectively increase the punching shear capacity. This increase in punching shear capacity results in a ductile flexural failure instead of a brittle punching shear failure. The shear reinforcement used for steel-RC slab-column connections can be classified into three main types:

- Shear heads

- Stirrups and bent bars
- Headed stud

The type of shear reinforcement to be used relies on strength and ductility considerations. However, other criteria such as proper anchorage in thin slabs, the ease of placing in the slab and economy have to be considered (Polak et al. 2005). Shear heads were introduced by Wheeler (1936) and was first incorporated into design codes in the ACI 318-71 code (ACI Committee 318 1971)based on the work done by Corley and Hawkins (1968). However, they interfere with the column reinforcement and cannot be used in relatively thin slabs in addition to being expensive to fabricate (Dilger and Ghali 1981). On the other hand, although proved to be effective in increasing the punching shear capacity, bent bars and stirrups are difficult to install in practice and their anchorage cannot be easily achieved in thin slabs.

Dilger and Ghali (1981) introduced the headed studs. Studs are preferred over stirrups and bent bars because of their feasibility to be installed in the congested regions around columns in thin slabs while having proper anchorage at the top and bottom to develop yield in the studs before failure (Mokhtar et al. 1985). In order to form stud rails, headed studs are usually arranged in the form of single-headed studs welded to a thin steel base plate or double-headed studs mechanically crimped into a steel channel. Test results showed a considerable increase in the capacity and ductility of slab-column connections when headed studs were used (Mokhtar et al. 1985; Elgabry and Ghali 1987; Megally and Ghali 1994; El-Salakawy et al. 1998, 2000; Birkle and Dilger 2008; Heinzmann et al. 2012).

Mokhtar et al. (1985) tested eight full-scale slab-column interior connections subjected to concentric loads in which seven connections were with shear studs while one specimen had no

shear reinforcement. The use of studs increased the shear capacity of the connections by 24 to 43% depending on the used configuration of the shear studs in each connection.

El-Salakawy et al. (1998) tested eight large-scale flat slab edge connections with openings and reinforced with shear studs. Test results showed that using stud shear reinforcement in slab-column connections increases the stiffness, the capacity and the ductility of the connections.

2.6.4. Effect of High Moment-to-Shear Ratio

El-Salakawy et al. (1998) studied the influence of high moment-to-shear ratio on the punching shear behaviour of slab-column edge connections with and without openings. The applied values of moment-to-shear ratio was a normal value of 0.3 m based on the analysis of a typical floor system under gravity loads and a higher value of 0.66 m to account for the effects of horizontal loads caused by earthquake or wind. It was found that increasing the moment-to-shear ratio decreased the punching capacity by about 47% for the connection without openings or shear reinforcement. In addition, an increase in the deflection for the same vertical shear force was also found. Test results showed that for the specimen subjected to high moment-to-shear ratio, the flexural cracks initiated at a vertical load is 17 to 25% less than that for the specimen with normal moment-to-shear ratio. The authors concluded that, the high moment-to-shear ratio extends the zone of the slab that is affected by high shear stresses around the column.

Marzouk et al. (2000) tested nine full-scale slab-column interior connections to study the effect of using high-strength light-weight concrete on the punching shear capacity. The test parameters included moment-to-shear ratio, the type of concrete and the steel reinforcement ratio. The specimens were subjected to low, medium and high moment-to-shear ratios with M/V = 0.15, 0.36, and 0.55 m respectively. The test results were compared with counterpart specimens subjected to

vertical shear force only. It was found that when increasing the moment-to-shear ratio from low to high for the specimen with a reinforcement ratio of 1.0%, maximum deflection at failure decreased by 44% and the ductility of the slabs decreased by 11%. When applying column load only on the specimens with a steel ratio of 0.5%, the ultimate deflection decreased by 20, 50, and 60% while the ductility increased by 33, 20, and 16% for the case of low, medium and high moments, respectively. In addition, the ultimate stiffness increased by 52, 49, and 42% for connections under low, medium, and high moment-to-shear ratios, respectively, when the steel reinforcement ratio was doubled from 0.5 to 1.0% . Also, it increased the stiffness degradation ratio by 22, 30, and 23%, respectively. From the comparison of test results it was concluded that, the ultimate load decreased as the moment transferred to the column increased. The ratio of the column load for the case of low, medium, and high moment-to-shear ratios to that of the column-load-only specimens with a steel ratio of 1.0% was 0.95, 0.79, and 0.61, respectively. However, the combined shear stresses due to column load and part of the moment transferred by shear were higher than those in the case of column load only.

2.6.5. Effect of Openings

El-Salakawy et al. (1998) tested eight large-scale slab-column edge connections with openings. The location of openings around the column was one of the tested parameters. The dimensions of the slabs were 1540 × 1020 × 120 mm and the columns were of 250 mm square cross sections. The openings were located either in front of the column or beside it. All the openings were 150 × 150 mm square with their sides parallel to the sides of the column. It was found that the existence of openings decreased the capacity and the stiffness of the connections. The openings at the front of the column decreased the stiffness by 32 to 45%, while the openings at the side of the column

decreased the stiffness by 16 to 25%. For the slabs subjected to higher moment-to-shear ratio, they found a larger decrease in capacity due to the existence of openings.

2.6.6. Effect of Using Fiber-Reinforced Concrete (FRC)

Swamy and Ali (1982) tested 19 full-scale slab-column interior connections to investigate the behaviour of fiber reinforced concrete in the slab column connections with and without shear reinforcement. The parameters studied were the amount, location, type of fibers, and the combination of steel fibers with shear reinforcement. It was found that adding 1% fiber volume to the concrete resulted in a 30% reduction in deflection and a 40% increase in the ultimate load. In addition, ductility and energy absorption capacity were increased by 100 and 300%, respectively. As a result of the reduction in deflections, the service loads can be increased by 30 to 50%. It was reported that the presence of fibers lead to a delay in the formation of diagonal cracking and enabled extensive cracking to occur at failure which transformed the mode of failure from brittle punching failure into more ductile shear failure. Also, it pushed the failure surface away from the column faces and so increased the punching shear resistance. In addition, providing fibers all over the slab had no significant effect than providing them in the vicinity of the column only.

Alexander and Simmonds (1992) tested six full-scale slab-column interior connections with the density of steel fibers as a parameter. It was found that adding 0.4% of 50 mm long corrugated steel fibers increased the ultimate shear capacity of the flat slab by 20%. Also, doubling the fiber content to 0.8% led to a further strength gain of about 7%. In addition, it was concluded that the use of fiber-reinforced concrete increased the ductility.

2.7. RESEARCH ON FRP-RC SLAB-COLUMN CONNECTIONS

2.7.1. Effect of Different Parameters

Due to the difference in properties between conventional steel bars and FRP bars, some research has been made to study the behaviour of concrete structures reinforced with FRP bars. In the following section, the effect of different parameters that affect the punching shear behaviour of slab-column connections reinforced with FRP bars will be discussed.

2.7.1.1. Effect of flexural reinforcement ratio

Matthys and Taerwe (2000) tested 17 slab-column interior connections with depths of 120 mm or 150 mm. Four of them were reinforced with steel grids while the other 13 were reinforced with CFRP grids. It was found that for FRP-reinforced slabs to obtain similar punching capacity as the steel-reinforced slabs, they should have sufficient high flexural stiffness by increasing flexural reinforcement ratio and/or slab depth. This also will decrease the deflections.

Ospina et al. (2003) tested four full-scale slab-column interior connections in which two reinforced with GFRP bars, one reinforced with GFRP grid, and one reinforced with steel bars. The tested flexural reinforcement ratios were 0.73, 087, and 1.46 %. Test results showed that the punching capacity of the slab increases with the increase of the elastic stiffness of the reinforcing grid. In addition, the ultimate deflection decreases as the top grid stiffness increases.

Hussein et al. (2004) tested four slab-column interior connections with reinforcement ratios varying between 1.05 and 1.67%. An increase of 14 and 10% in the ultimate capacity of the connections with 1.18 and 1.67% reinforcement ratio was found compared to the one with 1.05%.

Zaghloul (2007) tested 10 half-scale slab-column edge connections in which three connections reinforced with steel bars and seven reinforced with CFRP bars. Two connections was assigned to

investigate the effect of the flexural reinforcement ratio. It was found that increasing the reinforcement ratio by 46% increased the ultimate capacity by 21% without an increase in the post-cracking stiffness.

Gouda and El-Salakawy (2016) tested three full-scale slab-column interior connections reinforced with GFRP bars. Test results showed an increase in the capacity and the post-cracking stiffness of the connections by 8 and 20% and 50 and 110%, respectively, when the flexural reinforcement ratio was increased by 50 (from 0.65 to 0.98%) and 100% (from 0.65 to 1.3%), respectively. Also, increasing the reinforcement ratio by 50 and 100% decreased the deflection of the connections at service and at failure by 30 and 50% and 23 and 30%, respectively.

El-Gendy and El-Salakawy (2016b) tested three full-scale slab-column edge connections with different GFRP flexural reinforcement ratios of 0.9, 1.35 and 1.8%. It was found that increasing the reinforcement ratio by 50 and 100% increased the punching capacity by 14 and 21%, respectively. Also, a linear increase in the post-cracking stiffness with increasing the reinforcement ratio was reported. Increasing the reinforcement ratio by 50 and 100% increased the post-cracking stiffness by 62 and 119%, respectively, which in turn, decreased the deflections at service by 52 and 60% and at failure by 28 and 39%, respectively.

2.7.1.2. Effect of concrete compressive strength

Banthia et al. (1995) tested four slab-column interior connections. One specimen was reinforced with steel grid and the other three were reinforced with FRP grids. It was found that the use of HSC led to a stiffer response initially. However, a nominal increase in the total energy absorption capability occurred. Also, an insignificant increase in the capacity by 5% when the concrete compressive strength was increased from 41.5 to 53 MPa was found. It was concluded that there

is no need to modify the code equations of the steel-reinforced slabs when applying them to slabs reinforced with FRP reinforcement.

Zhang et al. (2005) tested one slab-column interior connection reinforced with GFRP bars with a concrete strength of 71 MPa. The results of this connection was compared to a similar connection made of normal strength concrete of 35 MPa tested by Hussein and Imtiaz (2004). It was reported that the use of HSC increased the punching capacity of the connection, however this increase was at a rate less than the rate of the square root of the concrete compressive strength. Also, it was reported that the concrete strength has little effect on the post-cracking stiffness and the energy absorption capacity of the connections.

Hassan et al. (2013) tested 10 full-scale slab-column interior connections subjected to concentric loading in which two connections were made of HSC of 76 MPa to study the effect of concrete compressive strength. Test results showed an increase in the punching shear capacity of the HSC connections than their NSC counterparts (38 MPa) by 27 and 7%. In addition, it was found that the use of HSC enhanced the un-cracked stiffness of the connections which resulted in lower deflections at the same load level compared to the NSC ones.

Gouda and El-Salakawy (2016) found that increasing the concrete compressive strength of full-scale slab-column interior connections subjected to eccentric loading by 67% increased the punching capacity and deflection at failure by 5 and 21%, respectively.

2.7.1.3. Effect of shear reinforcement

El-Ghandour et al. (2003) tested eight full-scale slab-column interior connections subjected to concentric loading in which two of them were reinforced with CFRP shear bands as shear reinforcement. The shear-reinforced slabs showed a slight increase in the punching shear capacity

and larger deformability compared to those without shear reinforcement. It was found that when using shear reinforcement in a slab with a GFRP flexural reinforcement of 0.38% the ultimate capacity was increased by 13.9%. This was attributed to the role of the shear reinforcement in preventing the punching shear failure at lower load levels. Also, the concrete contribution to the punching shear resistance was found to be reduced after the initiation of the major shear crack and accordingly, they proposed that only 50% of the concrete shear resistance to be considered.

Zaghloul (2007) tested two half-scale slab-column edge and interior connections to study the effect of CFRP shear reinforcement on the punching shear behaviour of such connections. A typical CFRP shear rails consisted of four legs 90 mm apart were used. The rails were placed orthogonally parallel to the column faces. For the interior connection, it was found that the shear reinforcement increased the ultimate capacity by 24.6 and 30.4% when the first leg of the rail was located at a distance of 0.5*d* and 0.85*d* from the column face, respectively. For the edge connection, the increase was only 9% with the first leg of the rail located 0.5*d* from the column face. Also, it was reported that the shear reinforcement increased the deformability of the connections.

Gouda and El-Salakawy (2016b) studied the effect of using a new type of GFRP studs with headed ends (Schoeck Canada Inc. 2013) as shear reinforcement in slab-column interior connections subjected to shear force and unbalanced moments. Test results showed an increase in both the capacity and the stiffness of the shear-reinforced connections, however the GFRP studs were not able to prevent the brittle punching shear failure.

El-Gendy and El-Salakawy (2016a) used the same new type of GFRP studs with headed ends as shear reinforcement in GFRP-RC edge connections. They arranged the headed studs (12-mm diameter) on six lines around the edge column (two perpendicular to each column face) forming

five and seven parallel peripheral rows of studs (six studs in each row) in their connections RD-75-M and RD-50-M, respectively, with a stud spacing of 120 and 80 mm (0.75 *d* and 0.50 *d*), respectively. They found that the GFRP headed studs significantly increased the capacity of both connections. They reported that connection RD-50-M (studs spaced at 0.50 *d*) failed in a flexural mode with substantial deformability; however, although showed significant deformability, connection RD-75-M (studs spaced at 0.75 *d*) failed in a mixed flexural/punching mode.

2.7.1.4. Effect of using fiber-reinforced concrete (FRC)

Banthia et al. (1995) investigated the punching shear behaviour of FRP reinforced slabs under the effect of using fiber reinforced concrete with normal and high compressive strengths. It was found that the use of steel fibers improved the ultimate load carrying capacity and the capability of energy absorption. When using SFRC, 11% increase in the capacity was found compared to the NSC while an increase of 17% in the capacity was found compared to the HSC. This increase was due to the cohesiveness, the capability to transfer stresses across a crack, and the improved strain capacity of SFRC which delayed the formation of large cracks and allowed the FRP reinforcement to achieve its full capacity.

2.7.2. Proposed Design Provisions

As a result of the research that has been carried out to investigate the punching shear behaviour of FRP-reinforced slabs, design provisions have been proposed as an alternative to the design provisions for punching shear of FRP-reinforced slabs.

El-Ghandour et al. (1999) found an overestimation of the concrete shear resistance of FRP-reinforced concrete slabs with low reinforcement ratios in the ACI 318-95 code (ACI Committee 318 1995) provisions as it ignores the influence of flexural reinforcement. As a result, they

suggested a modification to the ACI 318-95 (ACI Committee 318 1995) equation through multiplying the obtained shear strength value by the term $\left(\frac{\mathrm{E_{frp}}}{\mathrm{E_s}}\right)^{1/3}$ as follow:

$$V_{c\,,El} = V_{c,ACI\ 318}\ x\ \left(\frac{E_{frp}}{E_s}\right)^{1/3} = 0.33\sqrt{f_c'}\ \left(\frac{E_{frp}}{E_s}\right)^{1/3}\ b_o d \tag{2.45}$$

By applying this modification, they found that it leads to more accurate predictions of the punching capacity of their tested FRP-reinforced slabs without shear reinforcement.

Matthys and Taerwe (2000) suggested a modification to BS-8110 by introducing the equivalent reinforcement ratio $\rho_f \frac{E_f}{E_s}$ to account for the relatively low modulus of elasticity of FRP reinforcement:

The original BS-8110 equation:

$$v_{c,BS} = 0.79\ (100\rho_s)^{1/3}\left(\frac{400}{d}\right)^{1/4}\left(\frac{f_{ck}}{25}\right)^{1/3} \tag{2.46}$$

The modified equation:

$$V_{c,\ MT} = 1.36\ \frac{\left(100\ \rho_f \frac{E_f}{E_s} f_c'\right)^{1/3}}{d^{1/4}}\ b_o d \tag{2.47}$$

Where;

ρ_f = the reinforcement ratio of the tensile FRP mat

b_o = the control perimeter at a distance of 1.5 d away from the loaded area (mm)

However, Ospina et al. (2003) presented a modification to the equation proposed by Matthys and Taerwe (2000) as follows:

$$V_{c\,,\ osp.} = 2.77\left(\rho_f f_c'\right)^{1/3}\sqrt{\frac{E_{frp}}{E_s}}\ b_o d \tag{2.48}$$

Zaghloul (2007) improved his previous proposed equation in 2004 by introducing a shear perimeter size effect. He suggested a modification to the equation of one-way shear given by CSA/S806-02 (CSA 2002) to predict the punching capacity under the combination of shear force and unbalanced moment.

The original CSA/S806-02 equation:

$$v_{c,ACI} = 0.035\lambda\,\varphi_c\left(f_c'\rho E_f\frac{V_f}{M_f}d\right)^{1/3} \tag{2.49}$$

The modified equation:

$$V_{c,\ zag.} = 0.07(5.16\frac{d}{b_o} + 0.44)(f_c'\rho E_{FRP})^{1/3}b_o d \tag{2.50}$$

Ospina (2005) modified the one-way shear equation proposed by Tureyen and Frosch (2003) as follows:

Tureyen and Frosch (2003) model:

$$V_c = 0.4\sqrt{f_c'}b_o c \tag{2.51}$$

Ospina (2005) model:

$$V_c = 0.8\sqrt{f_c'}b_o c \tag{2.52}$$

Where;

b_o = the perimeter of critical section at *d*/2 away from the column face (mm)

c = the cracked transformed section neutral axis depth (mm), *c* = *kd*.

$$k = \sqrt{2\rho_f n_f + \left(\rho_f n_f\right)^2} - \rho_f n_f \tag{2.53}$$

Where;

ρ_f = the reinforcement ratio of the tensile FRP mat n_f = the modular ratio, $n_f = \frac{E_{frp}}{E_s}$

Since neither the CSA/S806-12 (CSA 2012) nor the ACI 440.1R-15 (ACI 2015) include design provisions regarding the design of FRP-RC slab-column connections with shear reinforcement, El-Gendy and El-Salakawy (2016a) modified the provisions regarding the design of FRP-RC slab-column connections without shear reinforcement to consider the shear reinforcement. The modifications are based on the relationship between the provisions regarding the slabs with and without shear reinforcement in both the CSA/A23.3-14 (CSA 2014) and the ACI 318-14 (ACI Committee 318 2014) for steel-RC structures as follows:

CSA/S806-12 Modified Provisions

In the CSA/A23.3-14 (CSA 2014) for steel-RC structures, the shear strength provided by the concrete, for slabs with studs shear reinforcement, inside (Eq. 2.7) and outside (Eq. 2.6) the shear reinforced zone represents 75 and 50% of the strength of slabs without shear reinforcement (Eq. 2.5), respectively. Therefore, for FRP-RC slabs, the shear strength equation in the CSA/S806-12 (CSA 2012) for slabs without shear reinforcement is multiplied by the same percentages (75 and 50%) to obtain Equations 2.54 and 2.55 for the shear strength provided by the concrete inside and outside the shear reinforced zone, respectively.

$$v_c = 0.041\lambda\,\varphi_c(E_F\rho_F f_c')^{\frac{1}{3}} \tag{2.54}$$

$$v_c = 0.028\lambda\,\varphi_c(E_F\rho_F f_c')^{\frac{1}{3}} \tag{2.55}$$

Moreover, the strength provided by the GFRP studs is calculated using Eq. 2.56 from the CSA/A23.3-14 (CSA 2014) with replacing the yield strength of the shear reinforcement, f_y, by the ultimate strength of the GFRP studs (f_{fu}) with a limiting strain of 5000 μs.

$$v_s = \frac{\varphi_s A_{vs} f_{fu}}{b_o s} \tag{2.56}$$

ACI 440.1R-15 Modified Provisions

The shear strength equations in the ACI 440.1R-15 (ACI 2015) for slabs without shear reinforcement were modified using the same previous procedure based on the ACI 318-14 code (ACI Committee 318 2014) for steel-RC structures. For FRP-RC slabs reinforced with studs, Equations 2.57 and 2.58 for the shear strength provided by the concrete inside and outside the shear reinforced zone, respectively, were obtained by multiplying Eq. 2.34, for slabs without shear reinforcement, by 75 and 50%, respectively. Those percentages were obtained based on Equations 2.13 and 2.12 for the shear strength provided by the concrete inside and outside the shear reinforced zone, respectively, for steel-RC slabs reinforced with studs, which represents 75 and 50% of the strength of slabs without shear reinforcement (Eq. 2.11).

$$V_n = V_c = 0.6\sqrt{f_c'} b_o c \tag{2.57}$$

$$V_n = V_c = 0.4\sqrt{f_c'} b_o c \tag{2.58}$$

Also, the strength provided by the GFRP studs or corrugated bars is calculated using Eq. 2.59 with replacing the yield strength of the shear reinforcement, f_y, by the ultimate strength of the GFRP studs or corrugated bars (f_{fu}) with a limiting strain of 4000 μs.

$$v_s = \frac{A_v f_{fu}}{b_o s} \tag{2.59}$$

CHAPTER 3

EXPERIMENTAL PROGRAM

3.1. INTRODUCTION

Based on the literature presented in the previous chapter, it is clear that the punching shear behaviour of slab-column edge connections depends on several parameters. This experimental study aims to study the effect of the flexural reinforcement ratio, and the shear reinforcement type and arrangement around the column (pattern) on the punching shear behaviour of slab-column edge connections.

3.2. TEST SPECIMENS

Seven full-scale slab-column edge connections were constructed and tested to failure. The dimensions and reinforcement distribution of the connections were obtained by performing an elastic analysis, according to the CSA/S806-12 (CSA 2012) standard, of a typical parking garage building consisting of three 6.5 m-long bays in both directions (Appendix A). Each connection simulates a portion of the slab bounded by the slab free edge and the lines of contra-flexure located at a distance of 0.2L from the column centrelines, where L is the distance between the centrelines of the columns (Fig. 3.1). The building was designed to carry a specified dead load of 5.8 kN/m^2 and a specified live load of 2.4 kN/m^2 (NRCC 2010), i.e., specified gravity load of 8.2 kN/m^2, which resulted in a moment-to-shear ratio of 0.4 m and a service load of 180 kN. The resulting connection dimensions from the analysis were 2,600×1,450×200 mm; however, the dimensions of actual connections were increased to 2,800×1,550×200 mm in order to allow for a 100 mm supporting clearance. The columns had a cross-section of 300×300 and extended for 1,000 mm above and below the slab. The control design was conducted using normal strength concrete (NSC)

with a compressive strength of 40 MPa, which resulted in a flexural reinforcement ratio of 1.8%. Then, two more reinforcement ratios of 0.9 and 1.35% were selected and the concrete strength was doubled in order to study the effect of flexural reinforcement ratio on high strength concrete (HSC) connections.

The connections were divided into Series I and Series II. Series I included three connections assigned to study the effect of flexural reinforcement ratio on the punching shear behaviour of HSC connections. These connections were reinforced with three different flexural reinforcement ratios of 0.90, 1.35 and 1.80% in the direction perpendicular to the slab free edge.

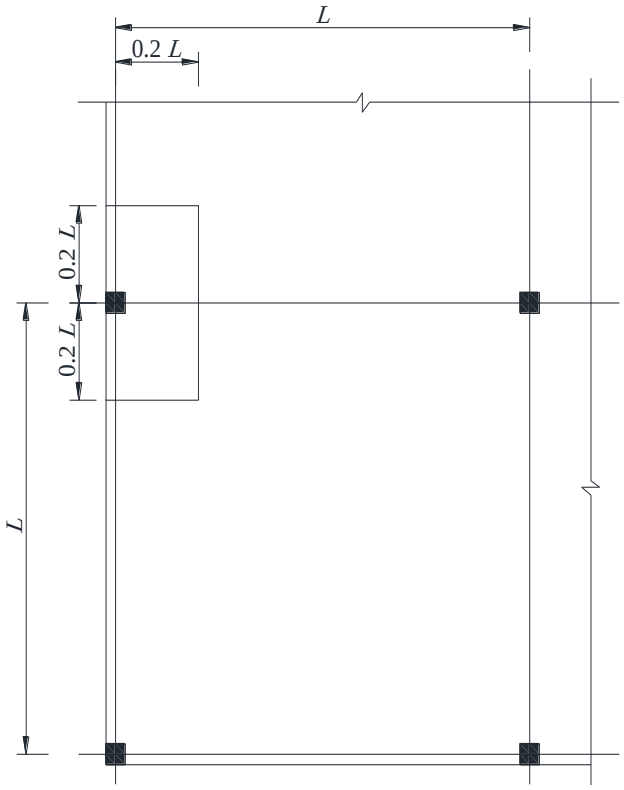

Figure 3.1: The studied portion of the slab

Series II included four NSC connections dedicated to investigate the effect of GFRP shear reinforcement type and pattern on the behaviour of slab-column edge connections. Two of the shear reinforced connections were reinforced with different ratios of GFRP headed studs, while

the other two were reinforced with different ratios of sand-coated (SC) GFRP corrugated bars. For each type of shear reinforcement, one connection had eight lines of shear reinforcement while the other one had six. These four connections had the same flexural reinforcement ratio of 0.90 % in the direction perpendicular to the slab free edge.

The designation of the connections consists of three parts; the first part is a letter indicating the concrete strength (N for normal strength and H for high strength), the second part is a number indicating the flexural reinforcement ratio in the direction perpendicular to the slab free edge (0.9 for ρ = 0.9%, 1.35 for ρ = 1.35% and 1.8 for ρ = 1.8%), the third part consists of a letter indicating the type of shear reinforcement (S for headed studs and C for corrugated bar) and a number indicating the number of shear reinforcement lines around columns (8 or 6 lines), whereas "XX" indicates that no shear reinforcement was used. For example, N-0.9-S6 denotes a NSC with 0.9% flexural reinforcement ratio and six lines of headed studs around the column. The characteristics of each connection are listed in Table 3.1.

Table 3.1: Details of test connections

Series	Connection	Concrete compressive strength, f'_c (MPa)	Concrete tensile strength, f_r (MPa)	Reinforcement ratio, ρ (%) and spacing, S (mm)				Shear reinforcement		
				Perpendicular to edge		Parallel to edge		Type	No. of stems per row	Ratio (%)
				ρ	s	ρ	s			
I	H-0.9-XX	81	5.0	0.9	192	0.82	232	NA	NA	NA
	H-1.35-XX	85	5.1	1.35	128	1.23	155			
	H-1.8-XX	80	4.9	1.8	96	0.64	116			
II	N-0.9-S8	43	3.0	0.9	192	0.82	232	Studs	8	0.69
	N-0.9-S6	44	3.4						6	0.52
	N-0.9-C8	43	3.2	0.9	192	0.82	232	Corrugated bars	8	0.39
	N-0.9-C6	45	3.4						6	0.29

All connections were reinforced using SC-GFRP bars with one orthogonal mesh in the tension side of the slab. Straight bars were used in the direction parallel to the free edge, while bent bars were used in the direction perpendicular to the free edge to provide sufficient anchorage. The columns were adequately reinforced with 4 No. 20M steel bars and No. 10M steel stirrups to prevent premature failure. The configuration of the shear reinforcement in Series II connections was selected based on the results of El-Gendy and El-Salakawy (2016a), where six lines of studs were used as discussed in section 2.7.1.3. The shear reinforcement was increased by adding two diagonal lines of shear reinforcement at each column corner and maintaining the diameter (12.7 mm) and spacing (0.75 d = 120 mm) of studs in connection N-0.9-S8. However, in order to provide the longest practical vertical stem (between the two bends) with a reasonable capacity, the 9.5-mm corrugated bar diameter was selected in connection N-0.9-C8. A larger bar diameter will result in a shorter vertical stem and, consequently, a higher possibility of missing diagonal cracks (inadequate anchorage). Accordingly, for connection N-0.9-S8 (with headed studs), the studs were arranged in five parallel peripheral rows (eight studs in each row) spaced at 120 mm (0.75 d) with a spacing between the column face and the first peripheral studs row of 64 mm (0.40 d). For connection N-0.9-C8 (with corrugated bars), eight corrugated bars with stems spaced at 120 mm (0.75d) were used. The spacing between the column face and the closest vertical stems of the corrugated bars was 40 mm (0.25 d). Based on the results of these two connections, which failed in flexure with strains in the vertical stems of the shear reinforcement well below the code limits as will be discussed later, it was decided to test two connections without diagonal lines of shear reinforcement, i.e., connections N-0.9-S6 and N-0.9-C6. The lines of shear reinforcement extended in the slabs such that the critical section outside the shear-reinforced zone is located at 624 mm (3.90 d) and 600 mm (3.75 d) from the column face in the direction perpendicular to the slab free

edge for connections with headed studs and corrugated bars, respectively. The reinforcement details of the test connections are shown in Figures 3.2 to 3.8.

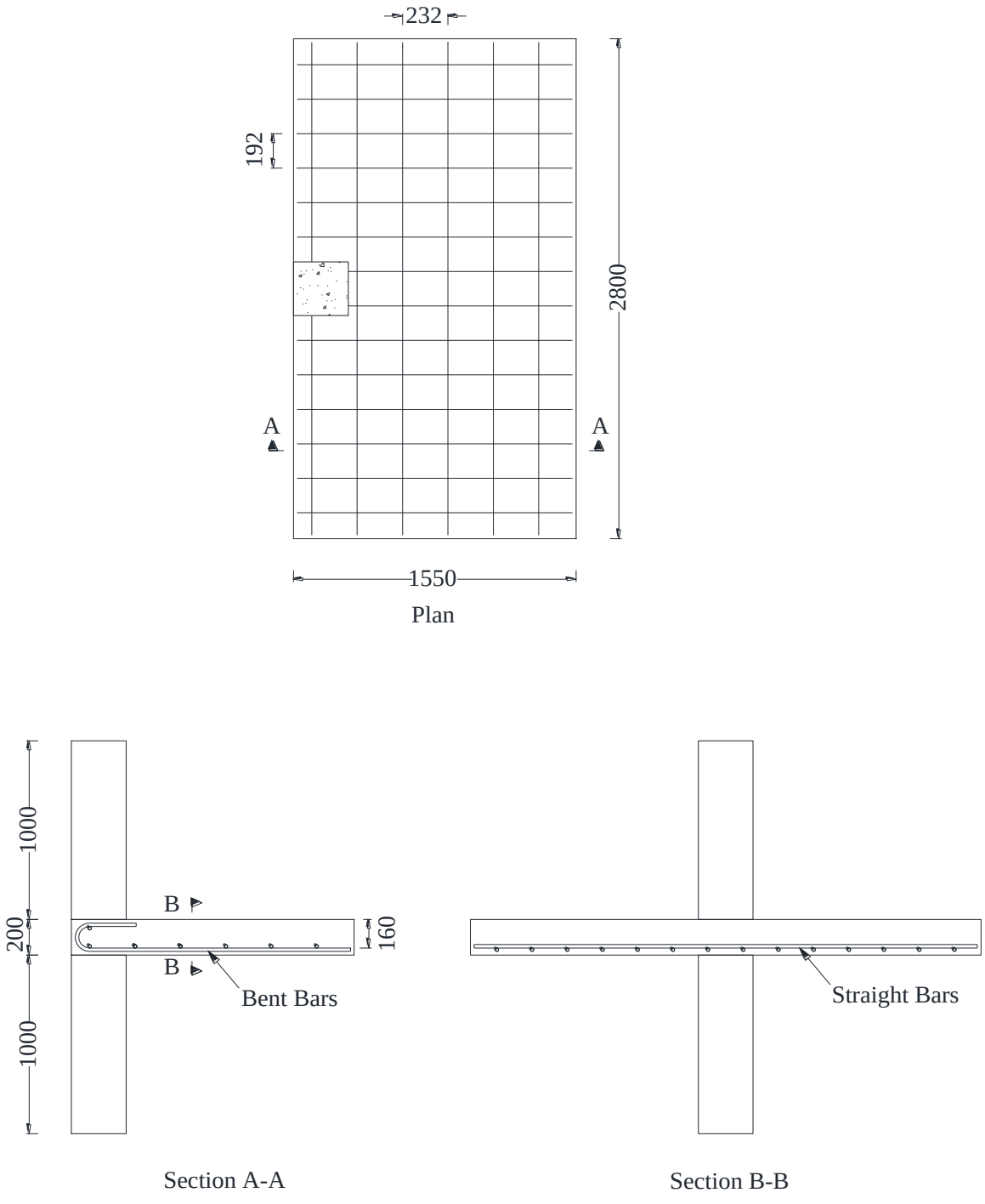

Figure 3.2: Dimensions and flexural reinforcement layout of connections with 0.9% reinforcement ratio (all dimensions are in mm)

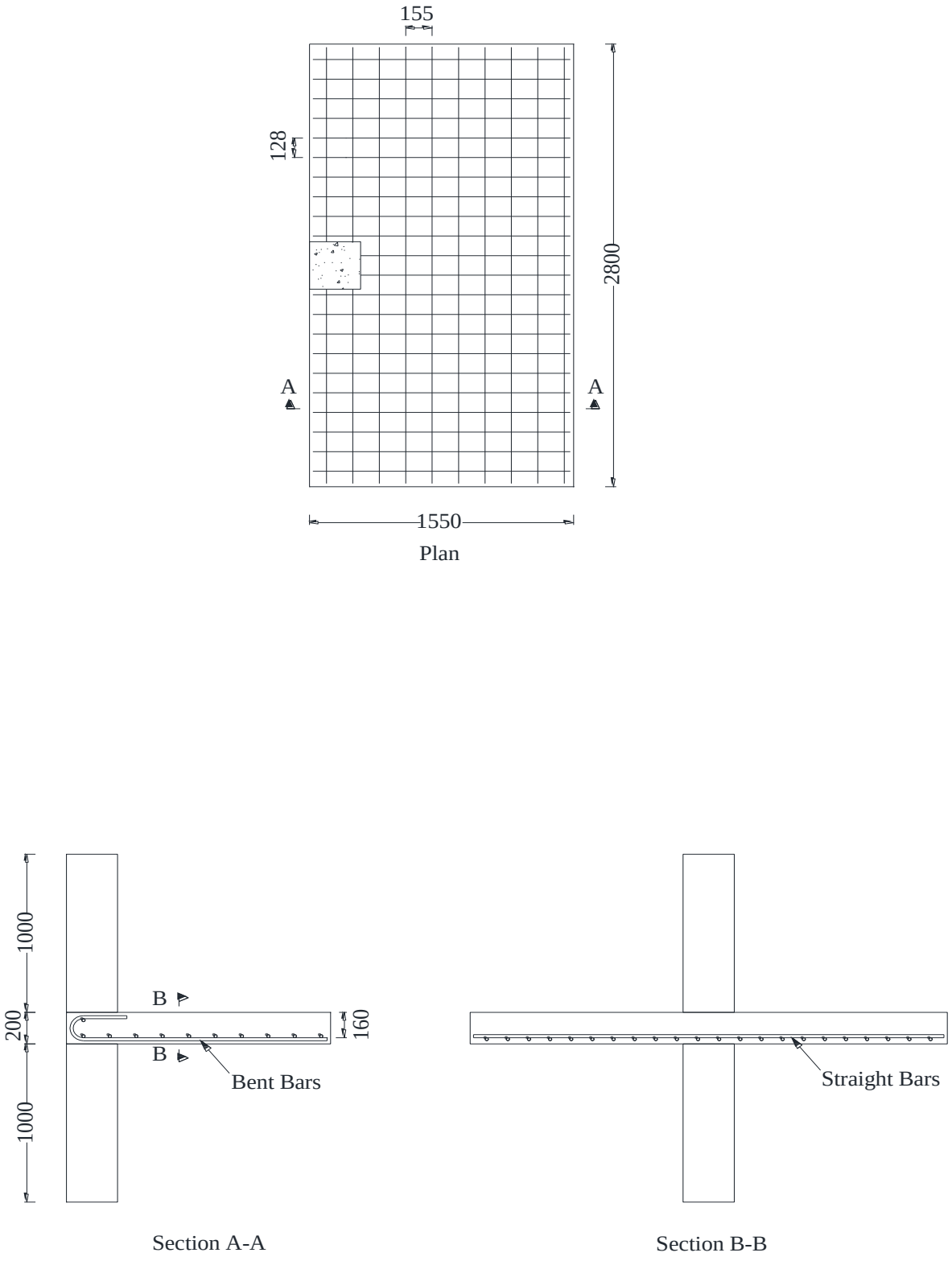

Figure 3.3: Dimensions and flexural reinforcement layout of connection H-1.35-XX (all dimensions are in mm)

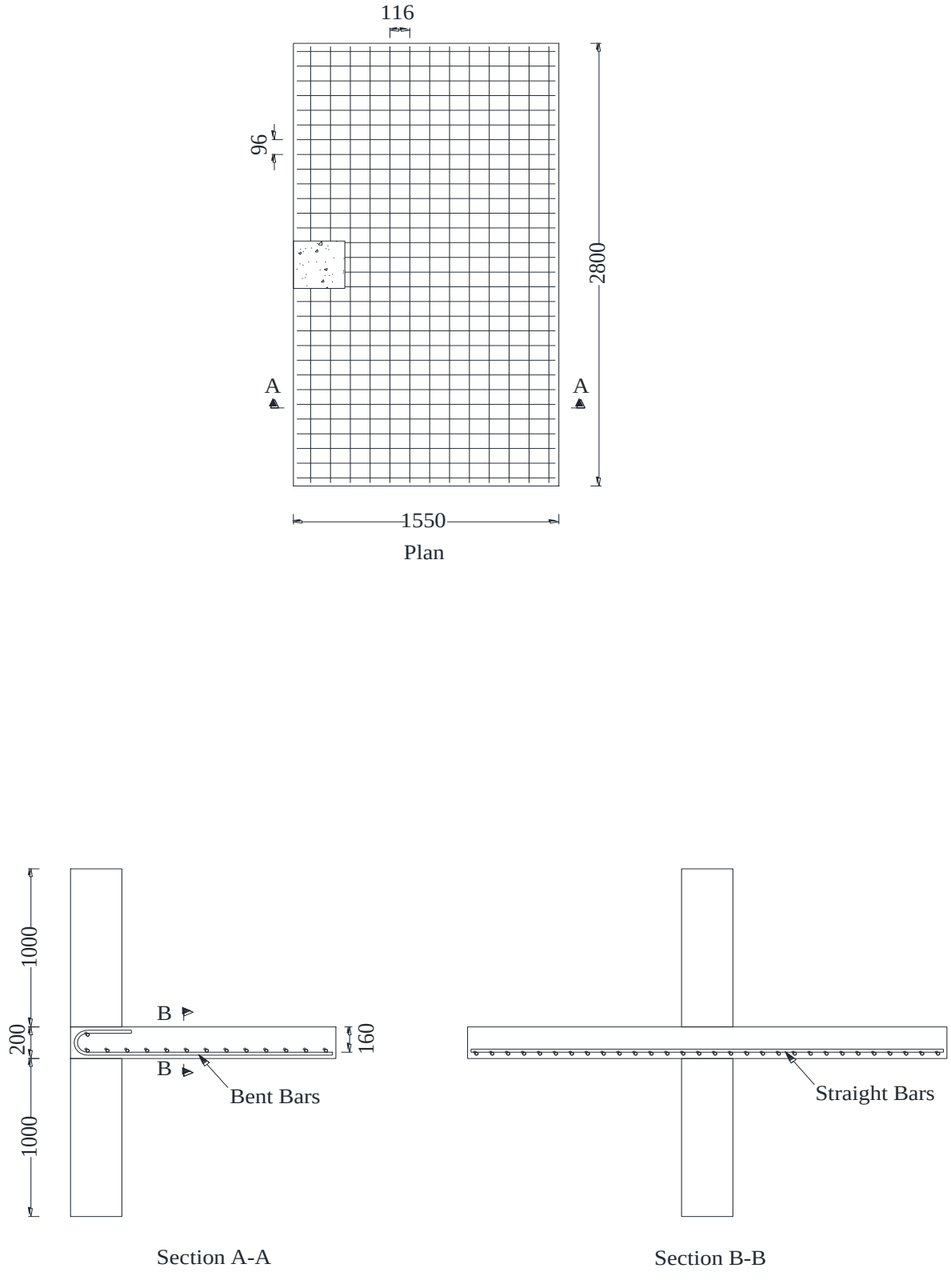

Figure 3.4: Dimensions and flexural reinforcement layout of connection H-1.8-XX (all dimensions are in mm)

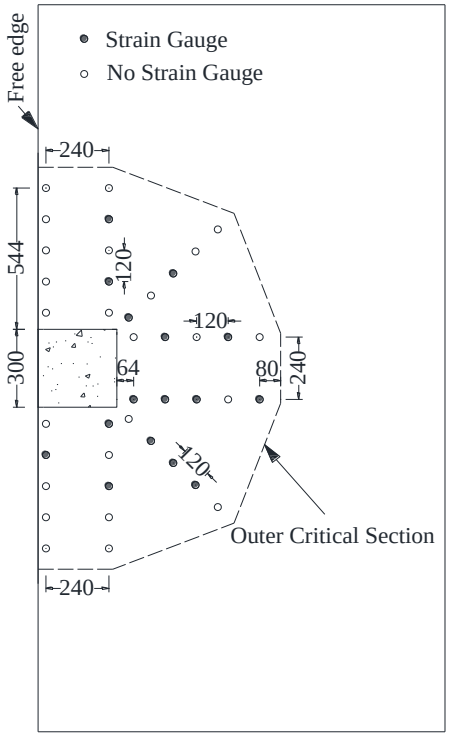

(a) Connection N-0.9-S8

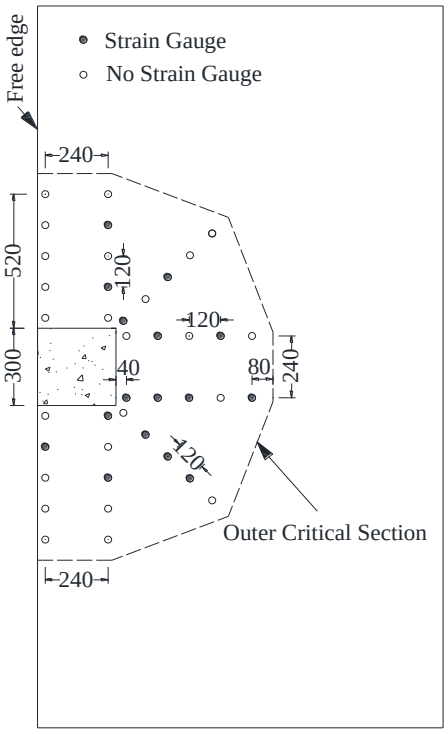

(b) Connection N-0.9-C8

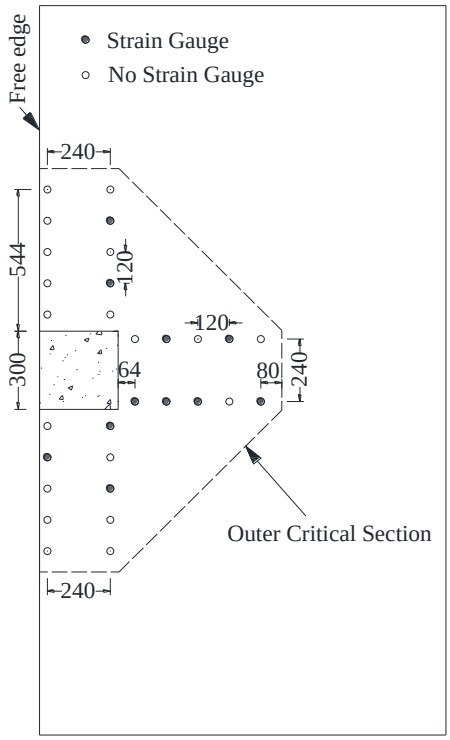

(c) Connection N-0.9-S6

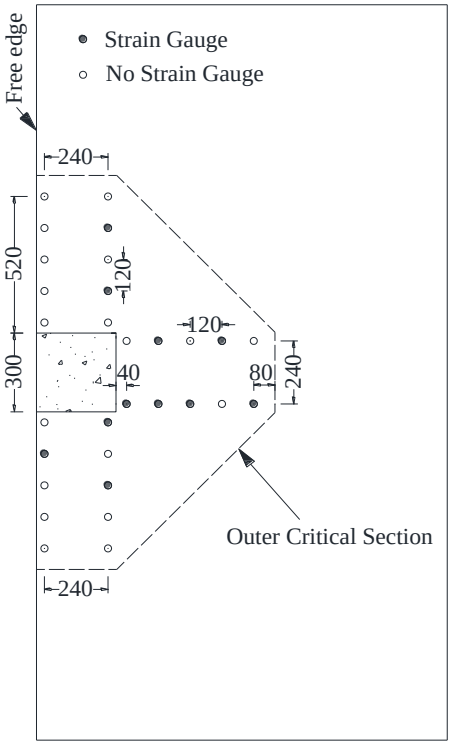

(d) Connection N-0.9-C6

Figure 3.5: Details of shear reinforcement (all dimensions are in mm)

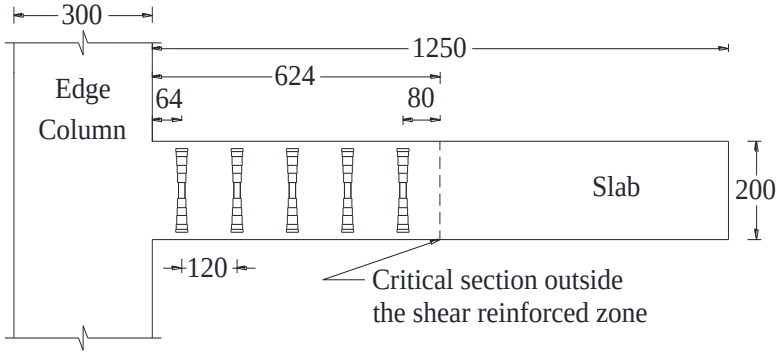

a) Connections with headed studs

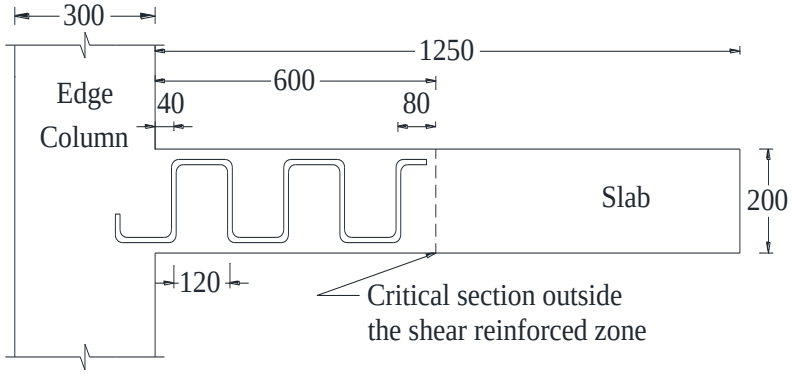

b) Connections with corrugated bars

Figure 3.6: Typical shear reinforcement arrangement (all dimensions are in mm)

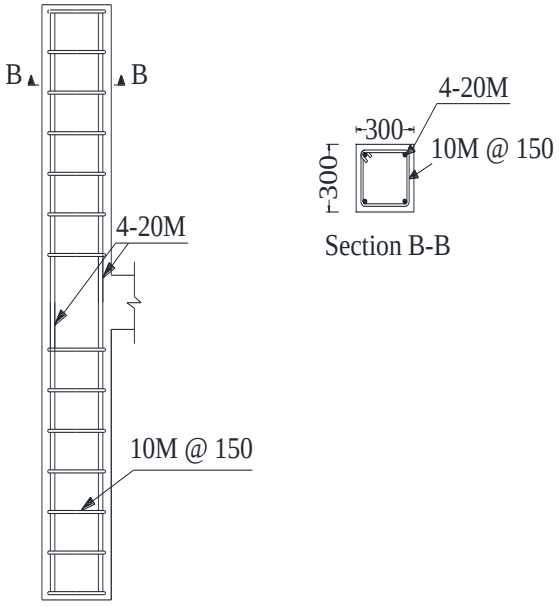

Figure 3.7: Details of column (all dimensions are in mm)

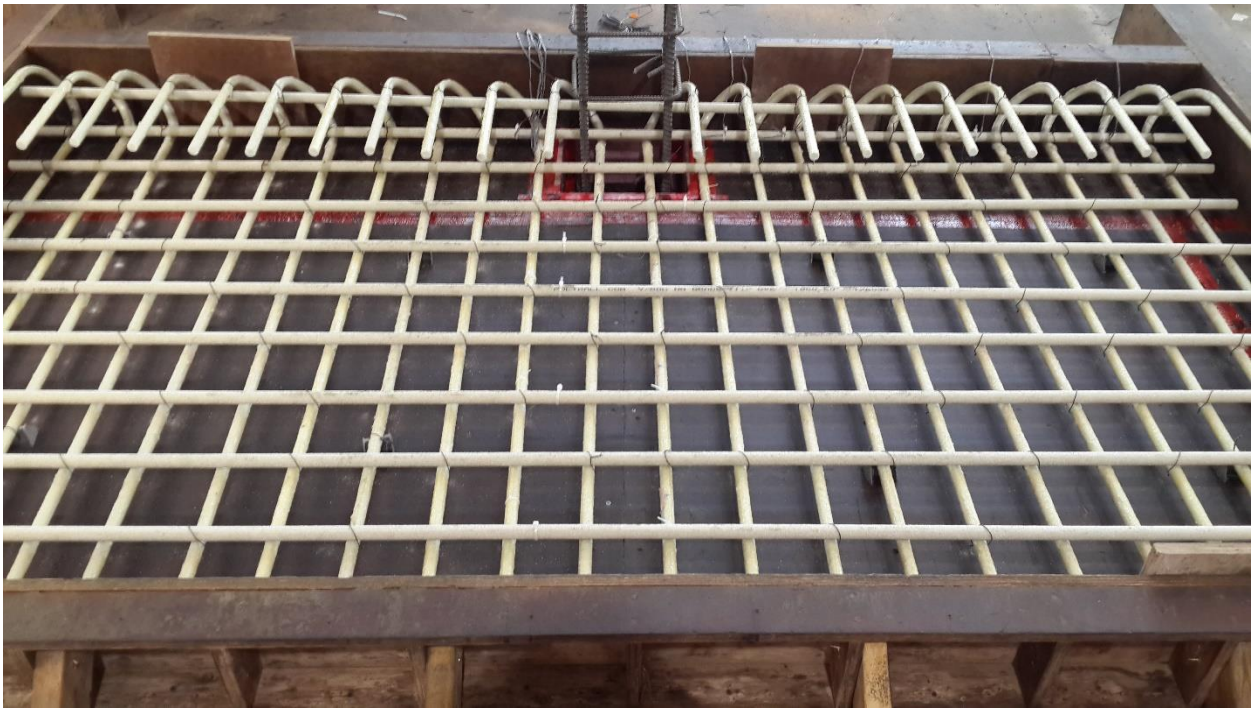

(a) Connection H-1.35-XX

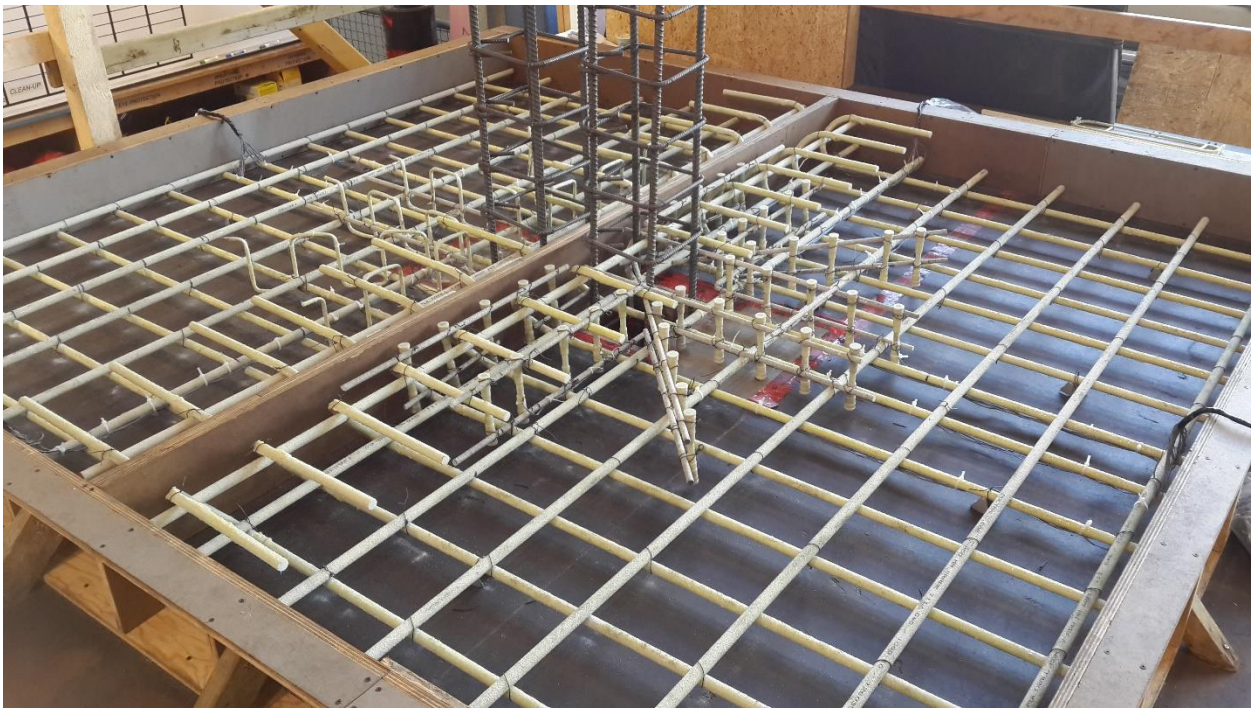

(b) Connections N-0.9-S8 and N-0.9-C8

Figure 3.8: Photos for the reinforcement configurations

3.3. MATERIALS

3.3.1. Concrete

All test connections were cast using normal-weight ready-mix concrete with a maximum aggregate size of 19 mm and a target 28-days compressive strengths of 40 and 80 MPa for the NSC and HSC connections, respectively (Table 3.1). All connections were wet-cured in the laboratory for 7 days. The actual concrete compressive and tensile strengths of each connection were determined on the day of testing by testing standard 100×200 mm and 150×300 mm concrete cylinders, respectively, in accordance with the CSA A23.1/A23.2-14 (CSA 2014).

3.3.2. GFRP Reinforcement

All slabs were reinforced in flexural using No. 20 SC-GFRP straight and bent bars (Pultrall Inc. 2015). The mechanical properties of these bars were obtained according to the ASTM 2011 and CSA/S806-12 (CSA 2012). In addition, two newly developed types of GFRP shear reinforcement were used; studs with headed ends and corrugated bars (Pultrall Inc. 2015) (Fig. 3.9). Table 3.2 shows the properties of the used GFRP reinforcement. The studs with headed ends were 170-mm long No.13 GFRP bars with 70-mm long cast-on tapered headed ends. The heads are made of a thermoplastic matrix reinforced with short discrete glass fibers. The outer diameter of the headed end is 25 mm (2 times the bar diameter) tapered in five steps towards the bar (Fig. 3a). The corrugated bars, on the other hand, are No.10 SC-GFRP bent bars with a 90° angle between the vertical stems and the horizontal portions. The total height of a corrugated bar is 160 mm, while the distance between the vertical stems is 120 mm (0.75 d).

Table 3.2: Mechanical properties of the used GFRP reinforcement

Bar Material	Bar Size	Effective Diameter (mm)	Effective Area (mm^2)	Tensile Strength (MPa)	Elasticity Modulus (GPa)	Ultimate Strain (%)
SC-GFRP (Straight)	No. 20	19.1	285	1484	65	2.3
SC-GFRP (Bent-Straight Portion)	No. 20	19.1	285	1266	54	2.4
GFRP (Studs)	No. 13	12.7	126.7	552[a]	68	0.8[a]
SC-GFRP (Corrugated Bars)[b]	No. 10	9.5	71.3	1280	52	2.5

[a] Usable design stress/strain provided by the manufacturer (corresponds to a pull-out load capacity of 70 kN)
[b] Properties are for the straight portion of the bar

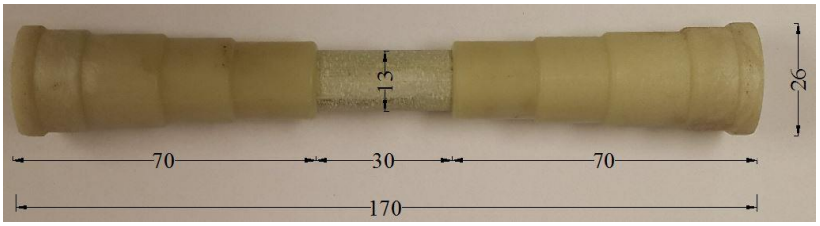

(a) Headed stud

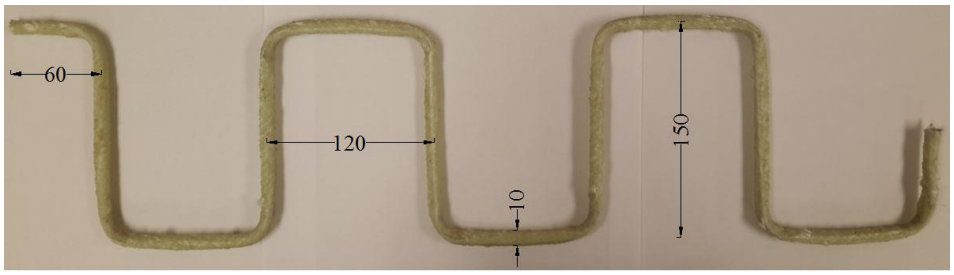

(b) Corrugated bar

Figure 3.9: Details of GFRP shear reinforcement (all dimensions are in mm)

3.4. INSTRUMENTATION

A real-time monitoring of the behaviour of the specimens during the test was provided in terms of the strains, deflections, and applied loads using strain gauges, PI-gauges, LVDTs, and load cells,

respectively. All the data was collected by a data acquisition system (DAQ) and stored in a personal computer. A total of 12 electrical strain gauges (6-mm long) were attached to the flexural reinforcement bars at critical locations in order to measure reinforcement strains (Fig. 3.10a). In addition, for connections reinforced with eight lines of shear reinforcement, 16 electrical strain gauges were attached at the mid-height of studs and corrugated bars legs, while for connections reinforced with six lines of shear reinforcement, 11 electrical strain gauges were used (Fig. 3.5). Moreover, two electrical strain gauges (40-mm long) and two PI-gauges were used to measure concrete surface strains at the column face in both orthogonal directions as shown in Figure 3.10b. In addition, a total of 12 linear variable displacement transducers (LVDTs) were used to measure the deflections of the slab at different locations as shown in Figure 3.10b. Three load cells (one load cell attached to each of the hydraulic machines) was used to measure the applied loads.

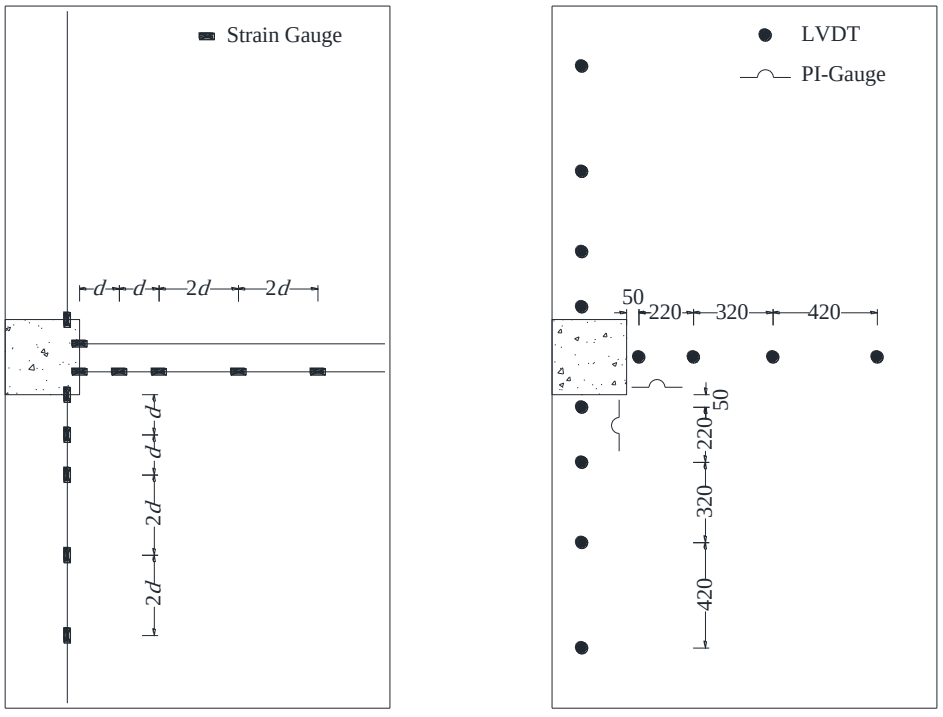

(a) Flexural Reinforcement Strain Gauges (b) PI-Gauges and LVDTs

Figure 3.10: Typical instrumentation arrangement (all dimensions are in mm)

3.5. TEST SET-UP AND TESTING PROCEDURE

All connections were tested in an upside-down position with respect to the position of a real structure with the vertical column load applied downward. Therefore, tension cracks appeared on the bottom surface of the slab. Stiff steel I-beams were used to simply support the connections at three edges through a 20-mm wide steel bearing plate, while the fourth edge was left free. Moreover, neoprene strips were placed between the slab and the bearing plate to have a uniform load distribution along the supported edges. Three heavy steel angles were placed on top of each supported edge of the slab to prevent any movement. C-shaped clamps were used to tighten the steel angles to the supporting steel I-beams, while keeping the corners of the slab free to lift. A hydraulic actuator and two hydraulic jacks, all attached to a rigid steel frame, were used to apply the vertical shear force and the lateral forces (causing the unbalanced moment), respectively. The actuator and one hydraulic jack were placed at the tip of the upper column stub, while the other hydraulic jack was placed at the tip of the lower column. A moment-to-shear ratio of 0.4 m was kept constant during the whole test for all connections and the loading was paused every 20 kN to mark the propagation of cracks. Figures 3.11 and 3.12 shows the details of the test setup use to test the connections in the laboratory.

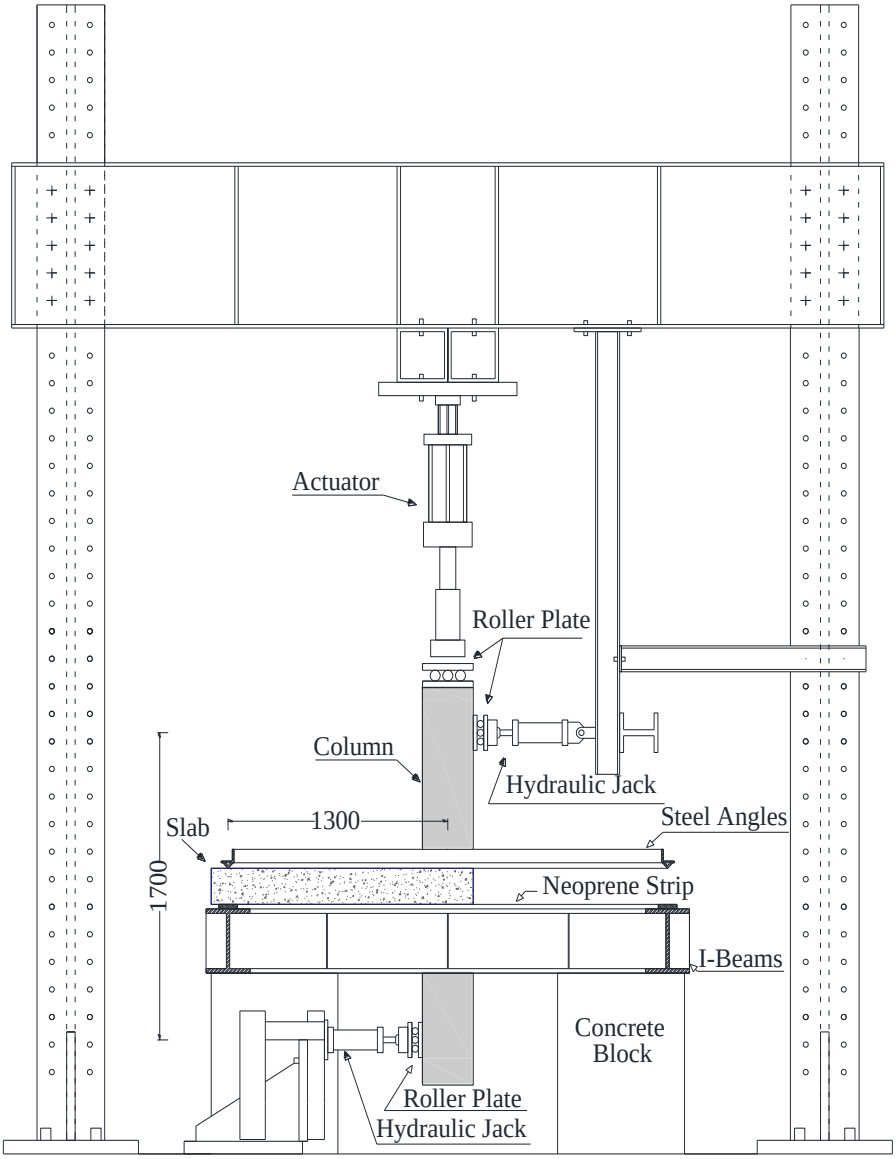

Figure 3.11: Schematic drawing for the test setup

Figure 3.12: Photo for the test setup

CHAPTER 4

EXPERIMENTAL RESULTS AND DISCUSSION

4.1. INTRODUCTION

In this chapter the experimental results of all test connections are presented. The behaviour of the connections was monitored throughout all the test where the deflection of the slabs and strains in both reinforcement and concrete at different locations were measured and recorded.

The analysis of each connection is presented in terms of the cracking pattern and mode of failure, deflection measurements, strain measurements and ultimate capacity. In addition, test results are compared to the predictions of the Canadian standard CSA/S806-12 (CSA 2012) and the American guideline ACI 440.1R-15 (ACI 2015). It is to be noted that, for all connections, the deflections at the column face are the deflection readings taken from the LVDT located 50 mm from the column face in the direction perpendicular to the free edge. Also, the reinforcement strain at the column face refers to the reinforcement strain readings taken from the strain gauge located 20 mm from the column face on one of the bars passing through the column perpendicular to the free edge. While the concrete strain at the column face are the concrete strain readings taken from the PI-gauge located at the same position on the compression face of the slab. Furthermore, all the flexural reinforcement strain profiles perpendicular and parallel to the free edge are established at increments of 20% of the failure load for one of the bars passing through the column in each direction.

4.2. SERIES I - EFFECT OF FLEXURAL REINFORCEMENT RATIO

Three connections with three different reinforcement ratios of 0.9, 1.35 and 1.8% were assigned to study the effect of GFRP flexural reinforcement ratio on the punching shear behaviour of HSC connections (H-0.9-XX, H-1.35-XX and H-1.8-XX). In addition, the results of the three HSC connections were compared, when applicable, to the results of three similar edge connections constructed with NSC reported by El-Gendy and El-Salakawy (2016b) to investigate the effect of concrete compressive strength. These three NSC will be designated as connections N-0.9-XX*, N-1.35-XX* and N-1.8-XX*.

4.2.1. Mode of Failure and Cracking Pattern

Regardless of the reinforcement ratio, all three connections failed in a brittle punching shear mode, characterized by a sudden drop in the load accompanied by the formation of a wide circumferential crack and column penetration through the slab.

All connections showed similar cracking behaviour, where flexural cracks were observed first at the inner corners of the column at a vertical load of 65, 60 and 63 for connections H-0.9-XX, H-1.35-XX and H-1.8-XX, respectively as listed in Table 4.1. These flexural cracks then propagated around the column periphery reaching the slab free edge. With increasing the load, radial cracks developed from the column faces towards the supports. Finally, circumferential cracks formed and connected the radial cracks together. This behaviour is similar to that reported by El-Gendy and El-Salakawy (2016b) for NSC connections. Also, increasing the reinforcement ratio decreased the average crack spacing as a result of the reduced bar spacing. The cracking pattern on the tension surface for the three connections is shown in Figure 4.1.

(a) Connection H-0.9-XX

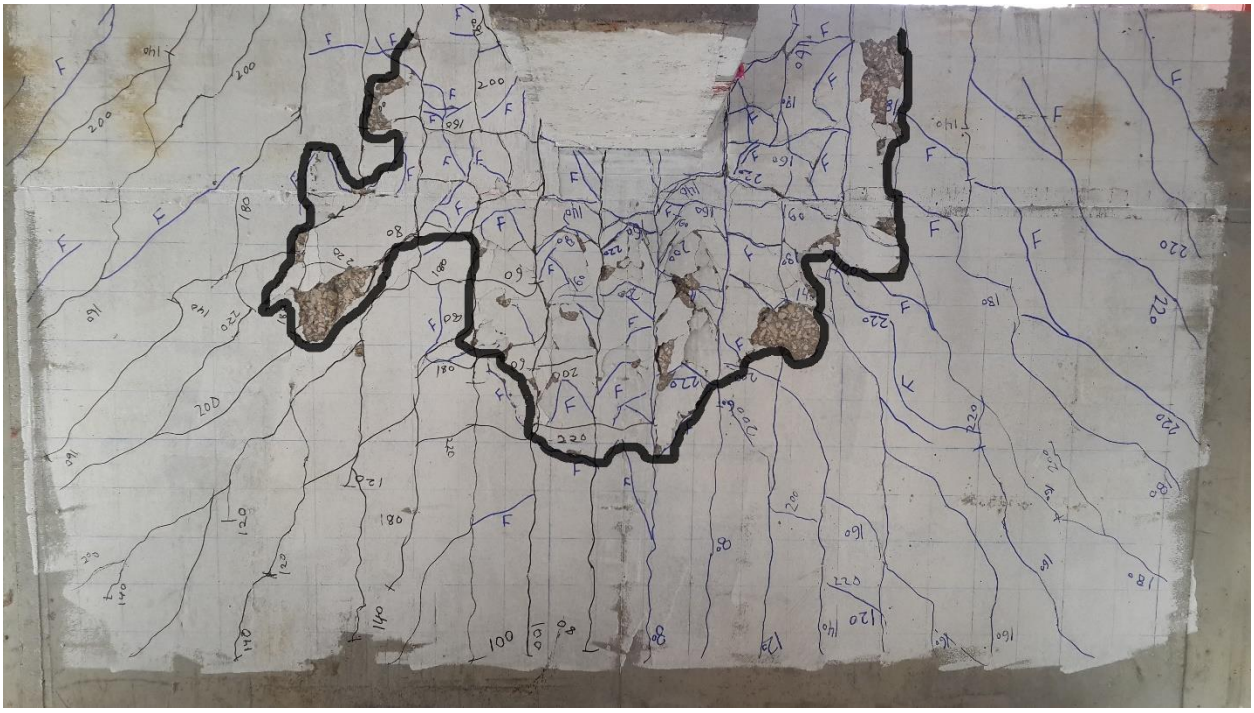

(b) Connection H-1.35-XX

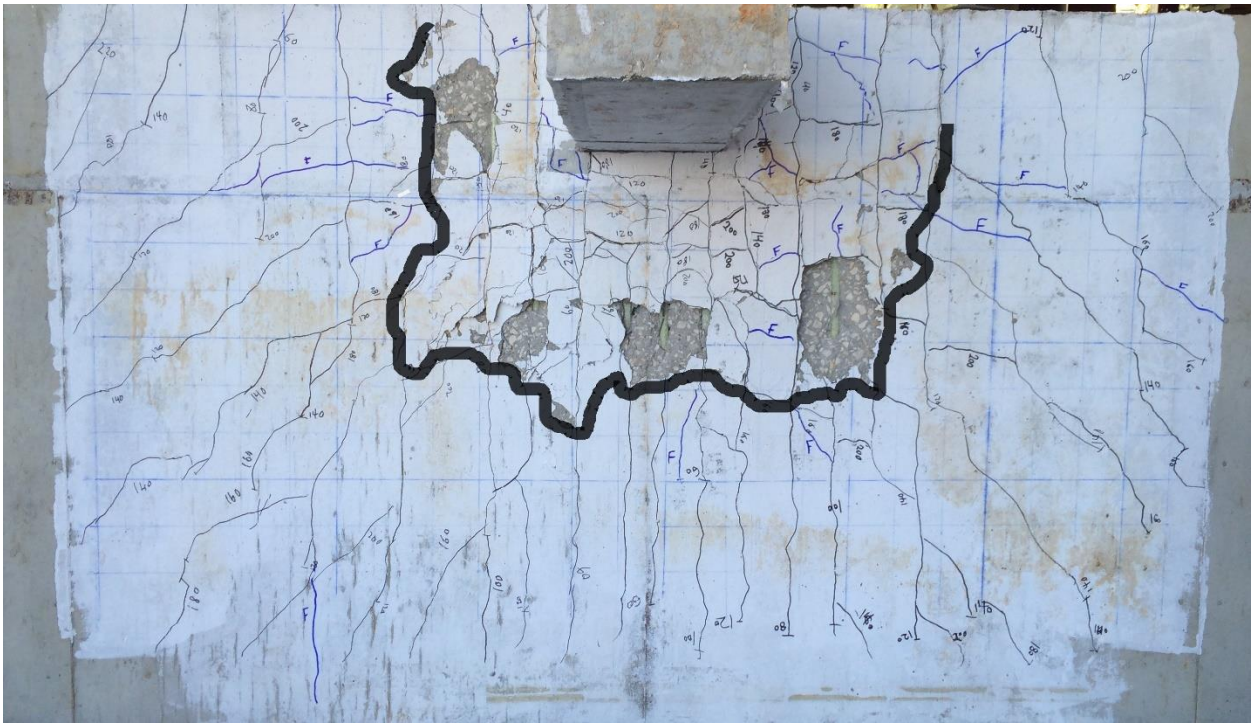

(c) Connection H-1.8-XX

Figure 4.1: Cracking pattern on the tension surface of the slab at failure

Also, the cracking pattern on the free edge of the three connections at failure is shown in Figure 4.2. For connection H-0.9-XX, the first crack formed at a distance of 130 mm from the corner of the bottom column and extended 100 mm in the transverse direction at a vertical load of 65 kN. With increasing the load this crack propagated with an average angle of 57^{o} with the horizontal reaching the top of the slab edge at a vertical load of 160 kN with the formation of other cracks at farther distances from the corner of the column. Finally, the punching failure occurred at this diagonal crack. Similarly, for connection H-1.35-XX, the first crack formed at a distance of 50 mm from the corner of the bottom column and extended 110 mm in the transverse direction at a vertical load of 60 kN. Other cracks then started to form at farther distances from the column corner at different loads. Eventually, the failure diagonal crack formed at the location of the first crack at a vertical load of 140 kN with an average angle of 60^{o} with the horizontal. For connection

H-1.8-XX, the first crack formed at a vertical load of 66 kN at a distance of 200 mm from the corner of the bottom column and extended 120 mm in the transverse direction. The failure diagonal crack formed at the corner of the bottom column at a vertical load of 160 kN with an average angle of 56^{o} with the horizontal.

(a) Connection H-0.9-XX

(b) Connection H-1.35-XX

(c) Connection H-1.8-XX

Figure 4.2: Cracking pattern on the free edge of the slab at failure

Moreover, the three connections were saw-cut in the direction perpendicular to the free edge after testing in order to investigate the internal cracking pattern inside the slabs as shown in Figure 4.3. In each connection, the diagonal shear crack propagated from the compression surface of the slab at the face of the column reaching the tension surface of the slab with different inclination angles. Increasing the reinforcement ratio increased the angle of inclination of the diagonal crack with the horizontal which pushed the failure crack on the tension surface of the slab towards the column.

The diagonal crack formed an angle of 22^{o}, 28^{o} and 30^{o} with the horizontal for connection H-0.9-XX, H-1.35-XX and H-1.8-XX, respectively.

(a) Connection H-0.9-XX

(b) Connection H-1.35-XX

(c) Connection H-1.8-XX

Figure 4.3: Internal cracking pattern in the direction perpendicular to the free edge at failure

Table 4.1: Test results

Connection	Cracking load (kN)	Concrete strain at failure (kN)	Deflection (mm)		Reinforcement strain (με)		Stiffness factor (kN/mm)	
			Service	Failure	Service	Failure	K_i	K_p
H-0.9-XX	65	-740	21.2	41.6	5,690	10,200	93.7	3.8
H-1.35-XX	60	-680	11.5	31.1	3,880	6,990	87.3	6.2
H-1.8-XX	63	-740	7.0	18.9	2,030	4,485	74.8	8.7

4.2.2. Deflections

Generally, the load-deflection curve of FRP-RC slab-column connections can be divided into two stages. The first stage represents the un-cracked behaviour, which depends mainly on the mechanical properties of concrete, consequently, the three connections showed comparable behaviour up to cracking. The second stage represents the cracked behaviour, which is mainly dependent on the axial rigidity of the reinforcing bars ($\rho_f E_f$). As a result, the three connections exhibited different post-cracking behaviour due to the different reinforcement ratios.

The relationship between the vertical load and the deflection measured at 50 mm from the face of the column in the direction perpendicular to the free edge for all connections is shown in Fig. 4.4. Increasing the reinforcement ratio increased the post-cracking stiffness of the connections, K_p, (the slope of the load-deflection curve after cracking) which in turn decreased the deflection at the same load level. Figure 4.5 shows an approximately linear increase in the post cracking stiffness with increasing the flexural reinforcement ratio. Connections H-1.8-XX and H-1.35-XX had 129 and 65% higher post-cracking stiffness, and 67 and 35% less deflection at service, respectively, than connection H-0.9-XX. At failure, these percentages were decreased to 55 and 25% less deflection, respectively, duo to the higher failure load of connections H-1.8-XX and H-1.35-XX than connection H-0.9-XX.

The use of HSC enhanced the un-cracked stiffness of the connections, K_i (the slope of the load-deflection curve before cracking) and the deformation behaviour of the connections. Connections H-0.9-XX, H-1.35-XX and H-1.8-XX had higher un-cracked stiffness than their counterpart NSC connections (N-0.9-XX*, N-1.35-XX* and N-1.8-XX*) by 83, 44 and 59% and, consequently, less deflection at service by 15, 10 and 34%, respectively.

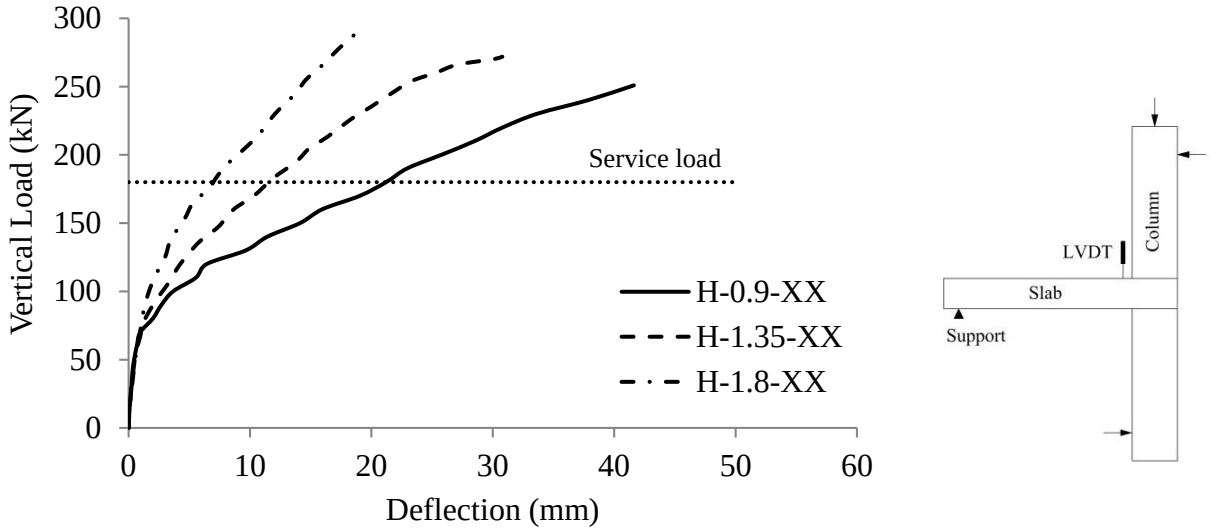

Figure 4.4: Vertical load-deflection relationship

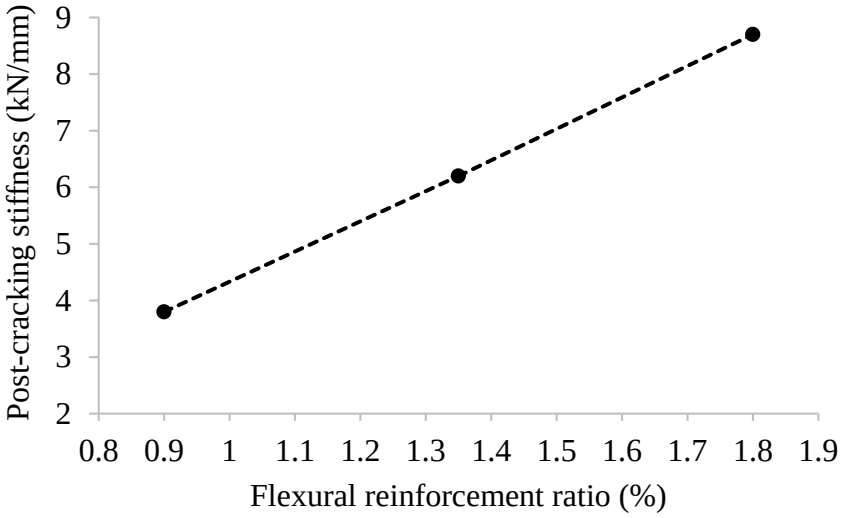

Figure 4.5: Reinforcement ratio vs. post cracking stiffness relationship

4.2.3. Flexural Reinforcement and Concrete Strains

The relationship between the vertical load and the flexural reinforcement and concrete strains measured at the column face in the direction perpendicular to the free edge is shown in Fig 4.6. Generally, at the un-cracked stage, the reinforcement strain readings were insignificant. After cracking, strains increased rapidly with increasing the load. A maximum reinforcement strain of 10,200 με, which represents 44% of the ultimate tensile strain of the GFRP bars, was measured in the connection with the lowest reinforcement ratio (H-0.9-XX). As expected, increasing the flexural reinforcement ratio decreased the reinforcement strains at the same load level as a direct result of providing additional reinforcement to carry the same load. Increasing the reinforcement ratio by 50 and 100% decreased the reinforcement strain at service in connections H-1.35-XX and H-1.8-XX by 32 and 64%, respectively. In addition, increasing the reinforcement ratio by 50 and 100% decreased the maximum reinforcement strain at failure by 31 and 56%, respectively. The maximum measured concrete strain was 740 με, which is considerably less than the theoretical concrete crushing strain defined by the CSA/S806-12 (CSA 2012) standard (3,500 με). This indicates that these connections exhibited a punching shear failure rather than a flexural failure.

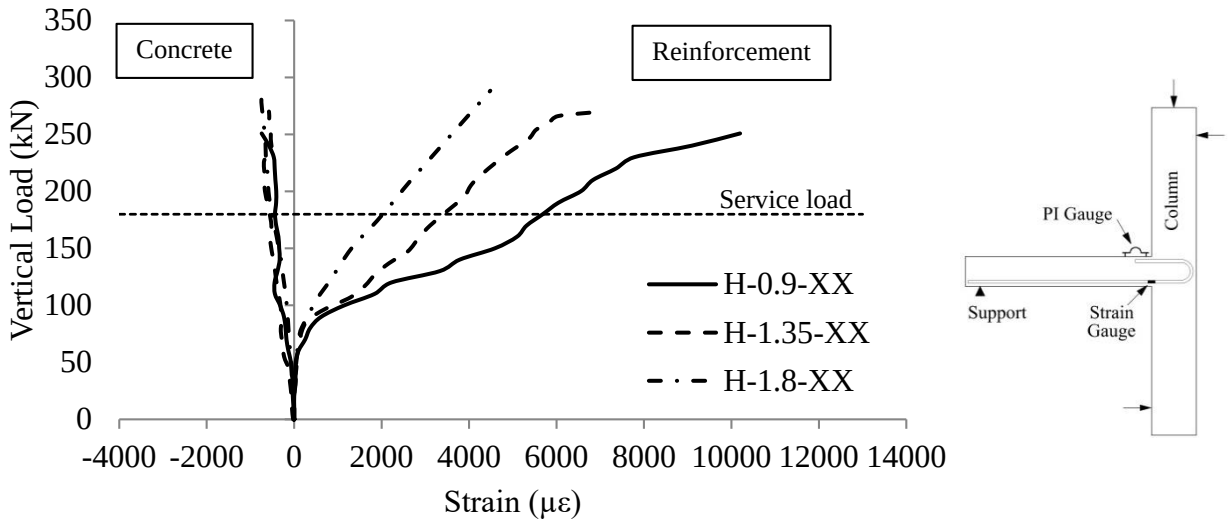

Figure 4.6: Vertical load-strain relationship

Moreover, the use of HSC reduced the reinforcement strains at the same load level. Connections H-0.9-XX, H-1.35-XX and H-1.8-XX had less reinforcement strains at service than their NSC counterparts by 18, 24 and 30%, respectively, because of their higher tensile strength, which delayed the formation of cracks. Also, the HSC connections had less concrete strains at failure than their NSC counterparts by 55, 28 and 8%, respectively.

The flexural reinforcement strain profiles for test connections in the direction perpendicular and parallel to the slab free edge at different loading levels (25, 50, 75, 100% of the failure load), are shown in Figures 4.7 and 4.8, respectively. For the three connections, the measured strains in both directions were inversely proportional to the distance from the column face, which implies that no bond slippage occurred. This result indicates the ability of SC-GFRP bars to develop strong bond with the concrete. This behaviour agrees with the findings of recent studies for both edge and interior connections (El-Gendy and El-Salakawy 2016b; Gouda and El-Salakawy 2016), and also with the findings of Hussein et al. (2004) and Dulude et al. (2013) for interior connections subjected to concentric loading.

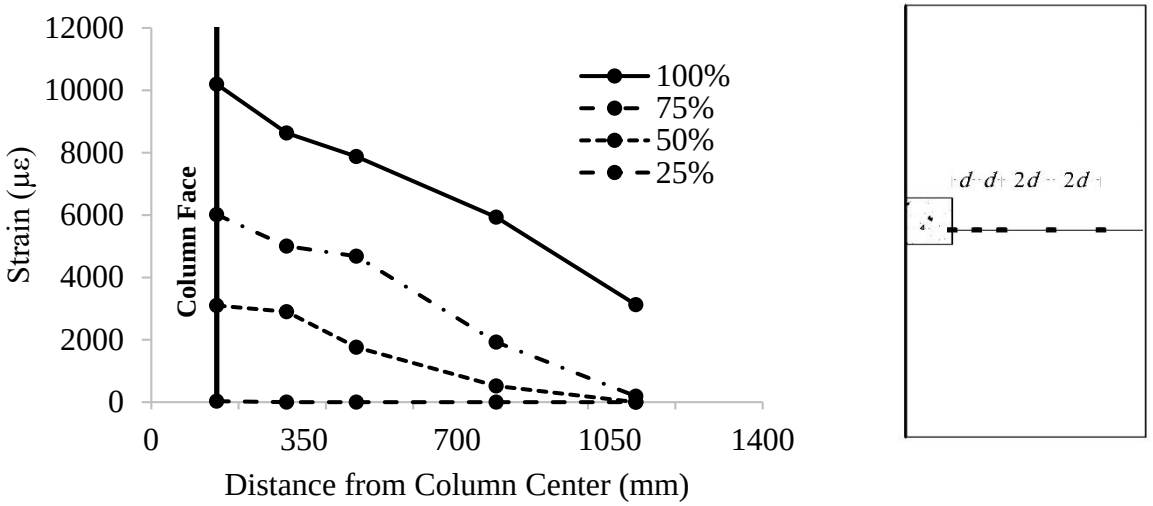

(a) Connection H-0.9-XX

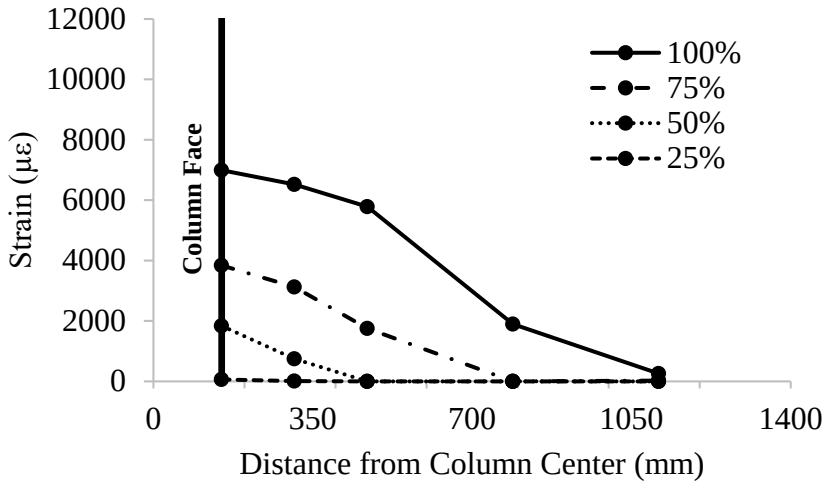

(b) Connection H-1.35-XX

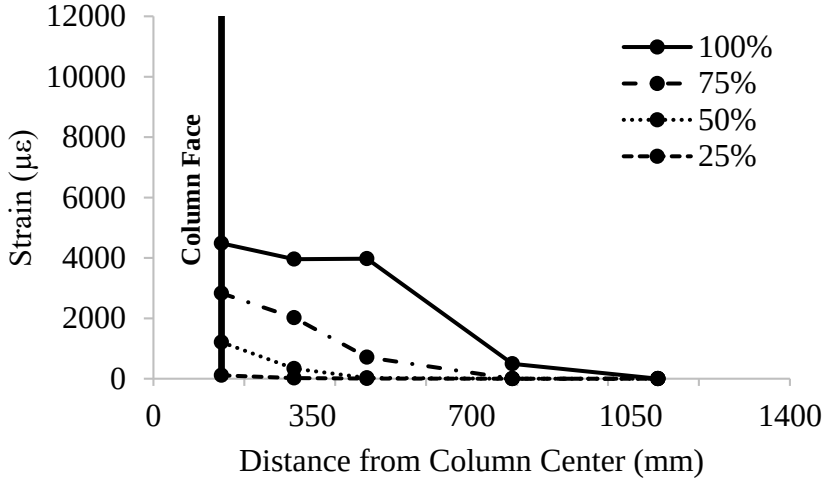

(c) Connection H-1.8-XX

Figure 4.7: Flexural reinforcement strain profile perpendicular to free edge

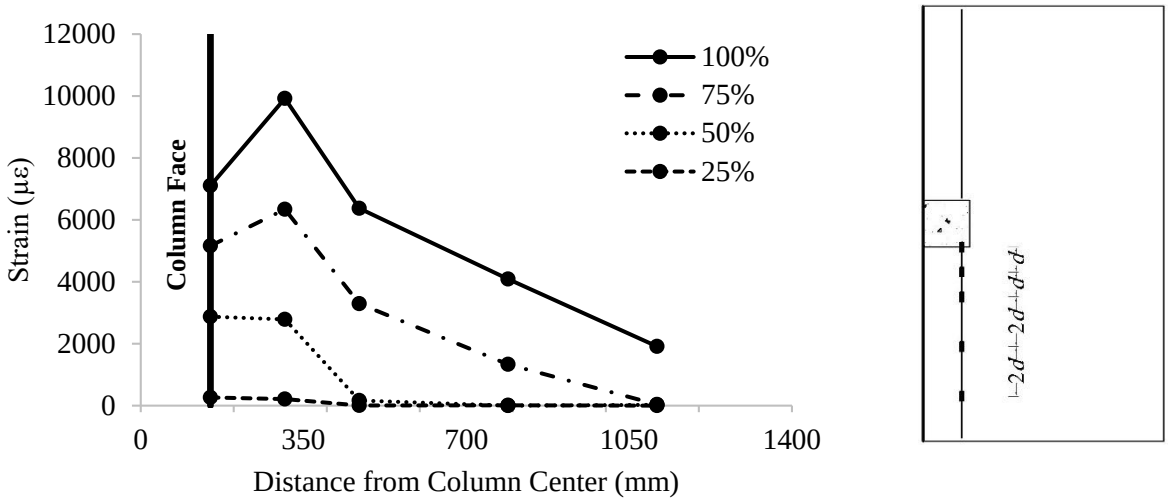

(a) Connection H-0.9-XX

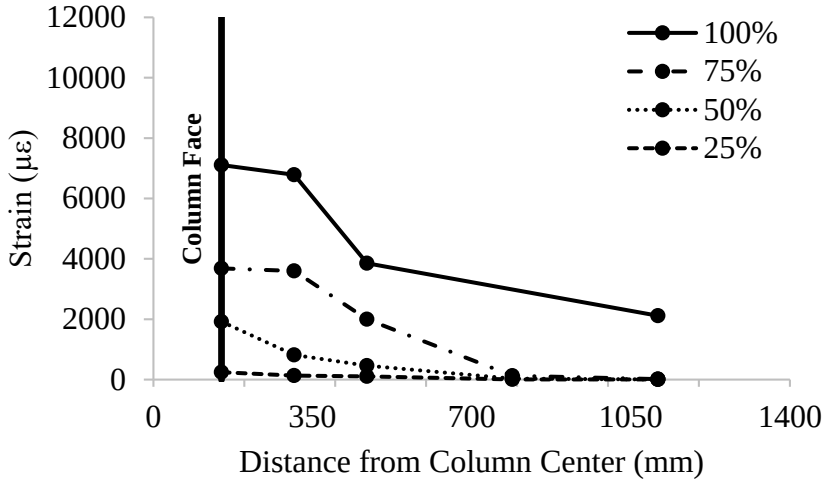

(b) Connection H-1.35-XX

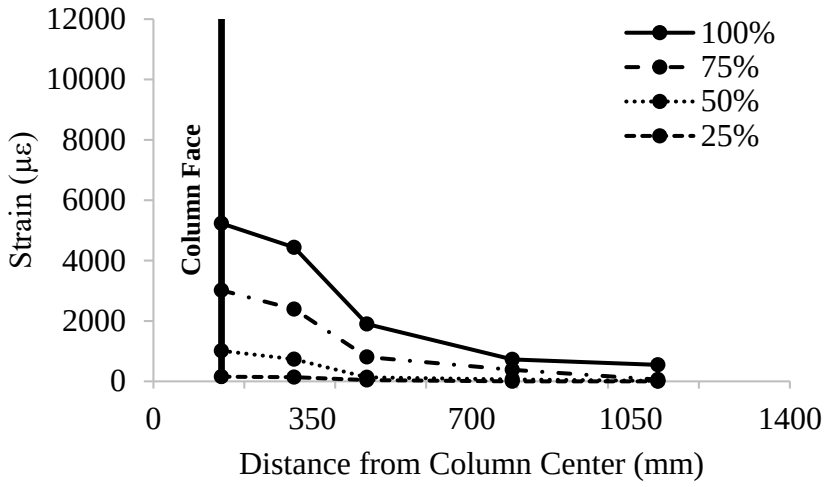

(c) Connection H-1.8-XX

Figure 4.8: Flexural reinforcement strain profile parallel to free edge

4.2.4. Ultimate Strength

The failure loads of connections were multiplied by $\sqrt[3]{80/f_c'}$ to eliminate the effect of concrete strength variation, where f_c' is the concrete compressive strength of each connection on the day of testing. To follow the CSA/S806-12 (CSA 2012) punching provisions, the cubic root was used instead of the common square root. Figure 4.9 shows the relationship between the flexural reinforcement ratio and the normalized capacity of the connections. Increasing the flexural reinforcement ratio by 50 and 100% in connections H-1.35-XX and H-1.8-XX increased the normalized capacity by 7 and 15%, respectively. This increase in punching capacity is due to the increased contribution of the dowel action to the shear strength of the connection and the increase in reinforcement axial rigidity, which contributed in delaying the propagation and opening of cracks, which increased the aggregate interlock contribution and the depth of un-cracked concrete. This increase in punching capacity was less than the increase found by El-Gendy and El-Salakawy (2016b) for the counterpart NSC connections at which the increase was 14 and 21% when increasing the flexural reinforcement ratio by 50 and 100%, respectively. This less increase in the

HSC connections can be attributed to the smoother crack surfaces of HSC as cracks tend to pass through the aggregate particles instead of going around it, which reduced the contribution of aggregate interlock component to the shear strength. However, the use of HSC slightly enhanced the punching shear capacity of the connections. Doubling the concrete compressive strength from 40 to 80 MPa resulted in 10, 3 and 5% increase in the punching capacity of connection H-0.9-XX, H-1.35-XX and H-1.8-XX, respectively, compared to their NSC counterparts.

Moreover, the flexural capacities of the connections, V_{flex}, were calculated using the yield line theory (Gar et al. 2014; El-Gendy and El-Salakawy 2016a) as listed in Table 4.2. Comparing the failure loads of the connections, V_{Test}, to the calculated flexural capacities, V_{flex}, showed low ratios which supports the punching shear failure mode of the connections.

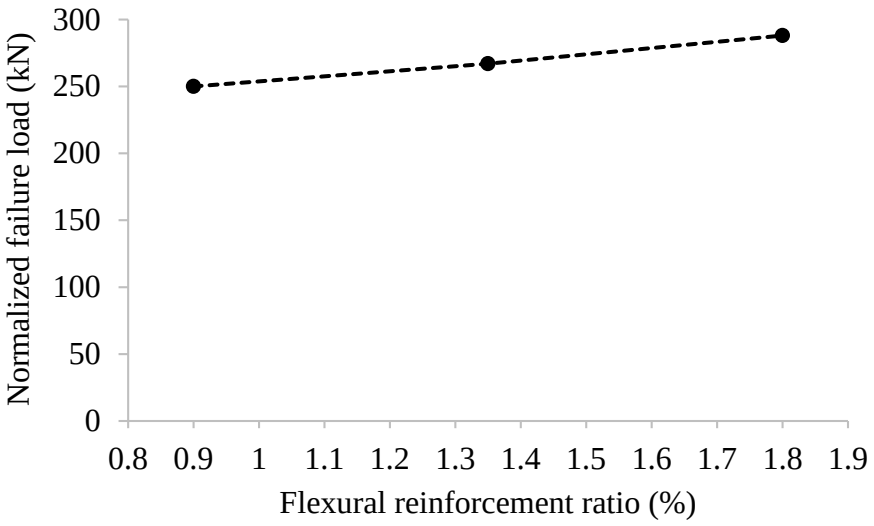

Figure 4.9: Reinforcement ratio vs. normalized capacity relationship

Table 4.2: Failure loads, normalized loads, and flexural capacities

Connection	Concrete strength, f_c' (MPa)	Failure load, V_{Test} (kN)	Normalized failure load (kN)	Flexural capacity		Failure mode
				V_{flex}[a] (kN)	V_{Test}/V_{flex}	
H-0.9-XX	81	251	250	391	0.64	Punching
H-1.35-XX	85	272	267	465	0.58	Punching
H-1.8-XX	80	288	288	507	0.57	Punching

[a] Calculated using actual f_c'

4.2.5. Code Comparisons

The ultimate capacity predictions of the CSA/S806-12 (CSA 2012) and the ACI 440.1R-15 (ACI 2015) and their ratios to the test failure loads are given in Table 4.3, considering all material and strength factors equals to unity. The CSA/S806-12 (CSA 2012) provided reasonable predictions with an acceptable safety margin yielding an average V_{Test}/V_{Pred} of 1.21±0.05 (COV = 4.5%). On the other hand, the ACI 440.1R-15 guideline highly underestimated the capacities with an average V_{Test}/V_{Pred} of 1.96±0.18 (COV = 9.1%). The reason behind this underestimated predictions might be that ACI equation accounts for the effect of the reinforcement axial rigidity implicitly when calculating the depth to the neutral axis, where the direct account for the axial rigidity showed better predictions as in the case of the CSA/S806-12 (CSA 2012).

It is to be noted that the CSA 2012 limits the maximum concrete compressive strength to be used in the punching shear equations to 60 MPa, however using the actual concrete strength and ignoring the 60 MPa limit, yielded a better predictions with an average V_{Test}/V_{Pred} of 1.1±0.05. This results agrees with the findings of Hassan et al. (2013) and Gouda and El-Salakawy (2016) for GFRP-RC interior connections and Marzouk et al. (1998) for steel-RC interior connections subjected to eccentric loading. As a result, the CSA/S806-12 (CSA 2012) equation can be

applicable to concrete strengths more than 60 MPa, however the safety margin will be reduced. Further investigation is needed regarding this issue.

Table 4.3: Code predictions

		CSA/S806-12		ACI 440.1R-15	
Connection	Failure load, V_{Test}	V_{Pred}[a]	V_{Test}/V_{Pred}	V_{Pred}[b]	V_{Test}/V_{Pred}
H-0.9-XX	251	196	1.27	116	2.16
H-1.35-XX	272	224	1.21	142	1.92
H-1.8-XX	288	248	1.16	159	1.81
Mean			1.21		1.96
SD			0.05		0.18
COV (%)			4.5		9.1

[a] Calculated using Eq. (2.33)
[b] Calculated using Eq. (2.34)

4.3. SERIES II - EFFECT OF SHEAR REINFORCEMENT TYPE AND PATTERN

Four NSC connections were assigned to study the effect of GFRP shear reinforcement type and pattern. Two connections were reinforced with different ratios of GFRP headed studs (N-0.9-S8 and N-0.9-S6), while the other two were reinforced with different ratios of GFRP corrugated bars (N-0.9-C8 and N-0.9-C6). The four connections were reinforced with the same flexural reinforcement ratio of 0.90 % in the direction perpendicular to the slab free edge. The results of the four connections were compared to the results of similar edge connection without shear reinforcement reported by El-Gendy and El-Salakawy (2016a) and designated as connections N-0.9-XX*.

4.3.1. Mode of Failure and Cracking Pattern

In case of using eight lines of shear reinforcement, both types of shear reinforcement were able to control the widening of diagonal shear cracks and prevented the punching of the column. Therefore, connections N-0.9-S8 and N-0.9-C8 failed in a pure flexural mode characterized by substantial deflections before crushing of concrete on the compression surface of the slab. However, when six lines of shear reinforcement were used, only the headed studs in connection N-0.9-S6 were able to fully control the shear cracks resulting in a deformable flexural failure. On the other hand, the relatively low reinforcement ratio of corrugated bars in connection N-0.9-C6, although managed to increase the punching capacity, did not enable the connection to reach its flexural capacity. Thus, connection N-0.9-C6 failed in punching shear inside the shear-reinforced zone. All four connections showed similar cracking behaviour to that of Series I connections except for lower cracking loads (Table 4.4) due to lower concrete strength. Also, only connection N-0.9-C6 showed a punching cone at failure as shown in Figure 4.10.

(a) Connection N-0.9-S8

(b) Connection N-0.9-C8

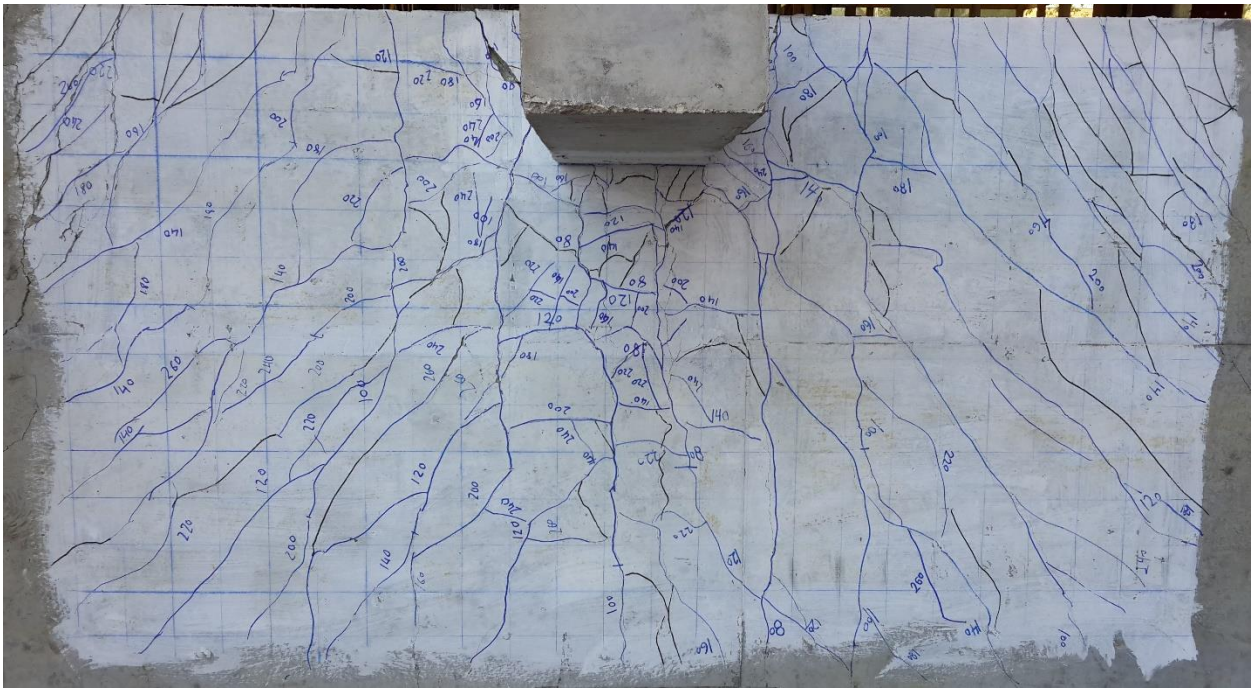

(c) Connection N-0.9-S6

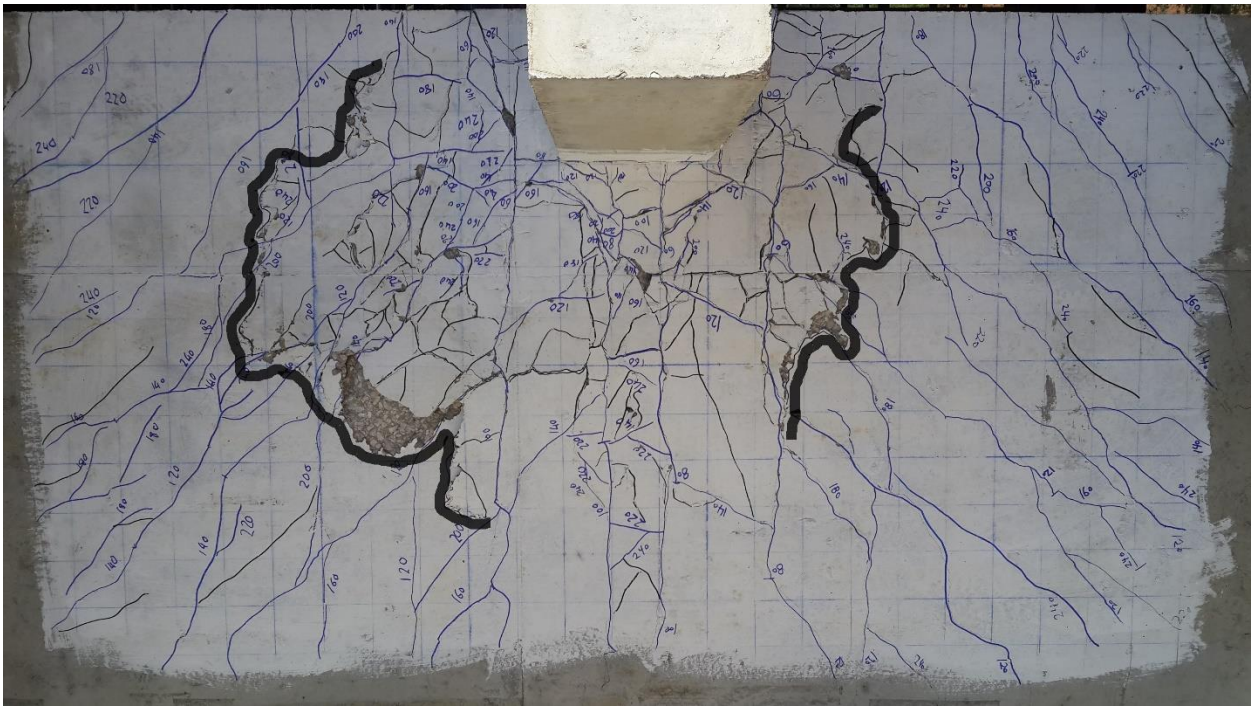

(d) Connection N-0.9-C6

Figure 4.10: Cracking pattern on the tension surface of the slab at failure

The cracking pattern on the free edge of the four connections at failure is shown in Figure 4.11. For connection N-0.9-S8, the first crack formed at a vertical load of 38 kN at a distance of 40 mm from the bottom column corner and extended to a height of 50 mm in the transverse direction. As the load increase, other cracks started to form at farther distances from the corner of the column. The main diagonal crack formed at 130 mm away from the corner of the bottom column with an approximate angle of 41^{o} with the horizontal at a vertical load of 160 kN. The headed studs managed to control the widening of this crack and prevented the brittle punching shear failure. Connection N-0.9-C8 showed similar behaviour. The first crack was formed at a vertical load of 40 kN at a distance of 50 mm from the bottom column corner and extended to a height of 90 mm in the transverse direction. The failure diagonal crack formed at the location of the first crack at a vertical load of 140 kN with an average angle of 45^{o} with the horizontal. Similarly, the corrugated bars managed to control the widening of the diagonal crack and prevented the brittle punching shear failure. Also, connection N-0.9-S6 showed the same cracking behaviour with the headed studs controlling the widening of the diagonal crack formed at 180 mm from the corner of the bottom column with an angle of 48^{o} with the horizontal. For connection N-0.9-C6, the first crack formed at a vertical load of 40 kN at a distance of 150 mm from the bottom column corner and extended to a height of 60 mm in the transverse direction. The main diagonal crack formed at 20 mm away from the corner of the bottom column with a steeper angle of 59^{o} with the horizontal at a vertical load of 100 kN. The corrugated bars was not able to fully control the propagation of this diagonal crack.

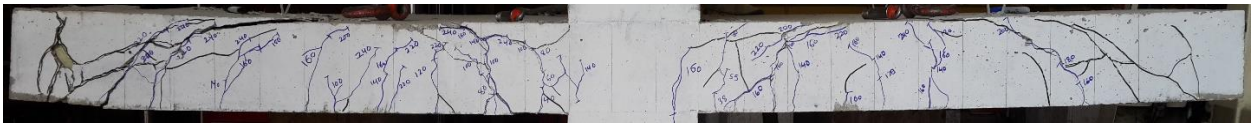

(a) Connection N-0.9-S8

(b) Connection N-0.9-C8

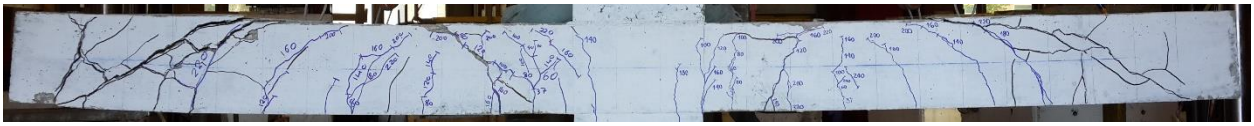

(c) Connection N-0.9-S6

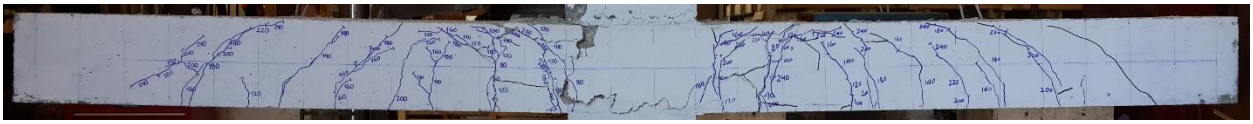

(d) Connection N-0.9-C6

Figure 4.11: Cracking pattern on the free edge of the slab at failure

In addition, connections N-0.9-S8 and N-0.9-C6 were saw-cut after testing in the direction perpendicular to the free edge to investigate the internal cracking pattern inside the slab as shown in Figures 4.12 and 4.13, respectively. For connection N-0.9-S8, it can be seen that the headed studs controlled the propagation of the diagonal shear crack preventing it from reaching the tension surface of the slab. The diagonal crack started from the column face at the compression surface of the slab and propagated above the upper heads of the first two studs in the parallel and diagonal directions located at 0.4*d* from the face of the column. The crack then propagated with a small angle of 29^{o} with the horizontal reaching the second stud in the perpendicular direction. Similar behaviour was reported by El-Gendy and El-Salakawy (2016a) and Lips et al. (2012) for FRP and steel-RC slab-column connections, respectively. In case of connection N-0.9-C6, it can be seen that the corrugated bars were not able to fully control the propagation of the diagonal shear crack

which caused the connection to fail in punching. The diagonal crack started from the column face at the compression surface of the slab and propagated to the tensile surface of the slab with an angle of 29^{o} with the horizontal passing through the first three vertical stems of the corrugated bar in the direction perpendicular to the free edge.

(a) Internal cracks for connection N-0.9-S8

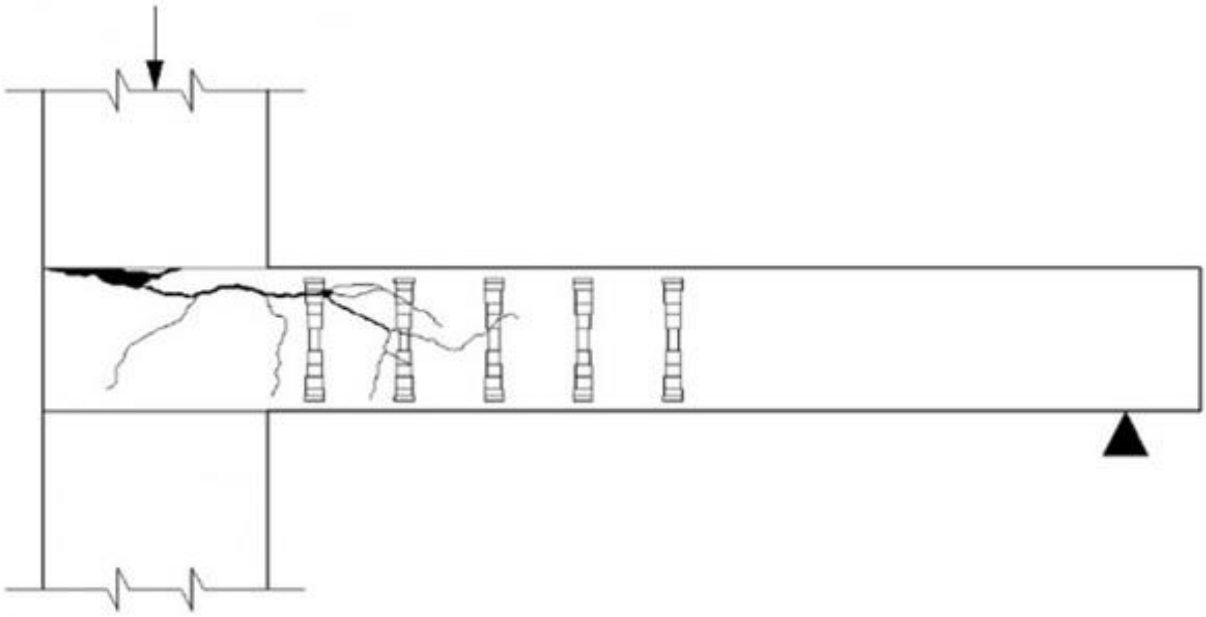

(b) Schematic drawing of internal cracks for connection N-0.9-S8

Figure 4.12: Internal cracking pattern in the direction perpendicular to the free edge at failure for connection N-0.9-S8

(a) Internal cracks for connection N-0.9-C6

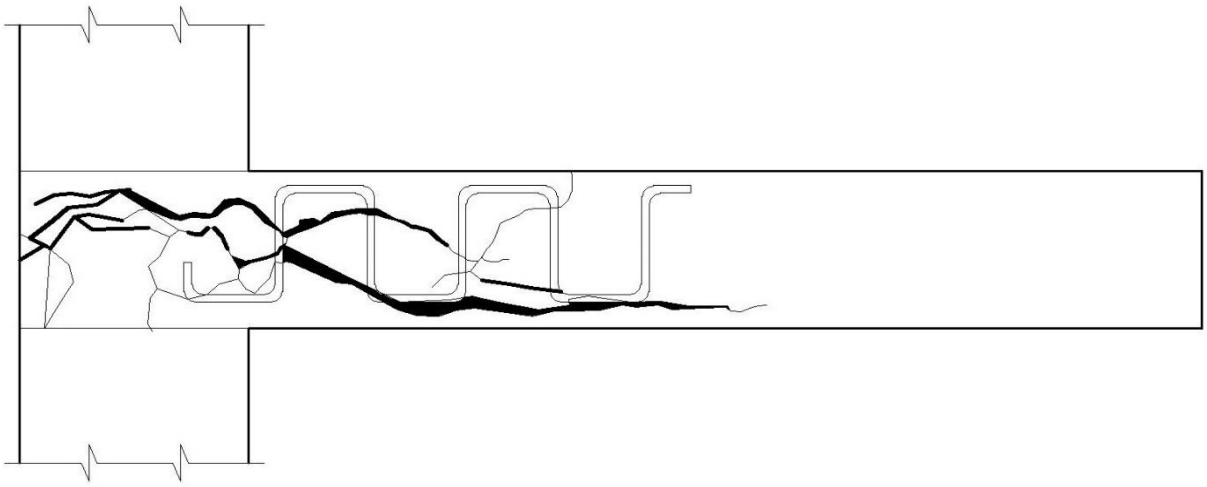

(b) Schematic drawing of internal cracks for connection N-0.9-C6

Figure 4.13: Internal cracking pattern in the direction perpendicular to the free edge at failure for connection N-0.9-C6

Table 4.4: Test results

Connection	Cracking load (kN)	Maximum deflection at failure (mm)	Maximum strain at failure (με)				Post-cracking stiffness, K_p (kN/mm)	Deformability factor, *J*
			Flexural reinforcement at column face					
			Perpendicular[a]	Parallel[a]	Concrete	Shear reinforcement		
N-0.9-S8	38	65.4	13,210[b]	12,530	-6,870	2,860	3.9	21.6
N-0.9-C8	40	68.6	10,910	12,760	-5,110	3,280	3.8	19.1
N-0.9-S6	37	63.7	12,500	10,570	-5,440	3,870	4.0	22.7
N-0.9-C6	40	46.1	8,660	9,150	-1,840	7,760	3.8	15.5

[a] Relative to slab free edge
[b] Malfunctioned at 85% of the failure load

4.3.2. Deflections

Although GFRP reinforcement does not yield, GFRP-RC connections can undergo substantial deflections before failure, especially when brittle punching failure is prevented, due to the relatively low modulus of elasticity of the GFRP reinforcement. The deformability factor, *J*, is used to assess this deformable behaviour and is calculated by Eq. (4.1), where *P* and Δ are the vertical load and displacement, respectively, and the subscripts *u* and *s* are the ultimate and service states, respectively. The Canadian standard CSA/S6-14 (CSA 2014) defines the service state as the state corresponding to a maximum compressive strain in concrete of 1,000 με.

$$J = \frac{P_u \Delta_u}{P_s \Delta_s} \tag{4.1}$$

The relationship between the vertical load and the deflection measured at 50 mm from the face of the column in the direction perpendicular to the free edge for all connections is shown in Fig. 4.14. Both types of shear reinforcement had an insignificant effect on the post-cracking stiffness of the connections. However, the presence of shear reinforcement substantially increased the deformability and the deflection at failure. Connections N-0.9-S8, N-0.9-C8 and N-0.9-S6 had 60, 41 and 68 % higher deformability and 66, 75 and 62 % higher deflection at failure, respectively, compared to connection N-0.9-XX* (without shear reinforcement with J = 13.5). These results were only 15 and 17%, respectively, in the case of connection N-0.9-C6, which failed in punching before exhibiting significant deflections.

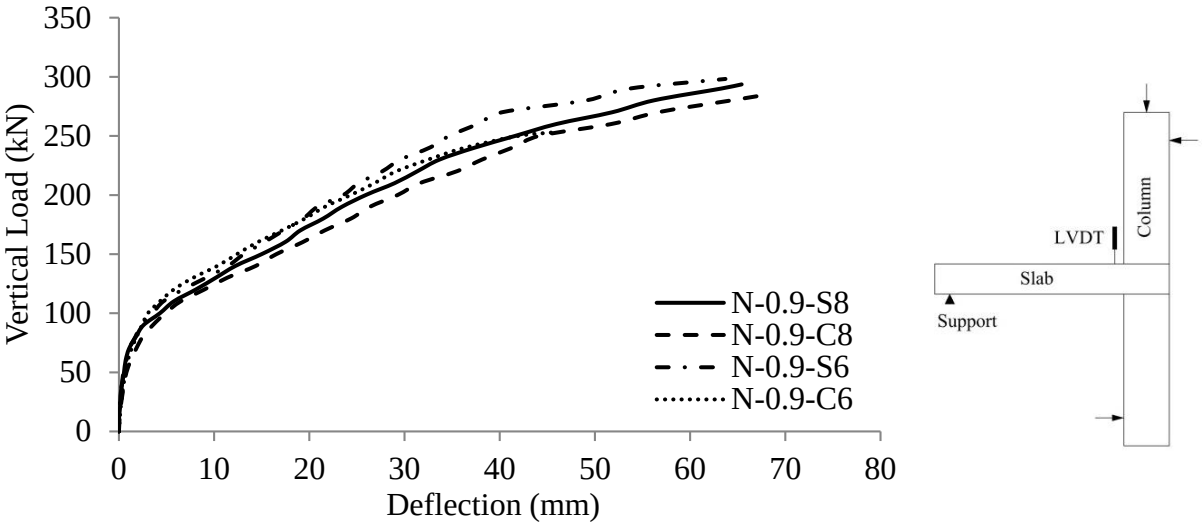

Figure 4.14: Vertical load-deflection relationship

4.3.3. Flexural Reinforcement and Concrete Strains

The relationship between vertical load and strains in flexural reinforcement and concrete measured at the column face in the direction perpendicular to the free edge is shown in Fig 4.15. The maximum recorded flexural strain was 13,210 με (55% of the ultimate strain of the GFRP bars) in connection N-0.9-S6 (with six lines of shear reinforcement). All connections had higher reinforcement strains at failure compared to connection N-0.9-XX* without shear reinforcement except connection N-0.9-C6, which experienced close strains. The maximum measured concrete strains for connections N-0.9-S8, N-0.9-C8 and N-0.9-S6 were 6,870, 5,110 and 5,440 με, respectively, which indicates the crushing of concrete that led to the pure flexural failure experienced by these connections. On the other hand, connection N-0.9-C6, which failed in punching before significant flexural stresses develop, experienced a considerably lower concrete strain of 1,840 με.

Figs. 4.16 and 4.17 show the flexural reinforcement strain profiles for the four connections in the direction perpendicular and parallel to the slab free edge, respectively, at different loading levels

(25, 50, 75, and 100% of the failure load). Similar to Series I connections, the measured strains in both directions were inversely proportional to the distance from the column face for the four connections, which indicates a good bond between the reinforcing bars and the surrounding concrete.

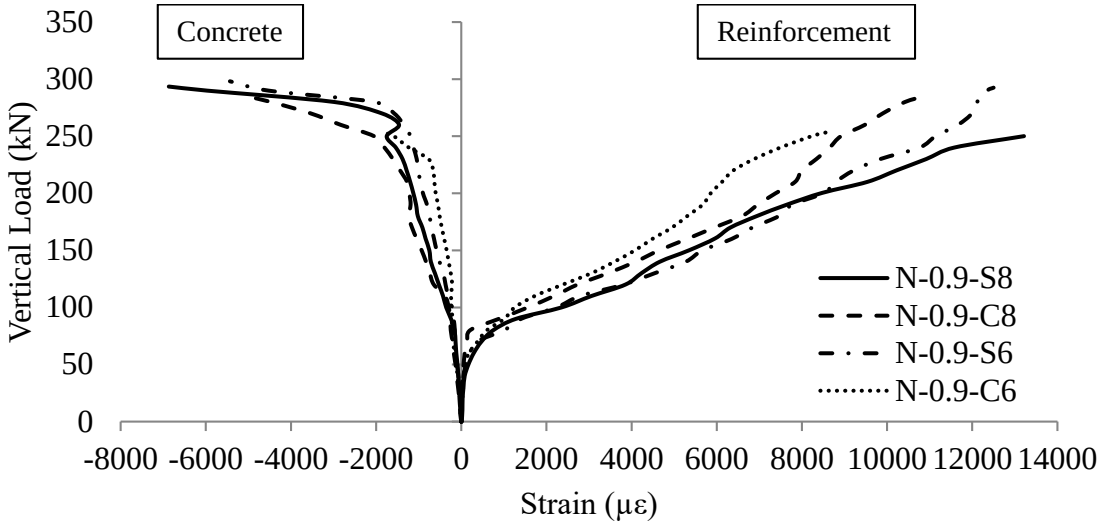

Figure 4.15: Vertical load-strain relationship

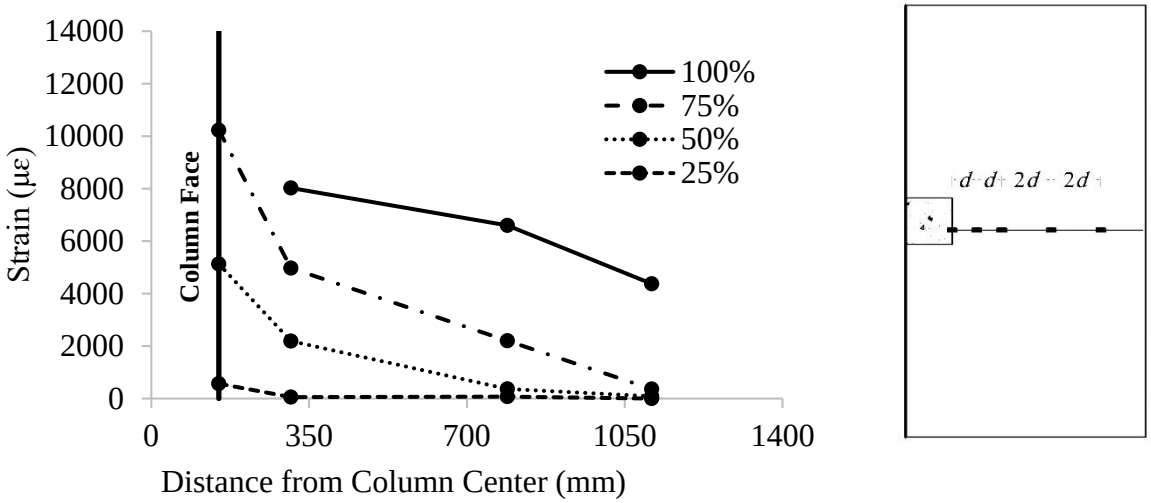

(a) Connection N-0.9-S8

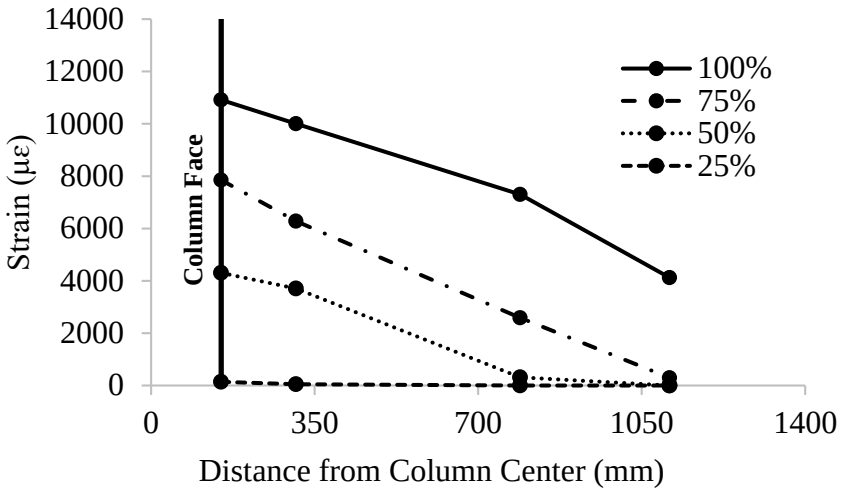

(b) Connection N-0.9-C8

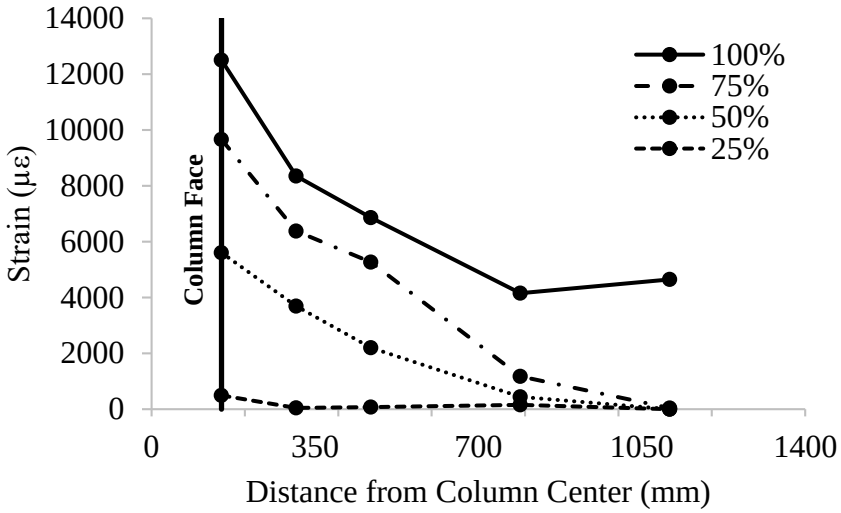

(c) Connection N-0.9-S6

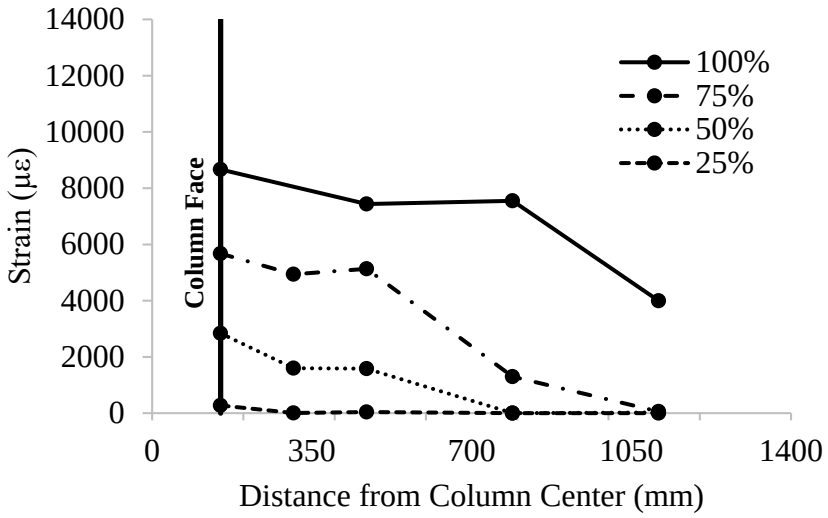

(d) Connection N-0.9-C6

Figure 4.16: Flexural reinforcement strain profile perpendicular to free edge

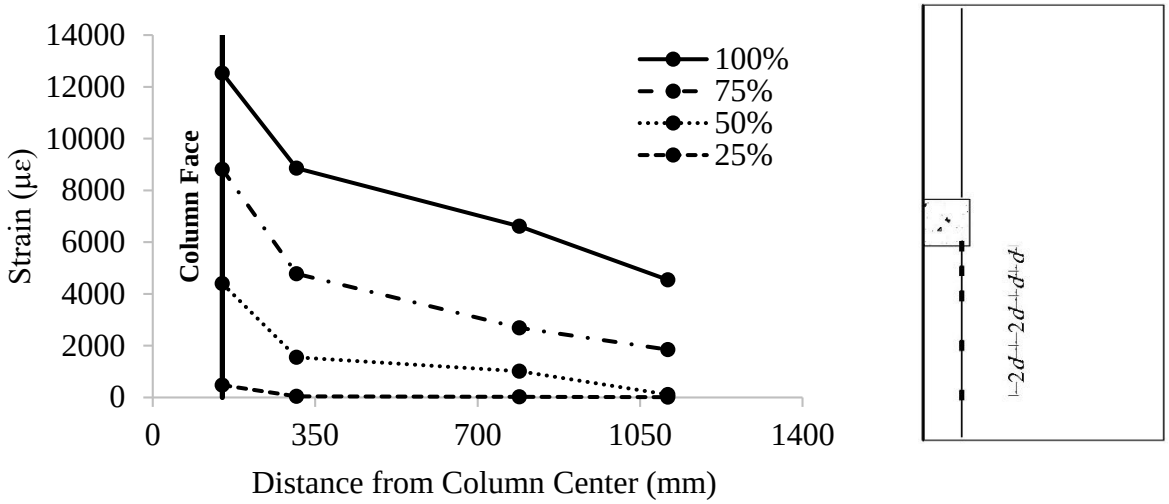

(a) Connection N-0.9-S8

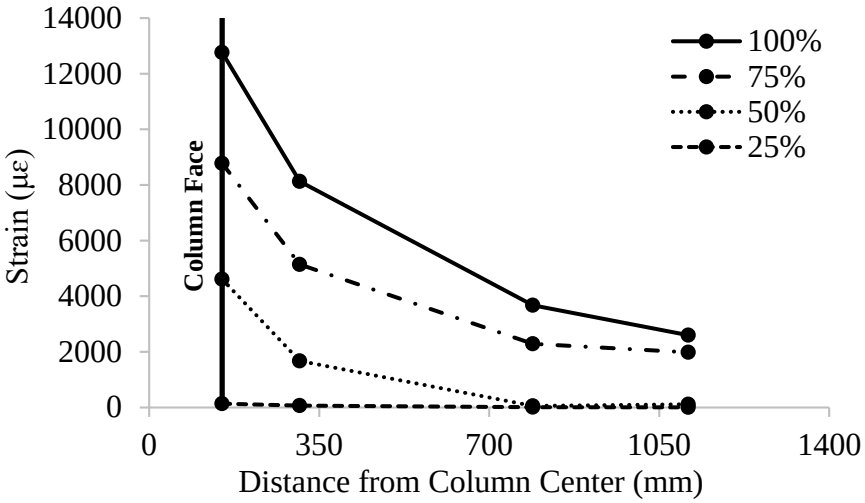

(b) Connection N-0.9-C8

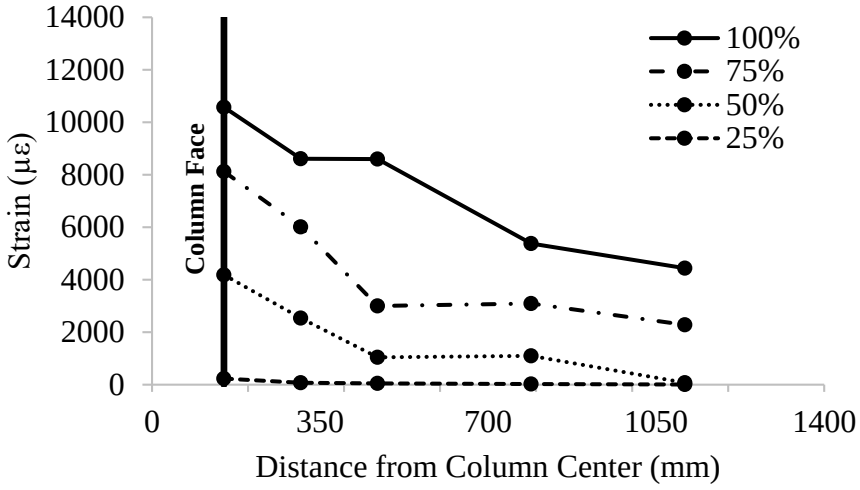

(c) Connection N-0.9-S6

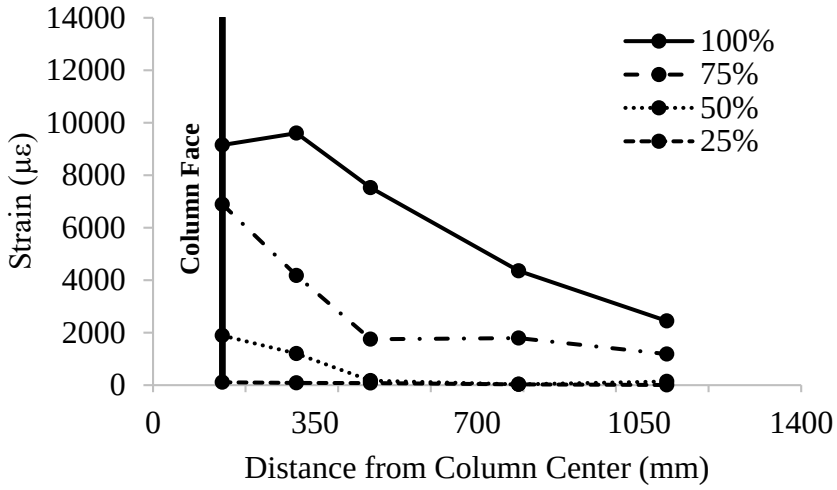

(d) Connection N-0.9-C6

Figure 4.17: Flexural reinforcement strain profile parallel to free edge

4.3.4. Shear Reinforcement Strains

Figures 4.18 and 4.19 show the strains in the vertical stems of the shear reinforcement in all directions at increments of 25% of the failure load versus the distance from the column face divided by the average effective slab depth, *d*, for connections with eight and six lines of shear reinforcement, respectively. The heads of the studs in connection N-0.9-S8 (with eight lines of shear reinforcement) provided adequate anchorage, which enabled most of the studs in the column vicinity to develop strains higher than 1,500 με before flexural failure. The highest strain reading of 2,860 με was measured in the first stud at a distance of 0.40 *d* from the column face in the direction parallel to the free edge. This value represents only 35% of the usable strain of the stud recommended by the manufacturer and 57 and 72% of the CSA/S806-12 (CSA 2012) and the ACI 440.1R-15 (ACI 2015) strain limits, respectively.

Similarly, the vertical stems of the corrugated bars were able to develop significant strains without apparent anchorage failure. Generally, as expected, the strains developed in the vertical stems of the corrugated bars in the counterpart connection N-0.9-C8 were higher than those in connection

N-0.9-S8 due to the smaller diameter (i.e. shear reinforcement ratio) and modulus of elasticity of the corrugated bars compared to the headed studs. The highest strain measured in the vertical stems of the corrugated bars in connection N-0.9-C8 was 3,280 με, which represents 66 and 82% of the CSA/S806-12 (CSA 2012) and ACI 440.1R-15 (ACI 2015) strain limits, respectively. The lower values of the strains recorded in the shear reinforcement in both connections with eight lines of shear reinforcement compared to the allowable limits in the North American standards suggests that the flexural capacities of the connections could still be reached with lower shear reinforcement ratios (less number of lines of shear reinforcement).

Reducing the number of lines of shear reinforcement to six resulted in higher strains in both headed studs and corrugated bars. For connection N-0.9-S6, however, the strains were still lower than the limits in the North American standards. The highest strain reading was 3,870 με, which represents 77 and 97% of the CSA/S806-12 (CSA 2012) and ACI 440.1R-15 (ACI 2015) strain limits. On the other hand, the vertical stems of the corrugated bars in connection N-0.9-C6 developed much higher strains due to their smaller diameter and modulus of elasticity. The highest strain reading was 7,760 με which highly exceeded the 5,000 and 4,000 με limits in the CSA/S806-12 (CSA 2012) and ACI 440.1R-15 (ACI 2015), respectively.

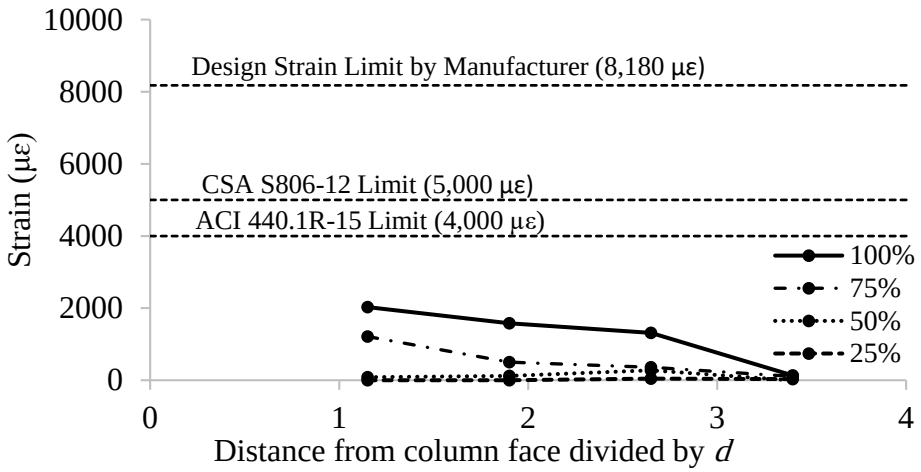

(a) Connection N-0.9-S8 (perpendicular)

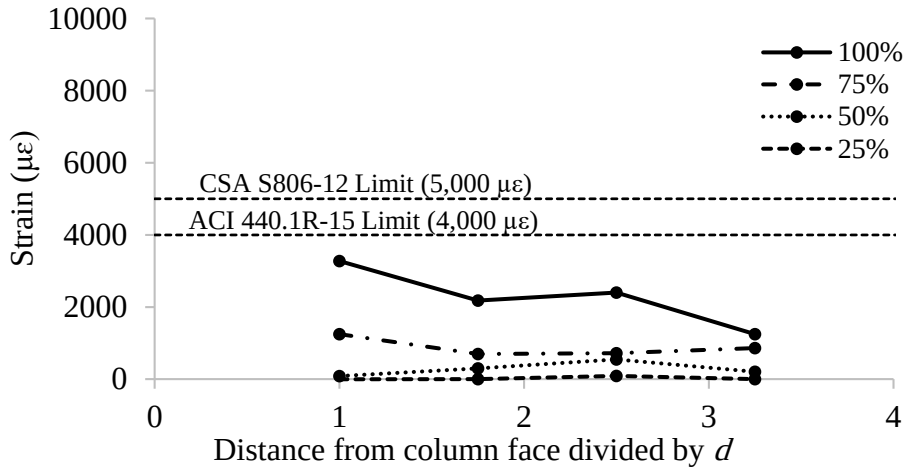

(b) Connection N-0.9-C8 (perpendicular)

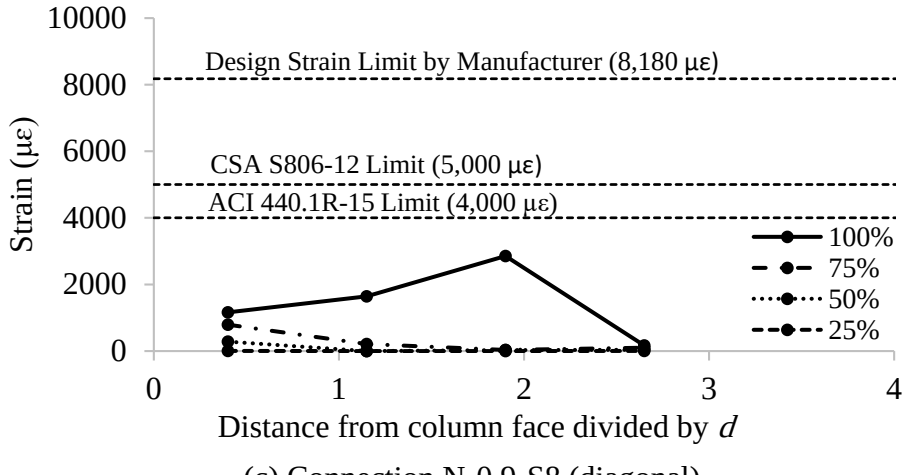

(c) Connection N-0.9-S8 (diagonal)

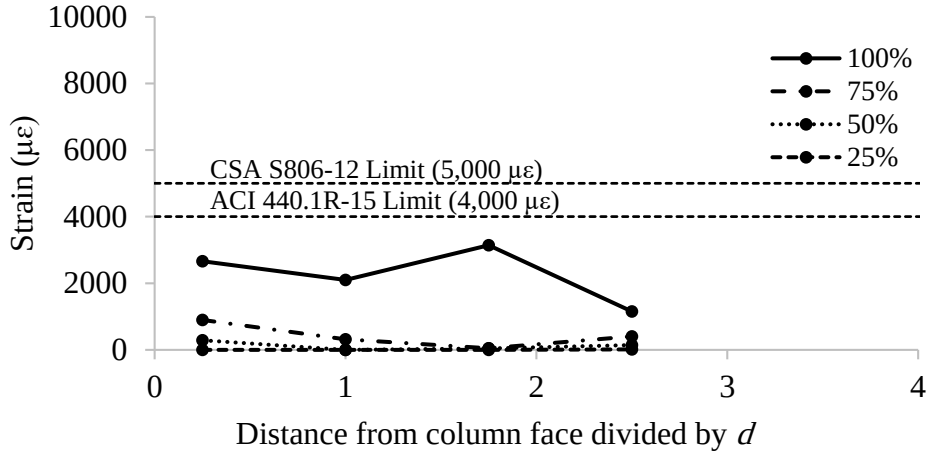

(d) Connection N-0.9-C8 (diagonal)

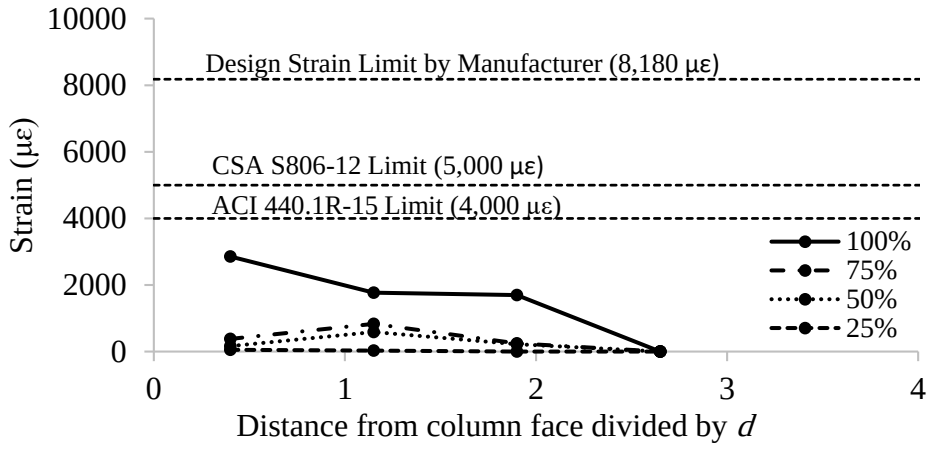

(e) Connection N-0.9-S8 (parallel)

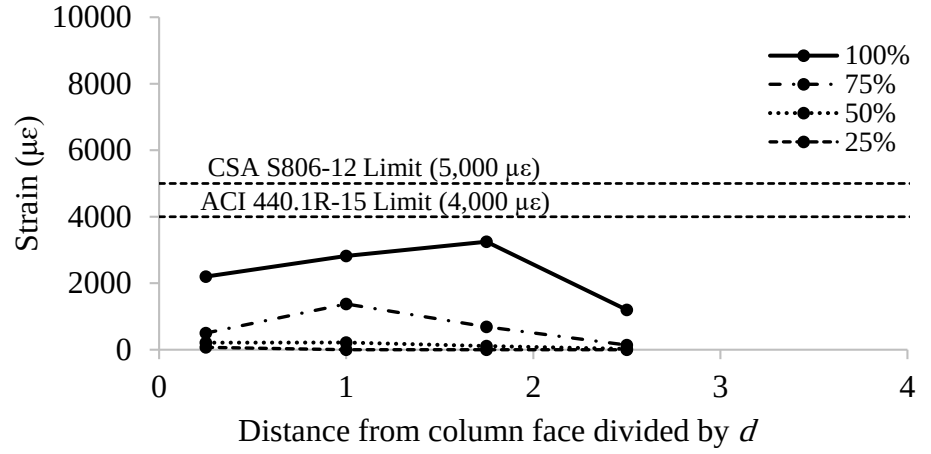

(f) Connection N-0.9-C8 (parallel)

Figure 4.18**:** Shear reinforcement strains vs. distance from column face for connections with eight lines of shear reinforcement

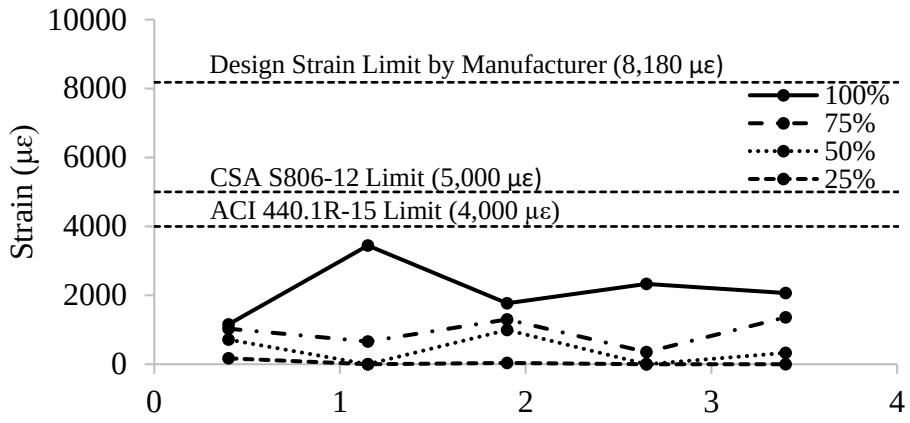

(a) Connection N-0.9-S6 (perpendicular)

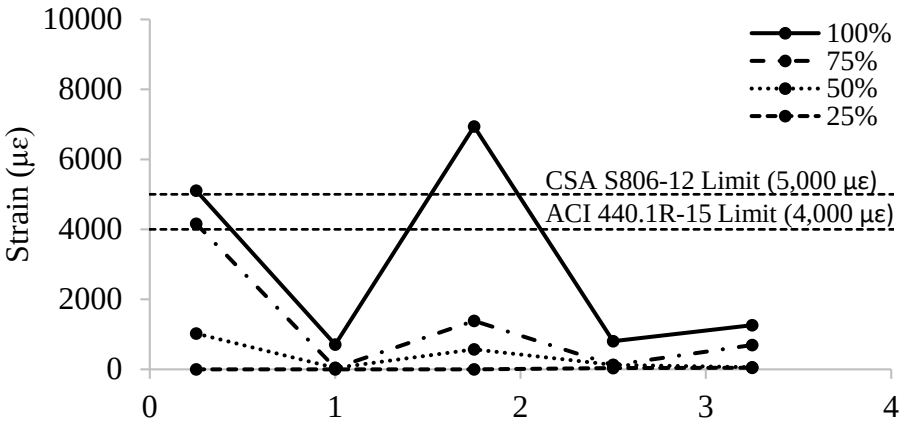

(b) Connection N-0.9-C6 (perpendicular)

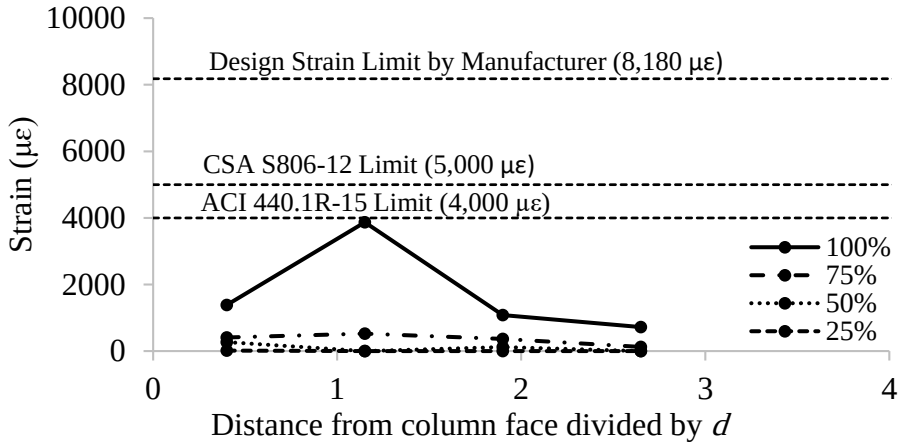

(c) Connection N-0.9-S6 (parallel)

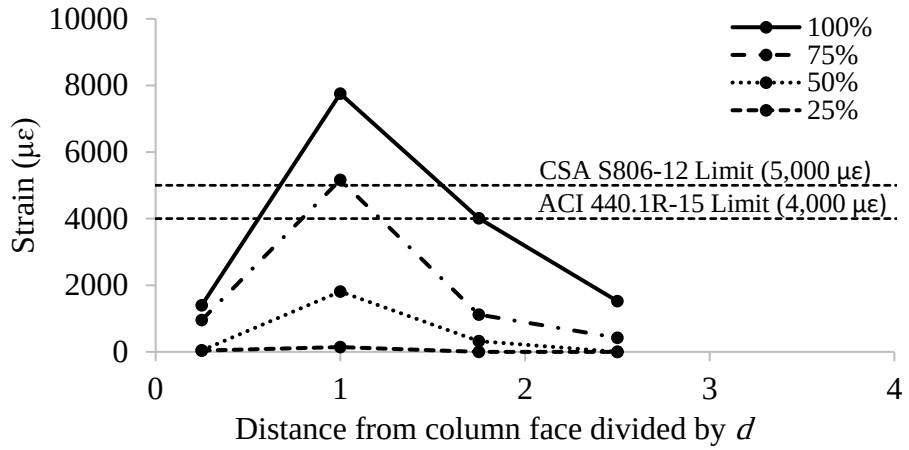

(d) Connection N-0.9-C6 (parallel)

Figure 4.19**:** Shear reinforcement strains vs. distance from column face for connections with six lines of shear reinforcement

4.3.5. Ultimate Strength

The failure loads of connections were multiplied by $\sqrt[3]{40/f_c'}$ to eliminate the effect of concrete strength variation, where f_c' is the concrete compressive strength of each connection on the day of testing. The use of eight lines of shear reinforcement significantly enhanced the ultimate capacity of the connections. Connections N-0.9-S8 and N-0.9-C8 had 26 and 23% higher capacity than connection N-0.9-XX*, respectively. This increase was 27 and 8% for connections N-0.9-S6 and N-0.9-C6, with six lines of shear reinforcement, respectively. The low increase in the capacity for connection N-0.9-C6 is attributed to the small reinforcement ratio (0.29%) and modulus of elasticity of the GFRP corrugated bars, which resulted in the rupture of the GFRP corrugated reinforcement before the connection reaches its flexural capacity. In addition, comparing the failure loads of the connections, V_{Test}, to the predicted flexural capacities calculated using the yield line theory (Table 4) supports the failure modes of the connections. All connections except connection N-0.9-C6 had high value of V_{Test}/V_{flex} (close to unity) which indicate flexural failure. Connection N-0.9-C6 had a border ratio of 0.82, which indicates the punching shear failure of the

connection with an increased capacity due to the presence of the low reinforcement ratio of GFRP corrugated bars.

Table 4.5: Failure loads, normalized loads, and flexural capacities

Connection	Concrete strength, f_c' (MPa)	Failure load, V_{Test} (kN)	Normalized failure load (kN)	Flexural capacity		Failure mode
				V_{flex}[a] (kN)	V_{Test}/V_{flex}	
N-0.9-S8	43	294	287	300	0.98	Flexural
N-0.9-C8	43	286	279	300	0.95	Flexural
N-0.9-S6	44	298	289	303	0.98	Flexural
N-0.9-C6	45	253	243	305	0.82	Punching (inside)

[a] Calculated using actual f_c'

4.3.6. Code Comparisons

The proposed equations by El-Gendy and El-Salakawy (2016a), discussed in Section 2.7.2 of this thesis, were used to predict the punching capacity of the four connections as listed in Table 4.6. The modified CSA/S806-12 (CSA 2012) equations yielded good predictions. For connections with shear studs, the predicted shear capacities were greater than the corresponding flexural capacities, which agree with test results. For connections with corrugated bars, the equations predicted shear failure for both connections with an average V_{Test}/V_{Pred} of 1.18. This does not agree with the test results of connection N-0.9-C8, which failed in flexure. On the contrary, the modified ACI 440.1R-15 (ACI 2015) equations highly underestimated the shear capacities with values less than the corresponding flexural capacities for all connections. For connection N-0.9-C6 with corrugated bars (failed in punching), the ratio of V_{Test}/V_{Pred} was 1.78.

Table 4.6: Code predictions

Connection	Failure load, V_{Test}	CSA/S806-12		ACI 440.1R-15	
		V_{Pred}[a]	V_{Test}/V_{Pred}	V_{Pred}[b]	V_{Test}/V_{Pred}
N-0.9-S8	294	389	0.76	282	1.04
N-0.9-C8	286	241	1.19	164	1.74
N-0.9-S6	298	325	0.92	230	1.30
N-0.9-C6	253	215	1.18	142	1.78

[a] Calculated using Eqs. (2.54) and (2.56)
[b] Calculated using Eqs. (2.57) and (2.59)

CHAPTER 5

CONCLUSIONS AND RECOMMENDATIONS

5.1. SUMMARY

This study investigated the punching shear behaviour of GFRP-RC slab-column edge connections. Seven full-scale slab-column edge connections were constructed and tested to failure under the combination of vertical shear force and unbalanced moment. Three connections were made of HSC while the other four were made of NSC. All connections were reinforced in flexure with sand-coated GFRP straight and bent bars. Newly developed GFRP shear reinforcement in the form of headed studs and bent bars were used as shear reinforcement in NSC connections. The parameters studied were flexural reinforcement ratio, shear reinforcement type and arrangement around the column (pattern).

5.2. CONCLUSIONS

Based on the presented experimental results and discussion, the following can be concluded:

Series I:

1. All tested connections failed in a brittle punching shear mode characterized by a sudden drop in the load accompanied by column penetration through the slab.

2. The sand-coated GFRP bars showed good bond with the surrounding concrete. In all connections, the flexural reinforcement strain profiles were inversely proportional to the distance from the column face, which implies that no bond slippage happened.

3. Increasing the flexural reinforcement ratio pushed the failure cone closer to the column due to the increased diagonal crack inclination angel with the horizontal (steeper). Increasing the flexural reinforcement ratio from 0.9% to 1.35 and 1.8% increased the inclination angle from 22^o to 28^o and 30^o, respectively.

4. The flexural reinforcement ratio had a considerable effect on the punching shear capacity, post-cracking stiffness and deflection of the HSC connections. Increasing the flexural reinforcement ratio by 50 and 100% increased the punching shear capacity by 7 and 15% and the post-cracking stiffness by 65 and 129%, respectively, and decreased the deflection at service by 35 and 67%, respectively.

5. The use of HSC enhanced the un-cracked stiffness which, in turn, decreased the deflection at service. Doubling the concrete compressive strength from 40 to 80 MPa resulted in 83, 44 and 59% increase in the un-cracked stiffness which resulted in 15, 10 and 34% less deflection at service for connections with reinforcement ratios of 0.9, 1.35 and 1.8%, respectively.

6. The use of HSC slightly enhanced the punching shear capacity of the connections. Doubling the concrete compressive strength from 40 to 80 MPa resulted in 10, 3 and 5% increase in the punching shear capacity for connections with reinforcement ratios of 0.9, 1.35 and 1.8%, respectively.

7. The CSA/S806-12 standard (CSA 2012) yielded reasonable predictions for the punching shear strength with an average V_{Test}/V_{Pred} of 1.21±0.05 (COV = 4.5%). However, the ACI 440.1R-15 guideline (ACI 2015) highly underestimated the capacities with an average V_{Test}/V_{Pred} of and 1.96±0.18 (COV = 9.1%).

8. For the CSA/S806-12 standard (CSA 2012), using the actual concrete strength over the 60 MPa limit yielded better predictions for HSC connections with an average V_{Test}/V_{Pred} of 1.1±0.05. However, Applying the 60 MPa limit will result in a higher margin of safety.

Series II:

1. Connections N-0.9-S8, N-0.9-C8 and N-0.9-S6 were able to reach their flexural capacities and failed in a pure flexural mode characterized by substantial deflections before crushing of concrete on the compression surface of the slab, while connection N-0.9-C6 failed in punching shear mode inside the shear-reinforced zone with a capacity less than its flexural capacity.

2. Similar to Series I, no bond slippage occurred between the sand-coated GFRP bars and the surrounding concrete as the flexural reinforcement strain profiles for all connections were inversely proportional to the distance from the column face.

3. Both the GFRP headed studs and corrugated bars managed to control the propagation of shear cracks and prevented the brittle punching shear failure in the column vicinity in case of using eight lines of shear reinforcement. However, when reducing the shear reinforcement ratio by using only six lines of shear reinforcement, only the headed studs were able to fully control the shear cracks and prevent the brittle punching shear failure.

4. The use of shear reinforcement enhanced the deformable behaviour and the capacity of the connections. Connections N-0.9-S8, N-0.9-C8, N-0.9-S6 and N-0.9-C6 had 60, 41, 68 and 15% higher deformability and 66, 75, 62 and 17% higher deflection at failure and 26, 23,

27 and 8% higher capacity, respectively, than the counterpart connection N-0.9-XX* without shear reinforcement.

5. The predictions of the modified CSA/S806-12 (CSA 2012) equations were in good agreement with the experimental results except for connection N-0.9-C8 which failed in flexure. In connection N-0.9-C8, the predicted failure mode was punching shear. On the other hand, the similarly-modified ACI 440.1R-15 (ACI 2015) equations underestimated the punching capacities of the connections.

5.3. RECOMMENDATIONS FOR FUTURE WORK

The following are suggestions for further studies:

1. The effect of different parameters on the punching shear behaviour of slab-column edge connections such as:
    a. The size effect (e.g., column size, column aspect ratio, column width-to-slab depth ratio and slab thickness).
    b. The effect of openings.
2. The effect of using headed studs and corrugated bars as shear reinforcement in slab-column edge connections with higher flexural reinforcement ratios.
3. The effect of using corrugated bars with larger bar diameter as shear reinforcement.
4. The effect of using different anchorage types in the direction perpendicular to the free edge such as headed-end bars.
5. Seismic behaviour of slab-column edge connections.
6. The punching shear behaviour of slab-column corner connections.

REFERENCES

ACI Committee 318. (1971). "Building Code Requirements for Reinforced Concrete." *ACI 318-71*, American Concrete Institute, Detroit, MI, 78.

ACI Committee 318. (1995). "Building Code Requirements for Structural Concrete." *ACI 318-95 and Commentary*, American Concrete Institute, Detroit, MI, 369.

ACI Committee 318. (2005). "Building Code Requirements for Structural Concrete." *ACI 318-05 and Commentary*, American Concrete Institute, Detroit, MI, 430.

ACI Committee 318. (2014). "Building code requirements for structural concrete and commentary." *ACI 318-14*, American Concrete Institute, Detroit, MI, 524.

ACI Committee 440. (2015). "Guide for the design and construction of structural concrete reinforced with fiber-reinforced polymer bars." *ACI 440.1R-15*, American Concrete Institute, Detroit, MI, 88.

Alexander, S.D.B. and Simmonds, S.H. (1992). "Punching Shear Tests of Concrete Slab-Column Joints Containing Fiber Reinforcement." *ACI Structural Journal*, 98(4): 425-432.

ASTM. (2011). "Standard test method for tensile properties of fiber reinforced polymer matrix composite bars." *ASTM D7205/D7205M*, American Society for Testing and Materials, ASTM International, West Conshohocken, PA, 15(3), 12.

Banthia, N., Al-Asaly, M. and Ma, S. (1995). "Behaviour of Concrete Slabs Reinforced with Fiber-Reinforced Plastic Grid." *Journal of Material in Civil Engineering*, 7(4): 252-256.

Birkle, G., and Dilger, W.H. (2008). "Influence of Slab Thickness on Punching Shear Strength." *ACI Structural Journal*, 105(2): 180-188.

British Standards Institution. (1997). "Structural Use of Concrete, *BS 8110*: Part 1: Code of Practice for Design and Construction." London, United Kingdom, 172.

Corley, W. G., and Hawkins, N. M. (1968). "Shearhead Reinforcement for Slabs." *ACI Journal Proceedings*, 65(10): 811-824.

CSA. (2002). "Design and Construction of Building Components with Fibre-Reinforced Polymers." *CSA/S806-02*, Canadian Standards Association, Toronto, ON, 177.

CSA. (2004). "Code for the design of concrete structures for buildings." *CSA/A23.3-04*, Canadian Standards Association, Toronto, ON, 240.

CSA. (2012). "Design and construction of building structures with fibre-reinforced polymers." *CSA/S806-12*, Canadian Standards Association, Toronto, ON, 206.

CSA. (2014). "Concrete materials and methods of concrete construction/Test methods and standard practices for concrete. *CSA A23.1/A23.2-14*, Canadian Standards Association, Toronto, ON, 690.

CSA. (2014). "Code for the design of concrete structures for buildings." *CSA/A23.3-14*, Canadian Standards Association, Toronto, ON, 297.

CSA. (2014). "Canadian highway bridge design code." *CSA/S6-14*, Canadian Standards Association, Toronto, ON, 894.

Dilger, W., Birkle, G. and Mitchell, D. (2005). "Effect of Flexural Reinforcement on Punching Shear Resistance." *ACI Structural Journal*, 32(4): 57-74.

Dilger, W. H., and Ghali, A. (1981). "Shear Reinforcement for Concrete Slabs." *Journal of the Structural Division*, 107(12): 2403-2420.

Dulude, C., Hassan, M., Ahmed, E., and Benmokrane, B. (2013). "Punching Shear Behaviour of Flat Slabs Reinforced with Glass Fiber-Reinforced Polymer Bars." *ACI Structural Journal*, 110(5): 723-734.

Elgabry, A., and Ghali, A. (1987). "Tests on Concrete Slab-Column Connections with Stud-Shear Reinforcement Subjected to Shear-Moment Transfer." *ACI Structural Journal*, 84(5): 433-442.

El-Gamal, S., El-Salakawy, E. F., and Benmokrane, B. (2005). "A New Punching Shear Equation for Two-Way Concrete Slabs Reinforced with FRP Bars." *ACI Special Publication*, SP-230, 877-894.

El-Gendy, M. G., and El-Salakawy, E. F. (2016a). "Effect of Shear Studs and High Moments on Punching Behaviour of GFRP-RC Slab-Column Edge Connections." *ASCE Journal of Composites for Construction*, 20(4), DOI: 10.1061/(ASCE) CC.1943-5614.0000668, 04016007.

El-Gendy, M. G., and El-Salakawy, E. F. (2016b). "Punching Shear Behaviour of GFRP-RC Slab-Column Edge Connections." in "Towards Sustainable Infrastructure with Fiber Reinforced Polymer Composites", *ACI Special Publication*, SP-06, in press, 20.

El-Ghandour, A. W., Pilakoutas, K., and Waldron, P. (1999). "New Approach for Punching Shear Capacity Prediction of Fiber-Reinforced Polymer Reinforced Concrete Flat Slabs." *ACI Structural Journal*, 188(13): 877-894.

El-Ghandour, A. W., Pilakoutas, K., and Waldron, P. (2003). "Punching Shear Behaviour of Fiber Reinforced Polymers Reinforced Concrete Flat Slabs: Experimental Study." *ASCE Journal of Composites for Construction*, 7(3): 258-265.

El-Salakawy, E. F., Polak, M. A., and Soliman, M. H. (1998). "Slab-column edge connections subjected to high moments." *Canadian Journal of Civil Engineering*, 25(3): 526-538.

El-Salakawy, E., Polak, M., and Soliman, M. (2000). "Reinforced concrete slab-column edge connections with shear studs." *Canadian Journal of Civil Engineering*, 27(2): 338-348.

European Standard, EN 1992-1-1. (2004). "Eurocode 2: Design of concrete structures, Part 1-1: General rules and rules for buildings." *British Standard*, London, United Kingdom, 230.

Gar, S. P., Mander, J., Head, M., and Hurlebaus, S. (2014). "FRP Slab Capacity Using Yield Line Theory." *ASCE Journal of Composites for Construction*, 18(6): 04014021.

Gardner, N. (1990). "Relationship of the Punching Shear Capacity of Reinforced Concrete Slabs with Concrete Strength." *ACI Structural Journal*, 87(1): 66-71.

Ghannoum, C. M. (1998). "Effect of High-Strength Concrete on the Performance of Slab-Column Specimens." MSc Thesis, McGill University, Montréal, QC, Canada.

Gouda, A., and El-Salakawy, E. (2016). "Punching Shear Strength of GFRP-RC Interior Slab-Column Connections Subjected to Moment Transfer." *ASCE Journal of Composites for Construction*, 20(1), DOI: 10.1061/(ASCE) CC.1943-5614.0000597, 04015037.

Hassan, M., Ahmed, E., and Benmokrane, B. (2013). "Punching-Shear Strength of Normal and High-Strength Two-Way Concrete Slabs Reinforced with GFRP Bars." *ASCE Journal of Composites for Construction*, 17(6): 04013003.

Hawkins, N. M., Bao, A., and Yamazaki, J. (1989). "Moment Transfer From Concrete Slabs to Columns." *ACI Structural Journal*, 86(6): 705-716.

Heinzmann, D., Etter, S., Villiger, S., and Jaeger, T. (2012). "Punching Tests on Reinforced Concrete Slabs with and without Shear Reinforcement." *ACI Structural Journal*, 109(6): 787-794.

Hussein, A., Rashid, I., and Benmokrane, B. (2004). "Two-way concrete slabs reinforced with GFRP bars." *Advanced Composite Materials in Bridges and Structures Conference*, Calgary, AB, Canada, 8.

ISIS Canada. (2007). "Reinforcing Concrete Structures with Fibre Reinforced Polymers - Design Manual No. 3." The Canadian Network of Centers of Excellence on Intelligent Sensing for Innovative Structures, *ISIS Canada Corporation*, University of Manitoba, Winnipeg, MB, Canada, 103.

Japan Society of Civil Engineering. (1997). "Recommendation for Design and Construction of Concrete Structures Using Continuous Fibre Reinforcing Materials." *Concrete Engineering*, Series 23, Tokyo, Japan 325.

Lips, S., Ruiz, M., and Muttoni, A. (2012). "Experimental Investigation on Punching Strength and Deformation Capacity of Shear-Reinforced Slabs." *ACI Structural Journal*, (109): 889-900.

Marzouk, H., Emam, M., and Hilal, M. (1996). "Effect of High-Strength Concrete Columns on the Behaviour of Slab-Column Connections." *ACI structural journal*, 93(5): 545-552.

Marzouk, H., Emam, M., and Hilal, M.S. (1998). "Effect of High-Strength Concrete Slab on the Behaviour of Slab-Column Connections." *ACI Structural Journal*, 95(3): 227-236.

Marzouk, H., and Hussein, A. (1991). "Experimental Investigation on the Behaviour of High-Strength Concrete Slabs." *ACI Structural Journal*, 88(6): 701-713.

Marzouk, H., Osman, M., and Helmy, S. (2000). "Behaviour of High-Strength Lightweight Aggregate Concrete Slabs under Column Load and Unbalanced Moment." *ACI Structural Journal*, 97(3): 860-866.

Matthys, S., and Taerwe, L. (2000). "Concrete Slabs Reinforced with FRP Grids. II: Punching Resistance." *ASCE Journal of Composites for Construction*, 4(3): 154-161.

Megally, S., and Ghali, A. (1994). "Design Considerations for Slab-Column Connections in Seismic Zones." *ACI Structural Journal*, 91(3): 303–314.

Mokhtar, A. S., Ghali, A. and Dilger, W. H. (1985). "Stud Shear Reinforcement for Flat Concrete Plates." *ACI Journal Proceedings*, 82(5): 676-683.

Mortin, J. D. (1989). "Connections of Concrete Slabs with Edge Columns." *Master's Thesis*, University of Calgary, Calgary, AB, Canada.

National Research Council of Canada. (2010). "National Building Code of Canada." *NBCC 2010*, National Research Council of Canada, Ottawa, ON, 1222.

Osman, M., Marzouk, H., and Helmy, S. (2000). "Behaviour of High-Strength Lightweight Concrete Slabs under Punching Loads." *ACI Structural journal*, 97(3): 492-498.

Ospina, C. E. (2005). "Alternative Model for Concentric Punching Capacity Evaluation of Reinforced Concrete Two-Way Slabs." *ACI Concrete International*, 27(9): 53-57.

Ospina, C. E., Alexander, S. D. B. and Cheng, J. J. R. (2003). "Punching of Two-Way Concrete Slabs with Fiber-Reinforced Polymer Reinforcing Bars or Grids." *ACI Structural Journal*, 100(5): 589-598.

Ozden, S., Ersoy, U., and Ozturan, T. (2006). "Punching Shear Tests of Normal- and High-Strength Concrete Flat Plates." *Canadian Journal of Civil Engineering*, 33(11): 1389-1400.

Park, R., and Gamble, W. L. (2000). "Reinforced Concrete Slabs." John Wiley & Sons, Inc., New York, USA, 736.

Polak, M. A., El-Salakawy, E. F. and Hammill, N. (2005). "Shear Reinforcement for Concrete Flat Slabs." *ACI Special Publication*, 232: 75-96.

Pultrall Inc. (2015). "V-ROD^{TM} – Technical Data Sheet." ADS Composites Group Inc., Thetford Mines, QC, Canada, http:// www.pultrall.com.

Richart, F.E. (1948). "Reinforced Concrete Wall and Column Footings, Part 1." *ACI Journal Proceedings*, Proc., 45(10): 97-127.

Ritchie, M., Ghali, A., Dilger, W., and Gayed, R. (2006). "Unbalanced moment resistance by shear in slab-column connections: experimental assessment." *ACI structural journal,* 103(1): 74-82.

Rizk, E., Marzouk, H., Hussein, A., and Hossin, M. (2011). "Effect of Reinforcement Ratio on Punching Capacity of RC Plates." *Canadian Journal of Civil Engineering,* 38(7): 729-740.

Schoeck Canada Inc. (2013). "Schock ComBAR - Technical Information." <http://www.schoeck.ca/en_ca/downloads?product=4&type=7&filter=1>.

Stein, T., Ghali, A., and Dilger, W. (2007). "Distinction between Punching and Flexural Failure Modes of Flat Plates." *ACI structural journal,* 104(3): 357-365.

Swamy, R.N., and Ali, S.A.R. (1982). "Punching Shear Behaviour of Reinforced Slab-Column Connections Made with Steel Fiber Concrete." *ACI Structural Journal,* 79(5): 392-406.

Tureyen, A. K., and Frosch, R. J. (2003). "Concrete Shear Strength: Another Perspective." *ACI Structural Journal,* 100(5): 609-615.

Vanderbilt, M. D. (1972). "Shear Strength of Flat Plates." *Journal of Structural Division,* 98(5): 961-973.

Wheeler, W. H. (1936). "Thin Flat-Slab Floors Prove Rigid Under Test." *Engineering News-Record,* 116(2): 49-50.

Widianto, Bayrak, O., and Jirsa, J. O. (2009). "Two-Way Shear Strength of Slab-Column Connections: Reexamination of ACI 318 Provisions." *ACI Structural Journal,* 106(2): 160-170.

Zaghloul, A. (2002). "Behaviour and Strength of CFRP-Reinforced Flat Plate Interior Column Connections Subjected to Shear and Unbalanced Moments." *Master's Thesis*, Carleton University, Ottawa, ON, Canada.

Zaghloul, A. (2007). "Punching Shear Strength of Interior and Edge Column-Slab Connections in CFRP Reinforced Flat Plate Structures Transferring Shear and Moment." *Ph.D. Thesis*, Carlton University, Ottawa, ON, Canada.

Zaghloul, A., and Razaqpur, A.G. (2004). "Punching Shear Strength of Concrete Flat Plates Reinforced with GFRP Grids." *4th International Conference on Advanced Composite Materials in Bridges and Structures*, Calgary, AB, Canada, 8.

Zhang, Q., Marzouk, H., and Hussein, A. (2005). "A preliminary study of high-strength concrete two-way slabs reinforced with GFRP bars." *Proceedings of the 33rd CSCE Annual Conference*, Toronto, ON, Canada, 10.

APPENDIX A

DESIGN OF TEST SPECIMENS

A.1. LAYOUT OF THE FLAT PLATE SYSTEM

A typical parking garage system consisting of three 6.5 m-long square bays is subjected to gravity loads and bending moment distribution as shown in Fig. A.1. The slab-column edge connections are bounded by the slab free edge and the lines of contra-flexure around the column as shown in Fig. A.2.

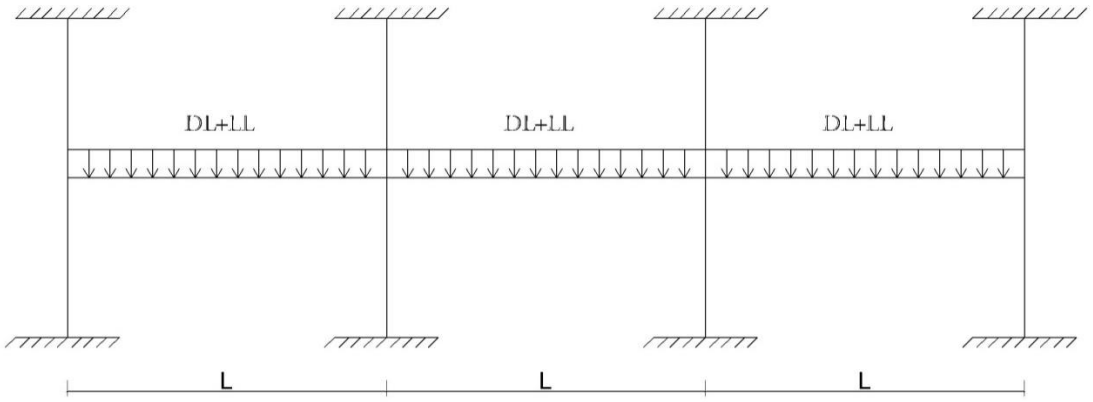

(a) Applied loads

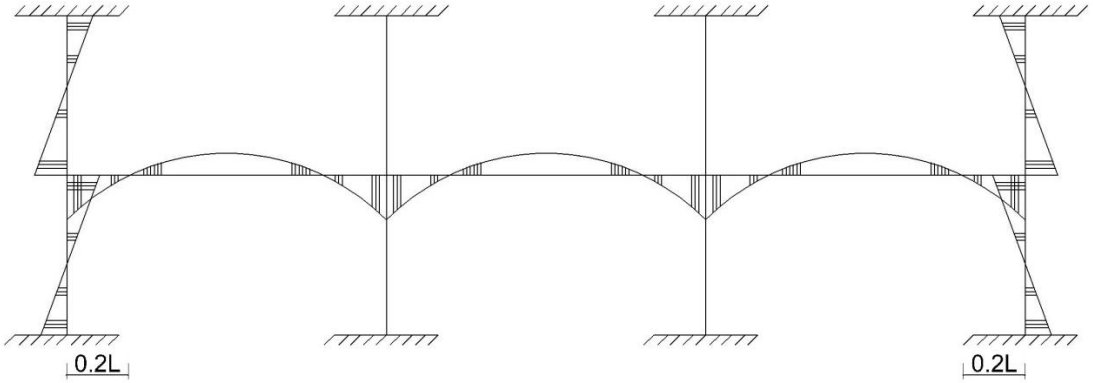

(b) Bending moment diagram

Figure A.1: Parking garage frame

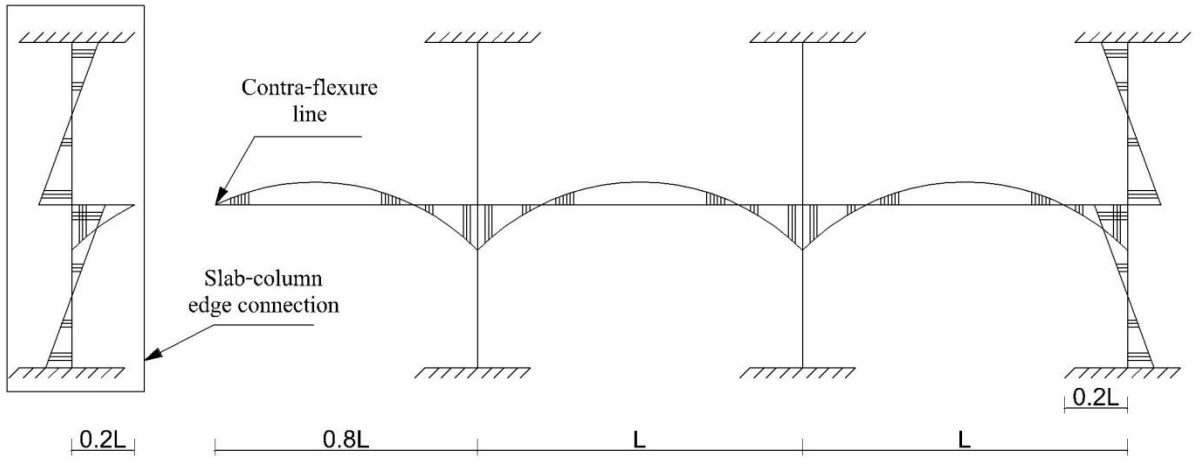

Figure A.2: Lines of contra-flexure

A.2. PROPERTIES OF CONCRETE

Compressive strength of concrete $f_c' = 35\ MPa$

Material resistance factor $\phi_c = 1.0$

Ultimate compressive strain of concrete $\varepsilon_{c_u} = 0.0035$

$\alpha_1 = 0.85 - 0.0015 f_c' = 0.85 - 0.0015(35) = 0.7975$

$\beta_1 = 0.97 - 0.0025 f_c' = 0.97 - 0.0025(35) = 0.8825$

A.3. LOADS (ACCORDING TO NRCC 2010)

$L.L. = 2.4\ kN/m^2$

$D.L. = self\ weight + partition\ allowance = 24 * 0.2 + 1.0 = 5.8\ kN/m2$

Factored load is the greater of $w_f = 1.4\ D.L. = 1.4 * 5.8 = 8.12\ kN/m^2$

or $= 1.25\ D.L. + 1.5\ L.L. = 1.25 * 5.8 + 1.5 * 2.4$

$= 7.25 + 3.6 = 10.85\ kN/m^2$ (It governs)

A.4. SLAB THICKNESS "h_s"

Minimum slab thickness $h_s = 1.1 * \frac{l_n\left(0.6+\frac{f_y}{1000}\right)}{30}$

$= 1.1 * \frac{6200\left(0.6+\frac{400}{1000}\right)}{30} = 227.3\ mm$

Take $h_s = 200\ mm$

A.5. DESIGN OF GFRP-RC PARKING GARAGE FLAT PLATE (ACCORDING TO CSA/S806-12 AND CSA/A23.3-14)

A.5.1. Properties of Reinforcement:

Material resistance factor $\phi_f = 1.0$

Use No. 20 bars:

$d_{b_{ext.}} = 22\ mm$ (Straight) $d_{b_{ext.}} = 20.5\ mm$ (Bent) $A_b = 285\ mm^2$

The mechanical properties of the used bars are shown in the following table:

Table A.1: Mechanical properties of the used GFRP bars

Bar type	f_{frp_u} (MPa)	E_{frp} (GPa)	ε_{frp_u} (%)
Straight bars	1,484	65	2.3
Bent bars	1,266	54	2.4

A.5.2. Design of Strip Perpendicular to the Free Edge

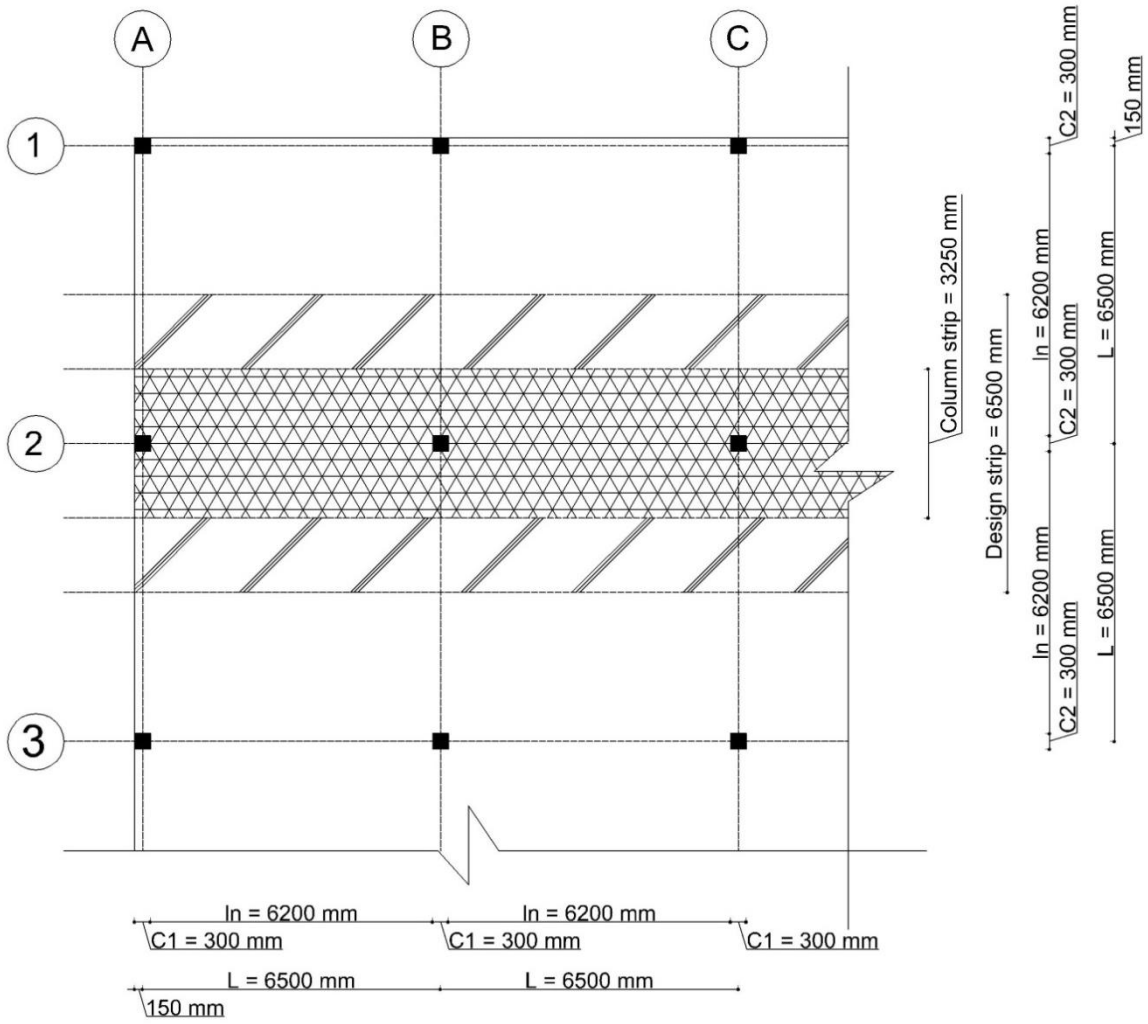

Figure A.2: Design strip perpendicular to the free edge

A.5.2.1. Effective depth "d"

Take concrete clear cover $= 19.5\ mm$

$\therefore\ d = h_s - clear\ cover - \frac{d_b}{2} = 200 - 19.5 - \frac{20.5}{2} = 170.25\ mm$

A.5.2.2. Design moments

$M_o = \frac{w_f * l_{2a} * l_n^2}{8} = \frac{10.85 * 6.5 * 6.2^2}{8} = 338.87\ kN.m$

Table A.2: Moment distribution in a design strip perpendicular to the free edge

Axis	A		B			C
l_n		6200			6200	
M_o%	0.26	0.52	0.7	0.65	0.35	0.65
M_{Design}	**88.11**	176.21	237.21	220.27	118.61	20.27

A.5.2.3. Reinforcement

$M_{Design} = 88.11\ kN.m$

Reinforcement for the total factored negative moment transferred to the exterior columns shall be placed within a band width $b_b = c + 3h_s$

- **For the part of the strip beneath the column $b_b = c + 3h_s$:**

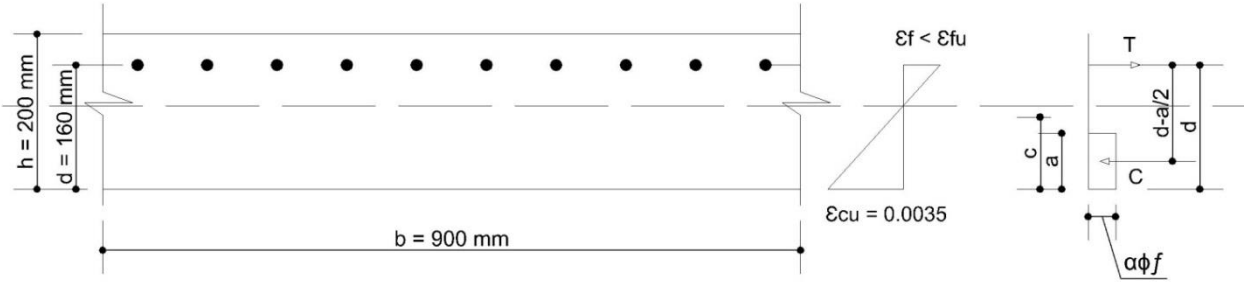

Figure A.3: Strain distribution and equivelant stress block for a slab cross section

$b_b = c + 3h_s = 300 + 3 * 200 = 900\ mm$

$M_r = \alpha_1 \phi_c f_c' b \beta c * \left(d - \frac{\beta c}{2}\right)$

$\therefore 88.11 * 10^6 = 0.7975 * 1.0 * 35 * 900 * 0.8825 * c * \left(170.25 - \frac{0.8825 * c}{2}\right)$

$9782.29c^2 - 3774357.91c + 88.11 * 10^6 = 0$

$\therefore c = 24.96\ mm$

From strain compatibility:

$\varepsilon_f = \varepsilon_{c_u} * \left(\frac{d}{c} - 1\right) = 0.0035 * \left(\frac{170.25}{24.96} - 1\right) = 20.37 * 10^{-3}$

$\therefore f_f = E_f * \varepsilon_f = 54000 * 20.37 * 10^{-3} = 1099.98\ MPa$

$\because C = T$

$\therefore \alpha_1 \phi_c f_c' b \beta c = \phi_f A_f f_f$

$0.7975 * 1.0 * 35 * 900 * 0.8825 * 24.96 = 1.0 * A_f * 1099.98$

$\therefore A_f = 503.06\ mm^2$

$A_{f_{min}} = \frac{400}{E_f} * A_g = \frac{400}{54000} * (200 * 900) = 1333.33\ mm^2$ (It governs)

$A_f = \frac{b}{s} * A_b \qquad \therefore 1333.33 = \frac{900}{s} * 285 \qquad \therefore s = 192.375\ mm$

$\therefore$ Use No. 20 @ 192 mm c/c

- **Check for the Balanced Reinforcement Ratio "ρ_b":**

$A_{f_{act}} = \frac{b}{s} * A_b = \frac{900}{192} * 285 = 1335.94\ mm^2$

$\rho = \frac{1335.94}{900 * 170.25} = 0.87\%$

$\rho_b = \alpha_1 \beta_1 \frac{\phi_c f_c'}{\phi_f f_{f_u}} * \frac{\varepsilon_{c_u}}{\varepsilon_{c_u} + \varepsilon_{fu}}$

$\rho_b = 0.7975 * 0.8825\ \frac{1.0 * 35}{1.0 * 1266} * \frac{0.0035}{0.0035 + 0.024} = 0.25\%$

$\therefore \rho > \rho_b$ Ok (over-reinforced)

- **For the Rest of the Strip:**

Use minimum reinforcement "$A_{s_{min}}$"

$A_{f_{min}} = \frac{400}{E_f} * A_g = \frac{400}{54000} * (200 * 1000) = 1481.48\ mm^2/m$ (It governs)

Or $A_{f_{min}} = 0.0025 A_g = 0.0025 * (200 * 1000) = 500\ mm^2/m$

Maximum spacing $s_{max} = 3h_s = 3 * 200 = 600\ mm$

Or $= 300\ mm$ (It governs)

$\therefore A_f = \frac{b}{s} * A_b \quad \therefore 1481.48 = \frac{1000}{s} * 285 \quad \therefore s = 192.375\ mm$

A.5.2.4. Development length for the reinforcement "l_d"

$$f_f = 0.5E_f\varepsilon_{c_u}\left[\left(1 + \frac{4\alpha_1\beta_1\phi_c f_c'}{\rho_f\phi_f E_f\varepsilon_{c_u}}\right)^{1/2} - 1\right]$$

$$= 0.5 * 54000 * 0.0035 * \left[\left(1 + \frac{4*0.7975*0.8825*1.0*35}{0.0087*1.0*54000*0.0035}\right)^{1/2} - 1\right]$$

$\therefore f_f = 643\ MPa$

$l_d = \frac{f_f}{3.1} k_2 \frac{d_b}{\sqrt{f_c'}}$ For $520\ MPa < f_{frp} \leq 1040\ MPa$

$k_2 = 1.0$ for normal density concrete

$l_d = \frac{643}{3.1} * 1.0 * \frac{20.5}{\sqrt{35}} = 718.8\ mm$

A.5.2.5. Check for serviceability

A.5.2.5.1. Service stress calculations

Specified load $w_s = D.L. + L.L. = 5.8 + 2.4 = 8.2\ kN/m^2$ **(NRCC 2010)**

Service moment $M_s = \frac{w_s * l_{2a} * l_n^2}{8} = \frac{8.2 * 6.5 * 6.2^2}{8} = 256.1\ kN.m$

Service moment at the edge connection $= M_s * 0.26 = 256.1 * 0.26 = 66.6\ kN.m$

$n = \frac{E_f}{E_c} = \frac{54000}{26622} = 2.03$

$k = \sqrt{2\rho n + (\rho n)^2} - \rho n = \sqrt{2 * 0.0087 * 2.03 + (0.0087 * 2.03)^2} - 0.0087 * 2.03 = 0.171$

$j = 1 - \frac{k}{3} = 1 - \frac{0.171}{3} = 0.9428$

∴ Service stress $f_s = \frac{M_s}{A_s jd} = \frac{66.6*10^6}{1335.94*0.9428*170.25} = 310.6\ MPa$

A.5.2.5.2. Check Crack Control Parameter

$d_c = h - d = 200 - 170.25 = 29.75\ mm$

$A = 2 * S * d_c = 2 * 192 * 29.75 = 11424\ mm$

$z = f_s k_p \frac{E_s}{E_f} \sqrt[3]{d_c A} = 310.6 * 1.2 * \frac{197000}{54000} \sqrt[3]{29.75 * 11424} = 94891\ N/mm > 45000\ N/mm$

Not OK

∴ Try reducing spacing and take No. 20 @ 96 mm c/c

$k = \sqrt{2\rho n + (\rho n)^2} - \rho n = \sqrt{2 * 0.0174 * 2.03 + (0.0174 * 2.03)^2} - 0.0174 * 2.03 = 0.233$

$j = 1 - \frac{k}{3} = 1 - \frac{0.233}{3} = 0.922$

Service stress $f_s = \frac{M_s}{A_s jd} = \frac{66.6*10^6}{2671.875*0.922*170.25} = 158.8\ MPa$

$A = 2 * S * d_c = 2 * 96 * 29.75 = 5712\ mm$

$z = f_s k_p \frac{E_s}{E_f} \sqrt[3]{d_c A} = 158.8 * 1.2 * \frac{197000}{54000} \sqrt[3]{29.75 * 5712} = 38506\ N/mm < 45000\ N/mm$

OK

A.5.2.5.3. Reinforcement Strain Limit

$0.25 f_u = 0.25 * 1266 = 316.5 MPa > f_s = 158.8\ MPa$ OK

Design Summary:

- **Use No. 20 @ 96 mm c/c for the whole specimen.**

A.5.3. Design of Strip Parallel to the Free Edge

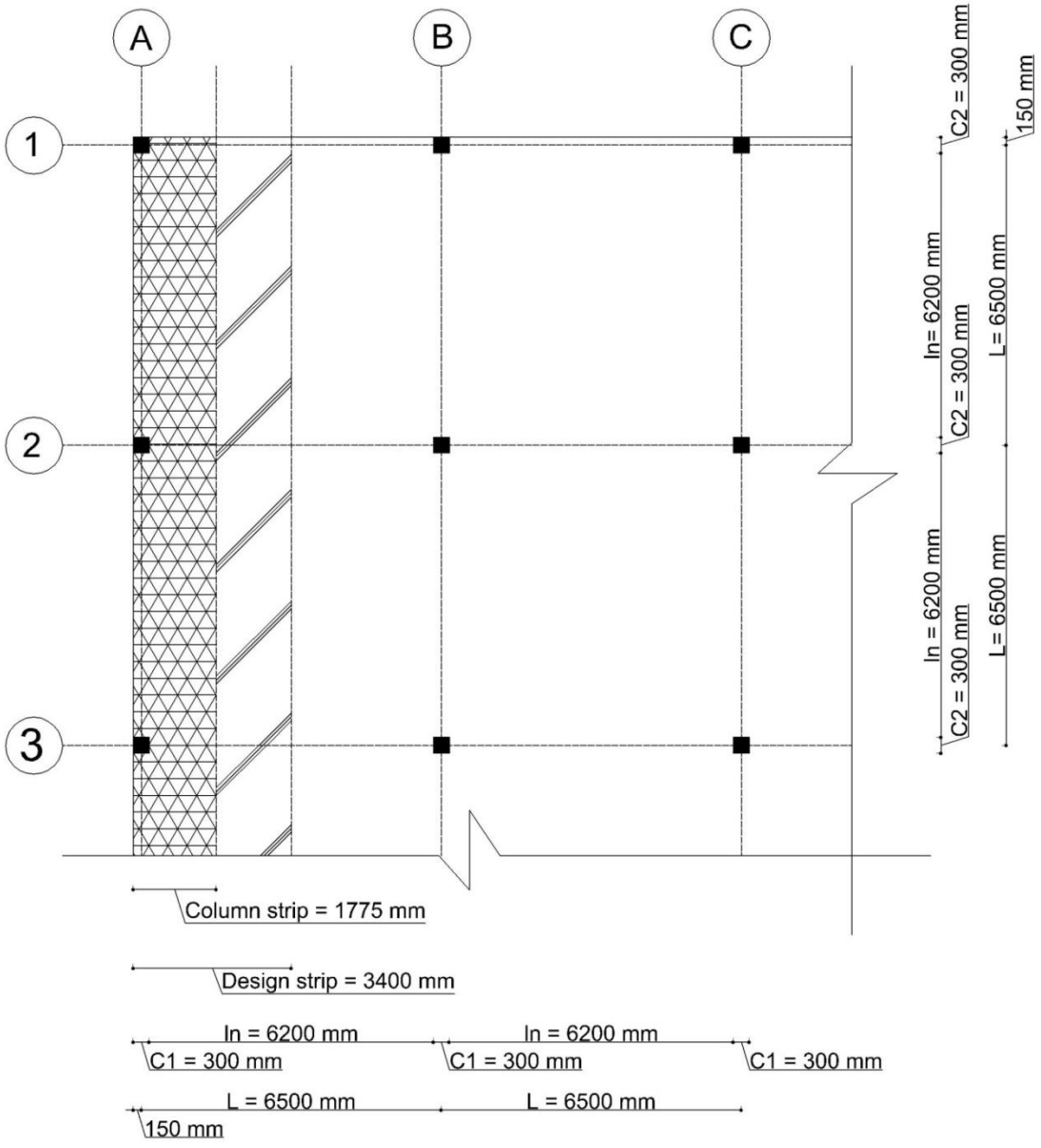

Figure A.4: Design strip strip parallel to the slab free edge

A.5.3.1. Effective depth "d"

$$d = h_s - clear\ cover - d_b - \frac{d_b}{2} = 200 - 19.5 - 20.5 - \frac{22}{2} = 149\ mm$$

A.5.3.2. Design moments

$M_o = \frac{w_f * l_a * l_n^2}{8} = \frac{10.85 * 3.4 * 6.2^2}{8} = 177.26\ kN.m$

Table A.3: Moment distribution in a design strip parallel to the free edge

Axis	1		2		3	
l_n		6200			6200	
M_o%	0.26	0.52	0.7	0.65	0.35	0.65
M_{Design}	46.09	92.17	**124.08**	115.22	62.04	115.22

A.5.3.3. Reinforcement

M_{Design}= 124.08kN.m

∵ 70% to 90% of the Negative moment at an interior column is to be taken by the column strip.

∴ 0.7M_{Design}= 0.7*124.08 = 86.86 kN.m

0.9M_{Design}= 0.9*124.08 = 111.67 kN.m

At interior columns, the band width b_b shall be designed to resist at least one-third of the total factored negative moment in the entire design strip.

- **For the Band Width $b_b = c + 1.5h_s$:**

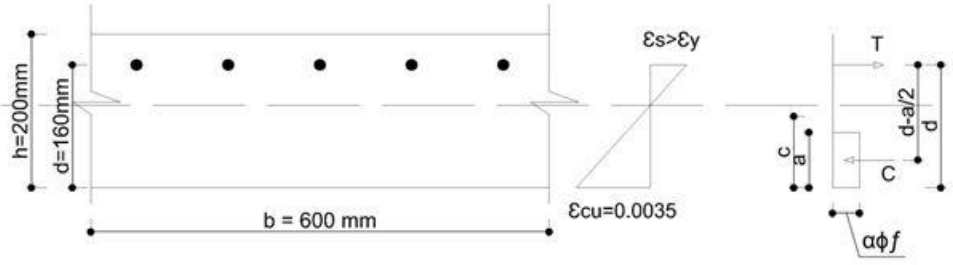

Figure A.5: Strain distribution and equivelant stress block

$b_b = c + 1.5h_s = 300 + 1.5 * 200 = 600\ mm$

$M = {}^{1}/_{3} * 124.08 = 41.36\ kN.m$

$M_r = \alpha_1 \phi_c f_c' b \beta c * \left(d - \frac{\beta c}{2}\right)$

$\therefore 41.36 * 10^6 = 0.7975 * 1.0 * 35 * 600 * 0.8825 * c * \left(149 - \frac{0.8825 * c}{2}\right)$

$6521.53c^2 - 2202170.64c + 41.36 * 10^6 = 0$

$\therefore c = 19.96\ mm$

From strain compatibility:

$\varepsilon_f = \varepsilon_{c_u} * \left(\frac{d}{c} - 1\right) = 0.0035 * \left(\frac{149}{19.96} - 1\right) = 22.63 * 10^{-3}$

$\therefore f_f = E_f * \varepsilon_f = 65374 * 22.63 * 10^{-3} = 1479.23\ MPa > f_{f_u}$

$\therefore$ Try $A_{f_{min}} = \frac{400}{E_f} * A_g = \frac{400}{65374} * (200 * 600) = 734.24\ mm^2$

$\alpha_1 \phi_c f_c' b \beta c = \phi_f A_f f_f$

$0.7975 * 1.0 * 35 * 600 * 0.8825 * \mathrm{c} = 1.0 * 734.24 * 65374 * \varepsilon_\mathrm{f}$

$\varepsilon_f = 3.08 * 10^{-4} * c = \varepsilon_{c_u} * \left(\frac{d}{c} - 1\right) = 0.0035 * \left(\frac{149}{c} - 1\right)$

$3.08 * 10^{-4} c^2 + 0.0035c - 0.5215 = 0$

$\therefore c = 35.86\ mm$

$\therefore \varepsilon_f = 3.08 * 10^{-4} * 35.86 = 11.04 * 10^{-3}$

$\therefore f_{frp} = 65374 * 11.04 * 10^{-3} = 721.83\ MPa < f_{f_u}$ <u>OK</u>

$\therefore M_r = \phi_f A_f f_f * \left(d - \frac{\beta c}{2}\right) = 1.0 * 734.24 * 721.83 * \left(149 - \frac{0.8825 * 35.86}{2}\right) * 10^{-6} =$

$70.58 kN.m > M_f = 41.36\ kN.m$ <u>OK</u>

$A_f = \frac{b}{s} * A_b \qquad \therefore 734.24 = \frac{600}{s} * 285 \qquad \therefore s = 232.89\ mm$

<u>Use No. 20 @ 232 mm c/c</u> $\qquad \therefore A_{f_{act}} = \frac{b}{s} * A_b = \frac{600}{232} * 285 = 737.07\ mm^2$

- **For the Rest of the Strip:**

<u>Use No. 20 @ 232 mm c/c</u>

$\therefore \rho_{frp} = \frac{737.07}{600*149} = 0.82\%$

A.5.3.4. Development length for the reinforcement "l_d"

$l_d = 1.15 \frac{k_1 k_2 k_3 k_4 k_5}{d_{cs}} \frac{f_f}{\sqrt{f_c'}} A_b$

Where;

$k_1 = 1.0$ for horizontal reinforcement placed in such a way that less than 300 mm of fresh concrete is cast in the member below the development length

$k_2 = 1.0$ for normal density concrete

$k_3 = 0.8$ for $A_b < 300 mm^2$

$k_4 = 1.0$ for GFRP

$k_5 = 1.0$ *s*and coated bars

$\therefore l_d = 1.15 * \frac{1*1*0.8*1*1}{2.5*22} * \frac{721.83}{\sqrt{35}} * 285 = 581.66\ mm$ OK

A.5.3.5. Serviceability check

A.5.3.5.1. Service stress calculations

Specified load $w_s = D.L. + L.L. = 5.8 + 2.4 = 8.2\ kN/m^2$ **(NRCC 2010)**

Service moment $M_s = \frac{w_s * l_{2a} * l_n^2}{8} = \frac{8.2 * 3.4 * 6.2^2}{8} = 133.96\ kN.m$

Service moment at the edge connection $= M_s * 0.7 * 0.33 = 133.96 * 0.7 * 0.33 = 31.3\ kN.m$

$n = \frac{E_f}{E_c} = \frac{65374}{26622} = 2.46$

$k = \sqrt{2\rho n + (\rho n)^2} - \rho n = \sqrt{2 * 0.0082 * 2.46 + (0.0082 * 2.46)^2} - 0.0082 * 2.46 = 0.182$

$j = 1 - \frac{k}{3} = 1 - \frac{0.182}{3} = 0.939$

Service stress $f_s = \frac{M_s}{A_s jd} = \frac{31.3*10^6}{737.07*0.939*149} = 303.5\ MPa$

A.5.3.5.2.Check crack control parameter

$d_c = h - d = 200 - 149 = 51\ mm$

$A = 2 * S * d_c = 2 * 232 * 51 = 23664\ mm$

$z = f_s k_p \frac{E_s}{E_f} \sqrt[3]{d_c A} = 303.5 * 1.2 * \frac{197000}{65374} \sqrt[3]{51 * 23664} = 116847\ N/mm > 45000\ N/mm$

Not OK

∴ Try reducing spacing and take No. 20 @ 116 mm c/c for the whole specimen

$k = \sqrt{2\rho n + (\rho n)^2} - \rho n = \sqrt{2 * 0.0164 * 2.46 + (0.0164 * 2.46)^2} - 0.0164 * 2.46 = 0.246$

$j = 1 - \frac{k}{3} = 1 - \frac{0.246}{3} = 0.918$

Service stress $f_s = \frac{M_s}{A_s jd} = \frac{31.3*10^6}{1474.14*0.918*149} = 155.23\ MPa$

$A = 2 * S * d_c = 2 * 116 * 51 = 11832\ mm$

$z = f_s k_p \frac{E_s}{E_f} \sqrt[3]{d_c A} = 155.23 * 1.2 * \frac{197000}{65374} \sqrt[3]{51 * 11832} = 47434\ N/mm \cong 45000\ N/mm$

OK

Design Summary:

- **Use No. 20 @ 116mm c/c for the whole strip.**

APPENDIX B

SHEAR CAPACITY OF CONNECTIONS

B.1. SHEAR CAPACITY OF CONNECTIONS WITHOUT SHEAR REINFORCEMENT

B.1.1 Properties of the Critical Section

$d_v = h_s$ – clear cover $-$ $d_b =$

$200 - 19.5 - 20.5 = 160\ mm$

$b_1 = c + \frac{d_v}{2} = 300 + \frac{160}{2} = 380\ mm$

$b_2 = c + 2 * \frac{d_v}{2} = 300 + 2 * \frac{160}{2} = 460\ mm$

$b_o = 2 * b_1 + b_2 = 2 * 380 + 460 = 1220\ mm$

$e = \frac{{b_1}^2}{2b_1 + b_2} = \frac{380^2}{2*380+460} = 118.4\ mm$

$J = 2\left(\frac{{b_1}^3 * d_v}{3} + \frac{{d_v}^3 * b_1}{12}\right) - b_o * d_v * e^2$

$= 2\left(\frac{380^3 * 160}{3} + \frac{160^3 * 380}{12}\right) - 1220 * 160 *$

$118.4^2 = 3377852377\ mm^4$

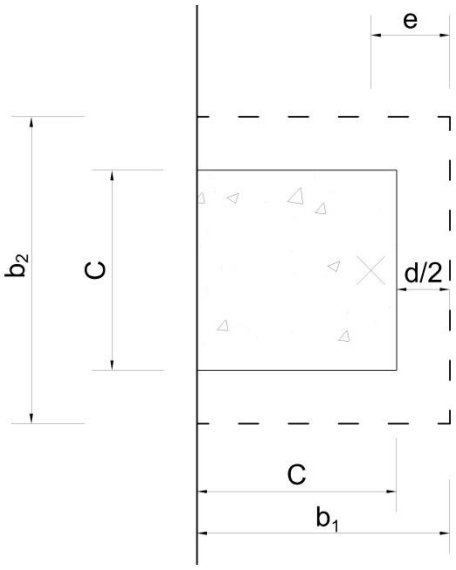

Figure B.1: Critical section at *d*/2 from column face

Where;

e = the distance between the centroid and the inner side of the critical section

J = property of the critical shear section corresponding to the polar moment of inertia

$\beta_c = \frac{c}{c} = 1$

$\gamma_v = 1 - \frac{1}{1 + \frac{2}{3}\sqrt{\frac{b_1}{b_2}}} = 1 - \frac{1}{1 + \frac{2}{3}\sqrt{\frac{380}{460}}} = 0.38$

$\frac{M_o}{V} = \frac{M}{V} - \left(b_1 - e - \frac{c}{2}\right)$

At $\frac{M}{V} = 0.4\ m$

$\frac{M_o}{V} = 0.4 - \left(0.38 - 0.1184 - \frac{0.3}{2}\right) = 0.2884\ m$

B.1.2 Connection H-0.9-XX

B.1.2.1 Material properties

B.1.2.1.1 Concrete

$f_c' = 81\ MPa$ $\phi_c = 1.0$ $\lambda = 1.0$

$E_c = 4700\sqrt{f_c'} = 4700 * \sqrt{81} = 42300\ MPa$

B.1.2.1.2 Flexural reinforcement

Reinforcement ratio perpendicular to the free edge, ρ_p = 0.0087

Reinforcement ratio parallel to the free edge, ρ_l = 0.0082

∴ Average reinforcement ratio, $\rho = \frac{\rho_p * b_2 + 2 * \rho_l * b_1}{b_o} = \frac{0.0087 * 460 + 2 * 0.0082 * 380}{1220} = 0.0084$

Modulus of elasticity perpendicular to the free edge, E_p = 54000 *MPa*

Modulus of elasticity parallel to the free edge, E_l = 65374 *MPa*

∴ Average modulus of elasticity, $E = \frac{E_p * b_2 + 2 * E_l * b_1}{b_o} = \frac{54000 * 460 + 2 * 65374 * 380}{1220} = 61085\ MPa$

Modular ratio, $n = \frac{E_f}{E_c} = \frac{61085}{42300} = 1.444$

B.1.2.2 Shear capacity according to CSA/S806-12

$v_r = v_c = \left(1 + \frac{2}{\beta_c}\right)\left[0.028\lambda\varphi_c\left(E_f\rho_f f_c'\right)^{1/3}\right] = \left(1 + \frac{2}{1}\right)\left[0.028 * 1.0 * 1.0 * (61085 * 0.0084 * 60)^{1/3}\right] = 2.63\ MPa$

Or $v_r = v_c = 0.147\lambda\varphi_c\left(0.19 + \alpha_s\frac{d_v}{b_o}\right)\left(E_f\rho_f f_c'\right)^{1/3} = 0.147 * 1.0 * 1.0 * \left(0.19 + 3 * \frac{160}{1220}\right) * (61085 * 0.0084 * 60)^{1/3} = 2.68\ MPa$

Or $v_r = v_c = 0.056\lambda\varphi_c\left(E_f\rho_f f_c'\right)^{1/3} = 0.056 * 1.0 * 1.0 * (61085 * 0.0084 * 60)^{1/3} =$ $1.755\ MPa$ (It governs)

$$V = {v_r}\Big/\left(\frac{1}{b_O * d} + \frac{0.2884\gamma}{J} * e\right) = 1.755 * 10^{-3}\Big/\left(\frac{1}{1220*160} + \frac{0.38*0.2884*1000}{3377852377} * 118.4\right) = 195.8\ kN$$

B.1.2.3 Shear capacity according to ACI 440.1R-15

$$k = \sqrt{2\rho n + (\rho n)^2} - \rho n = \sqrt{2 * 0.0084 * 1.444 + (0.0084 * 1.444)^2} - 0.0084 * 1.444 = 0.144$$

$$c = kd = 0.144 * 160 = 23.06\ mm$$

$$v_r = v_c = 0.8 * \frac{c}{d}\sqrt{f_c'} = 0.8 * \frac{23.06}{160}\sqrt{81} = 1.04\ MPa$$

$$V = {v_r}\Big/\left(\frac{1}{b_O * d} + \frac{0.2884\gamma}{J} * e\right) = 1.04 * 10^{-3}\Big/\left(\frac{1}{1220*160} + \frac{0.38*0.2884*1000}{3377852377} * 118.4\right) = 116\ kN$$

B.1.3 Connection H-1.35-XX

B.1.3.1 Material properties

B.1.3.1.1 Concrete

$f_c' = 85\ MPa$ $\phi_c = 1.0$ $\lambda = 1.0$

$$E_c = 4700\sqrt{f_c'} = 4700 * \sqrt{85} = 43332\ MPa$$

B.1.3.1.2 Flexural Reinforcement

Reinforcement ratio perpendicular to the free edge, ρ_p = 0.01305

Reinforcement ratio parallel to the free edge, ρ_l = 0.0123

Average reinforcement ratio, $\rho = \frac{\rho_p * b_2 + 2 * \rho_l * b_1}{b_o} = \frac{0.01305*460+2*0.0123*380}{1220} = 0.0126$

Modulus of elasticity perpendicular to the free edge, E_p = 54000 *MPa*

Modulus of elasticity parallel to the free edge, E_l = 65374 *MPa*

Average modulus of elasticity, $E = \frac{E_p * b_2 + 2 * E_l * b_1}{b_o} = \frac{54000*460+2*65374*380}{1220} = 61085\ MPa$

Modular ratio, $n = \frac{E_f}{E_c} = \frac{61085}{43332} = 1.41$

B.1.3.2 Shear capacity according to CSA/S806-12

$$v_r = v_c = \left(1 + \frac{2}{\beta_c}\right)\left[0.028\lambda\varphi_c\left(E_f\rho_f f_c'\right)^{1/3}\right] = \left(1 + \frac{2}{1}\right)\left[0.028 * 1.0 * 1.0 * (61085 * 0.0126 * 60)^{1/3}\right] = 3.01\ MPa$$

$$v_r = v_c = 0.147\lambda\varphi_c\left(0.19 + \alpha_s\frac{d_v}{b_o}\right)\left(E_f\rho_f f_c'\right)^{1/3} = 0.147 * 1.0 * 1.0 * \left(0.19 + 3 * \frac{160}{1220}\right) * (61085 * 0.0126 * 60)^{1/3} = 3.08\ MPa$$

$$v_r = v_c = 0.056\lambda\varphi_c\left(E_f\rho_f f_c'\right)^{1/3} = 0.056 * 1.0 * 1.0 * (61085 * 0.0126 * 60)^{1/3} = 2.01\ MPa$$

(It governs)

$$V = {v_r}\Big/\left(\frac{1}{b_O * d} + \frac{0.2884\gamma}{J} * e\right) = {2.01 * 10^{-3}}\Big/\left(\frac{1}{1220 * 160} + \frac{0.38 * 0.2884 * 1000}{3377852377} * 118.4\right) = 224.1\ kN$$

B.1.3.3 Shear capacity according to ACI 440.1R-15

$$k = \sqrt{2\rho n + (\rho n)^2} - \rho n = \sqrt{2 * 0.0126 * 1.41 + (0.0126 * 1.41)^2} - 0.0126 * 1.41 = 0.172$$

$$c = kd = 0.172 * 160 = 27.52\ mm$$

$$v_r = v_c = 0.8 * \frac{c}{d}\sqrt{f_c'} = 0.8 * \frac{27.52}{160}\sqrt{85} = 1.27\ MPa$$

$$V = {v_r}\Big/\left(\frac{1}{b_O * d} + \frac{0.2884\gamma}{J} * e\right) = {1.27 * 10^{-3}}\Big/\left(\frac{1}{1220 * 160} + \frac{0.38 * 0.2884 * 1000}{3377852377} * 118.4\right) = 141.7\ kN$$

B.1.4 Connection H-1.8-XX

B.1.4.1 Material properties

B.1.4.1.1 Concrete

$f_c' = 80\ MPa$ $\phi_c = 1.0$ $\lambda = 1.0$

$$E_c = 4700\sqrt{f_c'} = 4700 * \sqrt{80} = 42038\ MPa$$

B.1.4.1.2 Flexural Reinforcement

Reinforcement ratio perpendicular to the free edge, ρ_p = 0.0174

Reinforcement ratio parallel to the free edge, $\rho_l = 0.0164$

Average reinforcement ratio, $\rho = \frac{\rho_p * b_2 + 2 * \rho_l * b_1}{b_o} = \frac{0.0174 * 460 + 2 * 0.0164 * 380}{1220} = 0.017$

Modulus of elasticity perpendicular to the free edge, $E_p = 54000\ MPa$

Modulus of elasticity parallel to the free edge, $E_l = 65374\ MPa$

Average modulus of elasticity, $E = \frac{E_p * b_2 + 2 * E_l * b_1}{b_o} = \frac{54000 * 460 + 2 * 65374 * 380}{1220} = 61085\ MPa$

Modular ratio, $n = \frac{E_f}{E_c} = \frac{61085}{42038} = 1.45$

B.1.4.2 Shear capacity according to CSA/S806-12

$v_r = v_c = \left(1 + \frac{2}{\beta_c}\right)\left[0.028\lambda\varphi_c\left(E_f\rho_f f_c'\right)^{1/3}\right] = \left(1 + \frac{2}{1}\right)\left[0.028 * 1.0 * 1.0 * (61085 * 0.0127 * 60)^{1/3}\right] = 3.33\ MPa$

$v_r = v_c = 0.147\lambda\varphi_c\left(0.19 + \alpha_s\frac{d_v}{b_o}\right)\left(E_f\rho_f f_c'\right)^{1/3} = 0.147 * 1.0 * 1.0 * \left(0.19 + 3 * \frac{160}{1220}\right) * (61085 * 0.0127 * 60)^{1/3} = 3.4\ MPa$

$v_r = v_c = 0.056\lambda\varphi_c\left(E_f\rho_f f_c'\right)^{1/3} = 0.056 * 1.0 * 1.0 * (61085 * 0.017 * 60)^{1/3} = 2.22\ MPa$

(It governs)

$V = {v_r}\Big/\left(\frac{1}{b_O * d} + \frac{0.2884\gamma}{J} * e\right) = 2.22 * 10^{-3}\Big/\left(\frac{1}{1220 * 160} + \frac{0.38 * 0.2884 * 1000}{3377852377} * 118.4\right) = 247.66\ kN$

B.1.4.3 Shear capacity according to ACI 440.1R-15

$k = \sqrt{2\rho n + (\rho n)^2} - \rho n = \sqrt{2 * 0.017 * 1.45 + (0.017 * 1.45)^2} - 0.017 * 1.45 = 0.199$

$c = kd = 0.199 * 160 = 31.84\ mm$

$v_r = v_c = 0.8 * \frac{c}{d}\sqrt{f_c'} = 0.8 * \frac{31.84}{160}\sqrt{80} = 1.424\ MPa$

$V = {v_r}\Big/\left(\frac{1}{b_O * d} + \frac{0.2884\gamma}{J} * e\right) = 1.424 * 10^{-3}\Big/\left(\frac{1}{1220 * 160} + \frac{0.38 * 0.2884 * 1000}{3377852377} * 118.4\right) = 158.8\ kN$

B.2 SHEAR CAPACITY OF CONNECTIONS WITH SHEAR REINFORCEMENT

B.2.1 Introduction

The modified provisions of the CSA/A23.3-14 and the ACI 318-14 proposed by El-Gendy and El-Salakawy (2016a) (Section 2.7.2) were used to calculate the shear capacity of those connections.

B.2.2 Reinforcement Properties

B.2.2.1 Properties of headed end shear studs

No. 13 bars $A_b = 126.7\ mm^2$

Ultimate tensile strength $f_{frp_u} = 552\ MPa$

Ultimate tensile strain $\varepsilon_{frp_u} = 0.8\ \%$

Modulus of elasticity $E_{frp} = 67547\ MPa$

B.2.2.2 Properties of corrugated bars

No. 10 bars $A_b = 71.3\ mm^2$

Ultimate tensile strength $f_{frp_u} = 1280\ MPa$

Ultimate tensile strain $\varepsilon_{frp_u} = 2.5\ \%$

Modulus of elasticity $E_{frp} = 52000\ MPa$

B.2.2.3 Flexural reinforcement properties

Reinforcement ratio perpendicular to the free edge, $\rho_p = 0.0087$

Reinforcement ratio parallel to the free edge, $\rho_l = 0.0082$

∴ Average reinforcement ratio, $\rho = \frac{\rho_p * b_2 + 2 * \rho_l * b_1}{b_o} = \frac{0.0087 * 460 + 2 * 0.0082 * 380}{1220} = 0.0084$

Modulus of elasticity perpendicular to the free edge, $E_p = 54000\ MPa$

Modulus of elasticity parallel to the free edge, $E_l = 65374\ MPa$

∴ Average modulus of elasticity, $E = \frac{E_p * b_2 + 2 * E_l * b_1}{b_o} = \frac{54000 * 460 + 2 * 65374 * 380}{1220} = 61085\ MPa$

B.2.3. Connection N-0.9-S6

B.2.3.1. Concrete properties

$f_c' = 44\ MPa$ $\phi_c = 1.0$ $\lambda = 1.0$

B.2.3.2. Properties of outer critical section

$l_1 = 303\ mm$

$l_2 = 878\ mm$

$l_3 = 306\ mm$

$l_x = 924\ mm$

$l_y = 1548\ mm$

$d_v = 160\ mm$

$b_o = 2 * (l_1 + l_2) + l_3 = 2 * (303 + 878) + 306 =$

$\mathbf{2668\ mm}$

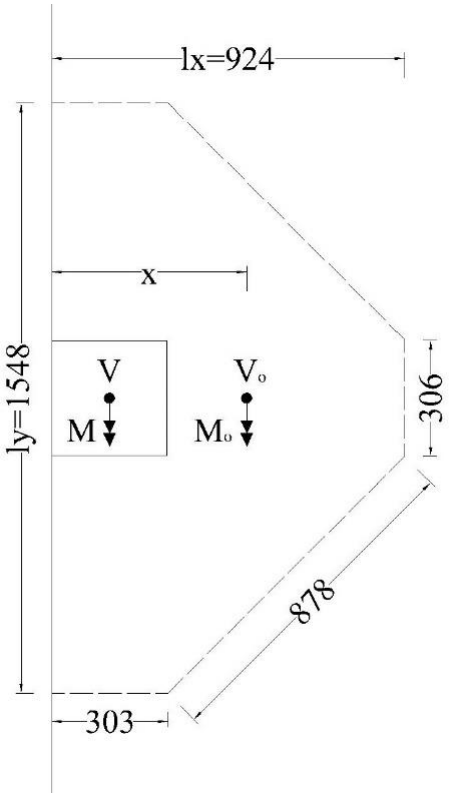

Figure B.2: Critical section outside the shear reinforced zone

To get distance X, we take the summation of the moments of the critical section segments about the free edge:

$\rightarrow 2 * \left(l_1 * \frac{l_1}{2} + l_2 * \frac{l_x + l_1}{2}\right) + l_3 * l_x = b_o * X$

$\rightarrow 2 * \left(303 * \frac{303}{2} + 878 * \frac{924 + 303}{2}\right) + 306 * 924 =$

$2668 * X$

$\therefore X = 544.2\ mm$

Calculating *J*:

$J = d \sum \frac{L}{3}\left(x_i^2 + x_i x_j + x_j^2\right)$

For segment 1: $x_i = -544.2\ mm$ $x_j = -241.2\ mm$

For segment 2: $x_i = -241.2\ mm$ $x_j = 379.8\ mm$

For segment 3: $x_i = 379.8\ mm$ $x_j = 379.8\ mm$

$\rightarrow J = \frac{160}{3} * \{2 * 303 * [(-544.2)^2 + (-544.2) * (-241.2) + (-241.2)^2] + 2 * 878 *$

$[(-241.2)^2 + (-241.2) * (379.8) + (379.8)^2] + 306 * [(379.8)^2 + (379.8) * (379.8) +$

$(379.8)^2]\} = 3.314 * 10^{10}\text{mm}^4$

$\gamma_v = 1 - \frac{1}{1+\frac{2}{3}\sqrt{\frac{l_x}{l_y}}} = 1 - \frac{1}{1+\frac{2}{3}\sqrt{\frac{924}{1548}}} = 0.34$

$\frac{M_o}{V} = \frac{M}{V} - \left(X - \frac{c}{2}\right)$

at $\frac{M}{V} = 0.4\ m$

$\frac{M_o}{V} = 0.4 - \left(0.5442 - \frac{0.3}{2}\right) = 0.0058\ m$

B.2.3.3. Capacity according to the modified CSA/A23.3-14

B.2.3.3.1. Shear strength at the inner critical section (d/2 from the column face)

<u>B.2.3.3.1.1. Concrete contribution</u>

$v_c = 0.041\lambda\phi_c\left(E_f\rho_f f_c'\right)^{\frac{1}{3}}$

$= 0.041 * 1.0 * 1.0 * (61085 * 0.0084 * 44)^{\frac{1}{3}} = 1.159\ \text{MPa}$

<u>B.2.3.3.1.2. Headed ends studs contribution</u>

$v_s = \frac{\phi_s A_v f_y}{b_o s} = \frac{\phi_s A_v f_{f_u}}{b_o s}$

$f_{f_u} = 0.005E_F = 0.005 * 67547 = 337.735\ \text{MPa}$

$\therefore\ v_s = \frac{1.0*(6*126.7)*337.735}{1220*120} = 1.754\ \text{MPa}$

B.2.3.3.1.3. Punching shear capacity

$v_r = v_c + v_{sF} = 1.159 + 1.754 = 2.913$ MPa

$V = {v_r}/{\left(\frac{1}{b_O * d} + \frac{0.2884\gamma}{J} * e\right)} = {2.913 * 10^{-3}}/{\left(\frac{1}{1220*160} + \frac{0.38*0.2884*1000}{3377852377} * 118.4\right)} = 324.95$ kN

B.2.3.3.2. Shear strength at the outer critical section (3.9d from the column face)

B.2.3.3.2.1. Punching shear capacity

$v_r = v_c = 0.028\lambda\phi_c\left(E_f\rho_f f_c'\right)^{\frac{1}{3}}$

$= 0.028 * 1.0 * 1.0 * (61085 * 0.0084 * 44)^{\frac{1}{3}} = 0.7914$ MPa

$V = {v_r}/{\left(\frac{1}{b_O * d} + \frac{0.2884\gamma}{J} * e\right)} = {0.7914 * 10^{-3}}/{\left(\frac{1}{2668*160} + \frac{0.34*0.0058*1000}{3.314*10^{10}} * 379.8\right)} = 334.6\ kN$

Shear failure is expected to be **inside** the shear reinforced zone

B.2.3.4. Capacity according to the modified ACI 318-14

B.2.3.4.1. Shear strength at the inner critical section (d/2 from the column face)

B.2.3.4.1.1. Concrete contribution

$E_c = 4700\sqrt{f_c'} = 4700 * \sqrt{44} = 31176.3$ MPa

$n_f = \frac{E_f}{E_c} = \frac{61085}{31176.3} = 1.96$

$k = \sqrt{2\rho_f n_f + \left(\rho_f n_f\right)^2} - \rho_f n_f = \sqrt{2 * 0.0084 * 1.96 + (0.0084 * 1.96)^2} - 0.0084 * 1.96 =$

0.166

$c = kd = 0.166 * 160 = 26.56$ mm

$V_c = \frac{3}{5}\lambda\sqrt{f_c'}b_o c$

$= \frac{3}{5} * 1.0 * \sqrt{44} * 1220 * 26.56 = 128963$ N

$\therefore v_c = \frac{V_c}{b_o d} = \frac{128963}{1220*160} = 0.66$ MPa

B.2.3.4.1.2. Headed ends studs contribution

$f_{f_u} = 0.004E_f = 0.004 * 67547 = 270.19$ MPa

$v_s = \frac{A_v f_y}{b_o s} = \frac{A_v f_{f_u}}{b_o s} = \frac{(6*126.7)*270.19}{1220*120} = 1.4$ MPa

B.2.3.4.1.3. Punching shear capacity

$v_n = v_c + v_{sF} = 0.66 + 1.4 = 2.06$ MPa

$V = {v_r}\Big/\left(\frac{1}{b_O*d} + \frac{0.2884\gamma}{J} * e\right) = 2.06 * 10^{-3}\Big/\left(\frac{1}{1220*160} + \frac{0.38*0.2884*1000}{3377852377} * 118.4\right) = 230$ kN

B.2.3.4.2. Shear strength at the outer critical section (3.9d from the column face)

B.2.3.4.2.1. Punching shear capacity

$V_n = V_c = \frac{2}{5}\lambda\sqrt{f_c'}b_o c$

$= \frac{2}{5} * 1.0 * \sqrt{44} * 2668 * 26.56 = 189427.78\ N$

$\therefore v_n = v_c = \frac{V_c}{b_o d} = \frac{189427.78}{2668*160} = 0.444\ MPa$

$V = {v_r}\Big/\left(\frac{1}{b_O*d} + \frac{0.2884\gamma}{J} * e\right) = 0.444 * 10^{-3}\Big/\left(\frac{1}{2668*160} + \frac{0.34*0.0058*1000}{3.314*10^{10}} * 379.8\right) = 187.6\ kN$

Shear failure is expected to be **outside** the shear reinforced zone.

B.2.4. Connection N-0.9-S8

B.2.4.1. Concrete properties

$f_c' = 43\ MPa$ $\phi_c = 1.0$ $\lambda = 1.0$

B.2.3.2. Properties of outer critical section

$l_1 = 285\ mm$

$l_2 = 495\ mm$

$l_3 = 495\ mm$

$l_4 = 270\ mm$

$l_x = 924\ mm$

$l_y = 1548\ mm$

$d_v = 160\ mm$

$b_o = 2 * (l_1 + l_2 + l_3) + l_4 = 2 * (285 + 495 + 495) + 270 = \mathbf{2820\ mm}$

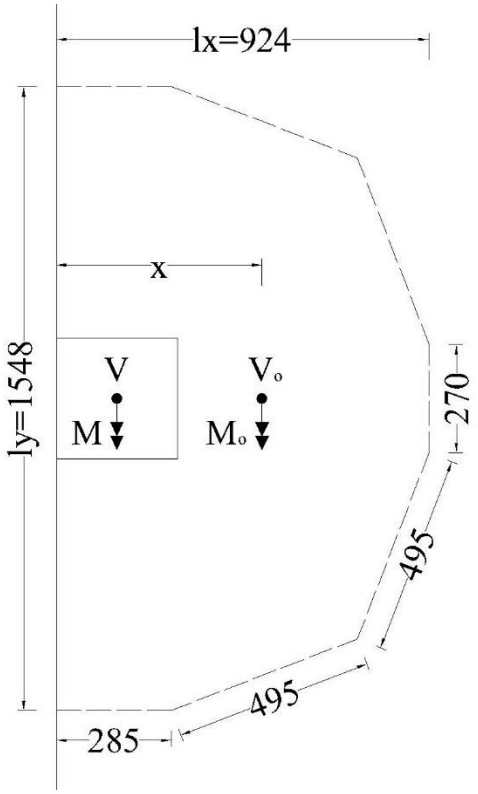

Figure B.3: Critical section outside the shear reinforced zone

To get distance X, we take the summation of the moments of the critical section segments about the free edge:

$2 * \left(285 * \frac{285}{2} + 495 * \frac{285+747}{2} + 495 * \frac{747+924}{2}\right) + 270 * 924 = 2820 * X$

$\therefore X = 591.7\ mm$

Calculating *J*:

$J = d \sum \frac{L}{3}\left(x_i^2 + x_i x_j + x_j^2\right)$

For segment 1: $x_i = -591.7\ mm$ $x_j = -306.7\ mm$

For segment 2: $x_i = -306.7\ mm \quad x_j = 155.3\ mm$

For segment 3: $x_i = 155.3\ mm \quad x_j = 332.3\ mm$

For segment 4: $x_i = 332.3\ mm \quad x_j = 332.3\ mm$

$$\therefore J = \frac{160}{3} * \{2 * 285 * [(-591.7\ )^2 + (-591.7\ ) * (-306.7\ ) + (-306.7)^2] + 2 * 495 *$$

$$[(-306.7)^2 + (-306.7) * (155.3) + (155.3)^2] + 2 * 495 * [(155.3\ )^2 + (155.3\ ) * (332.3) +$$

$$(332.3)^2] + 270 * [(332.3)^2 + (332.3) * (332.3) + (332.3)^2]\} = 3.734 * 10^{10}\ \text{mm}^4$$

$$\gamma_v = 1 - \frac{1}{1+\frac{2}{3}\sqrt{\frac{l_x}{l_y}}} = 1 - \frac{1}{1+\frac{2}{3}\sqrt{\frac{924}{1548}}} = 0.34$$

$$\frac{M_o}{V} = \frac{M}{V} - \left(X - \frac{c}{2}\right)$$

at $\frac{M}{V} = 0.4\ m$

$$\frac{M_o}{V} = 0.4 - \left(0.5917 - \frac{0.3}{2}\right) = -0.0417\ m$$

B.2.4.3. Capacity according to the modified CSA/A23.3-14

B.2.4.3.1. Shear strength at the inner critical section (d/2 from the column face)

B.2.4.3.1.1. Concrete contribution

$$v_c = 0.041\lambda\phi_c\left(E_f\rho_f f_c'\right)^{\frac{1}{3}}$$

$$= 0.041 * 1.0 * 1.0 * (61085 * 0.0084 * 43)^{\frac{1}{3}} = 1.15\ \text{MPa}$$

B.2.4.3.1.2. Headed ends studs contribution

$$v_s = \frac{\phi_s A_v f_y}{b_o s} = \frac{\phi_s A_v f_{f_u}}{b_o s}$$

$$f_{f_u} = 0.005E_F = 0.005 * 67547 = 337.735\ MPa$$

$$\therefore\ v_s = \frac{1.0*(8*126.7)*337.735}{1220*120} = 2.338\ MPa$$

B.2.4.3.1.3. Punching shear capacity

$v_r = v_c + v_{sF} = 1.15 + 2.338 = 3.488\ MPa$

$V = {v_r}\Big/\left(\frac{1}{b_O * d} + \frac{0.2884\gamma}{J} * e\right) = {3.488 * 10^{-3}}\Big/\left(\frac{1}{1220*160} + \frac{0.38*0.2884*1000}{3377852377} * 118.4\right) = 389.13\ kN$

B.2.4.3.2. Shear strength at the outer critical section (3.9d from the column face)

B.2.3.3.2.1. Punching shear capacity

$v_r = v_c = 0.028\lambda\phi_c\left(E_f\rho_f f_c'\right)^{\frac{1}{3}}$

$= 0.028 * 1.0 * 1.0 * (61085 * 0.0084 * 43)^{\frac{1}{3}} = 0.785$ MPa

$V = {v_r}\Big/\left(\frac{1}{b_O * d} + \frac{0.2884\gamma}{J} * e\right) = {0.785 * 10^{-3}}\Big/\left(\frac{1}{2820*160} + \frac{0.34*0.0417*1000}{3.734*10^{10}} * 591.7\right) = 321.6\ kN$

Shear failure is expected to be **outside** the shear reinforced zone

B.2.4.4. Capacity according to the modified ACI 318-11

B.2.4.4.1. Shear strength at the inner critical section (d/2 from the column face)

B.2.4.4.1.1. Concrete contribution

$E_c = 4700\sqrt{f_c'} = 4700 * \sqrt{43} = 30820\ MPa$

$n_f = \frac{E_f}{E_c} = \frac{61085}{30820} = 1.98$

$k = \sqrt{2\rho_f n_f + \left(\rho_f n_f\right)^2} - \rho_f n_f = \sqrt{2 * 0.0084 * 1.98 + (0.0084 * 1.98)^2} - 0.0084 * 1.98 =$

0.167

$c = kd = 0.167 * 160 = 26.72\ mm$

$V_c = 0.6\lambda\sqrt{f_c'} b_o c$

$= 0.6 * 1.0 * \sqrt{43} * 1220 * 26.72 = 128257.2\ N$

$\therefore v_c = \frac{V_c}{b_o d} = \frac{128257.2}{1220*160} = 0.657\ MPa$

B.2.4.4.1.2. Headed ends studs contribution

$f_{f_u} = 0.004E_f = 0.004 * 67547 = 270.19\ MPa$

$v_s = \frac{A_v f_y}{b_o s} = \frac{A_v f_{f_u}}{b_o s} = \frac{(8*126.7)*270.19}{1220*120} = 1.87$ MPa

B.2.4.4.1.3. Punching shear capacity

$v_n = v_c + v_{sF} = 0.657 + 1.87 = 2.527\ MPa$

$V = {v_r}\Big/\left(\frac{1}{b_O*d} + \frac{0.2884\gamma}{J} * e\right) = 2.527 * 10^{-3}\Big/\left(\frac{1}{1220*160} + \frac{0.38*0.2884*1000}{3377852377} * 118.4\right) = 281.9\ kN$

B.2.4.4.2. Shear strength at the outer critical section (3.9d from the column face)

B.2.4.4.2.1. Punching shear capacity

$V_n = V_c = 0.4\lambda\sqrt{f_c'}b_o c$

$= 0.4 * 1.0 * \sqrt{43} * 2812 * 26.72 = 197081.56\ N$

$\therefore v_n = v_c = \frac{V_c}{b_o d} = \frac{197081.56}{2812*160} = 0.438\ MPa$

$V = {v_r}\Big/\left(\frac{1}{b_O*d} + \frac{0.2884\gamma}{J} * e\right) = 0.438 * 10^{-3}\Big/\left(\frac{1}{2820*160} + \frac{0.34*0.0417*1000}{3.734*10^{10}} * 591.7\right) = 179.4\ kN$

Shear failure is expected to be **outside** the shear reinforced zone.

B.2.5. Connection N-0.9-C6

B.2.5.1. Concrete properties

$f_c' = 45\ MPa$ $\phi_c = 1.0$ $\lambda = 1.0$

B.2.5.2. Properties of outer critical section

$l_1 = 303\ mm$

$l_2 = 844\ mm$

$l_3 = 306\ mm$

$l_x = 900\ mm$

$l_y = 1500\ mm$

$d_v = 160\ mm$

$b_o = 2 * (l_1 + l_2) + l_3 = 2 * (303 + 844) + 306 =$

$\mathbf{2600\ mm}$

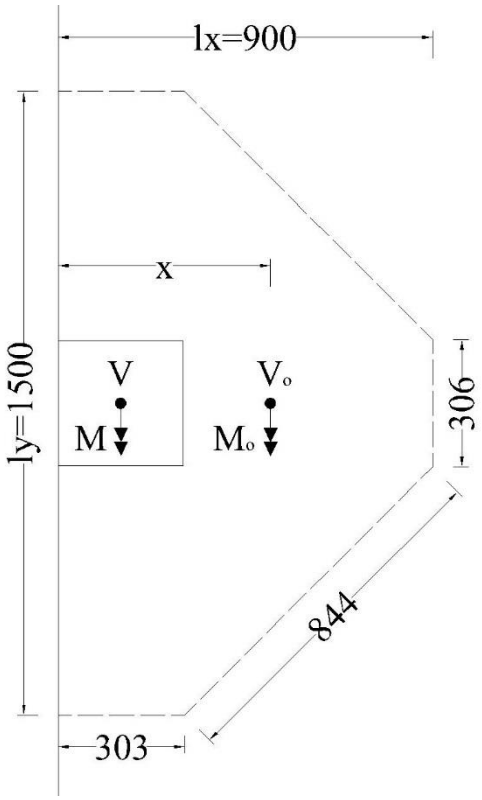

Figure B.4: Critical section outside the shear reinforced zone

To get distance X, we take the summation of the moments of the critical section segments about the free edge:

$\rightarrow 2 * \left(l_1 * \frac{l_1}{2} + l_2 * \frac{l_x + l_1}{2}\right) + l_3 * l_x = b_o * X$

$\rightarrow 2 * \left(303 * \frac{303}{2} + 844 * \frac{900+303}{2}\right) + 306 * 900 =$

$2600 * X$

$\therefore X = 531.75\ mm$

Calculating *J*:

$J = d \sum \frac{L}{3}\left(x_i^2 + x_i x_j + x_j^2\right)$

For segment 1: $x_i = -531.75\ mm$ $x_j = -228.75\ mm$

For segment 2: $x_i = -228.75\ mm \quad x_j = 368.25\ mm$

For segment 3: $x_i = 368.25\ mm \quad x_j = 368.25\ mm$

$\rightarrow J = \frac{160}{3} * \{2 * 303 * [(-531.75)^2 + (-531.75) * (-228.75) + (-228.75)^2] + 2 * 844 *$

$[(-228.75)^2 + (-228.75) * (368.25) + (368.25)^2] + 306 * [(368.25)^2 + (368.25) *$

$(368.25) + (368.25)^2]\} = 3.074 * 10^{10}\text{mm}^4$

$\gamma_v = 1 - \frac{1}{1+\frac{2}{3}\sqrt{\frac{l_x}{l_y}}} = 1 - \frac{1}{1+\frac{2}{3}\sqrt{\frac{900}{1500}}} = 0.3405$

$\frac{M_o}{V} = \frac{M}{V} - \left(X - \frac{c}{2}\right)$

at $\frac{M}{V} = 0.4\ m$

$\frac{M_o}{V} = 0.4 - \left(0.53175 - \frac{0.3}{2}\right) = 0.01825\ m$

B.2.5.3. Capacity according to the modified CSA/A23.3-14

B.2.5.3.1. Shear strength at the inner critical section (d/2 from the column face)

<u>B.2.5.3.1.1. Concrete contribution</u>

$v_c = 0.041\lambda\phi_c\left(E_f\rho_f f_c'\right)^{\frac{1}{3}}$

$= 0.041 * 1.0 * 1.0 * (61085 * 0.0084 * 45)^{\frac{1}{3}} = 1.168$ MPa

<u>B.2.5.3.1.2. Corrugated bars contribution</u>

$v_s = \frac{\phi_s A_v f_y}{b_o s} = \frac{\phi_s A_v f_{f_u}}{b_o s}$

$f_{f_u} = 0.005E_F = 0.005 * 52000 = 260\ MPa$

$\therefore\ v_s = \frac{1.0*(6*71.29)*260}{1220*120} = 0.76\ MPa$

<u>B.2.5.3.1.3. Punching shear capacity</u>

$v_r = v_c + v_{sF} = 1.168 + 0.76 = 1.928\ MPa$

$$V = {v_r}\Big/\left(\frac{1}{b_O * d} + \frac{0.2884\gamma}{J} * e\right) = 1.928 * 10^{-3}\Big/\left(\frac{1}{1220*160} + \frac{0.38*0.2884*1000}{3377852377} * 118.4\right) = 215.07\ kN$$

B.2.5.3.2. Shear strength at the outer critical section (3.75d from the column face)

<u>B.2.5.3.2.1. Punching shear capacity</u>

$$v_r = v_c = 0.028\lambda\phi_c\left(E_f\rho_f f_c'\right)^{\frac{1}{3}}$$

$$= 0.028 * 1.0 * 1.0 * (61085 * 0.0084 * 45)^{\frac{1}{3}} = 0.797 \text{ MPa}$$

$$V = {v_r}\Big/\left(\frac{1}{b_O * d} + \frac{0.2884\gamma}{J} * e\right) = 0.797 * 10^{-3}\Big/\left(\frac{1}{2600*160} + \frac{0.3405*0.01825*1000}{3.074*10^{10}} * 368.25\right) =$$

$321.6\ kN$

Shear failure is expected to be **<u>inside</u>** the shear reinforced zone

B.2.5.4. Capacity according to the modified ACI 318-11

B.2.5.4.1. Shear strength at the inner critical section (d/2 from the column face)

<u>B.2.5.4.1.1. Concrete contribution</u>

$$E_c = 4700\sqrt{f_c'} = 4700 * \sqrt{45} = 31528.6\ MPa$$

$$n_f = \frac{E_f}{E_c} = \frac{61085}{31528.6} = 1.94$$

$$k = \sqrt{2\rho_f n_f + \left(\rho_f n_f\right)^2} - \rho_f n_f = \sqrt{2 * 0.0084 * 1.94 + (0.0084 * 1.94)^2} - 0.0084 * 1.94 =$$

0.165

$$c = kd = 0.166 * 160 = 26.4\ mm$$

$$V_c = 0.6\lambda\sqrt{f_c'} b_o c$$

$$= 0.6 * 1.0 * \sqrt{45} * 1220 * 26.4 = 129634.7\ N$$

$$\therefore v_c = \frac{V_c}{b_o d} = \frac{129634.7}{1220*160} = 0.664\ MPa$$

B.2.5.4.1.2. Corrugated bars contribution

$f_{f_u} = 0.004E_f = 0.004 * 52000 = 208\ MPa$

$v_s = \frac{A_v f_y}{b_o s} = \frac{A_v f_{f_u}}{b_o s} = \frac{(6*71.29)*208}{1220*120} = 0.61$ MPa

B.2.5.4.1.3. Punching shear capacity

$v_n = v_c + v_{sF} = 0.664 + 0.61 = 1.274\ MPa$

$V = {v_r}\Big/\left(\frac{1}{b_O*d} + \frac{0.2884\gamma}{J} * e\right) = {1.274 * 10^{-3}}\Big/\left(\frac{1}{1220*160} + \frac{0.38*0.2884*1000}{3377852377} * 118.4\right) = 142.1\ kN$

B.2.5.4.2. Shear strength at the outer critical section (3.75d from the column face)

B.2.5.4.2.1. Punching shear capacity

$V_n = V_c = 0.4\lambda\sqrt{f_c'}b_o c$

$= 0.4 * 1.0 * \sqrt{45} * 2600 * 26.4 = 184180.4\ N$

$\therefore v_n = v_c = \frac{V_c}{b_o d} = \frac{184180.4}{2600*160} = 0.443\ MPa$

$V = {v_r}\Big/\left(\frac{1}{b_O*d} + \frac{0.2884\gamma}{J} * e\right) = {0.443 * 10^{-3}}\Big/\left(\frac{1}{2600*160} + \frac{0.3405*0.01825*1000}{3.074*10^{10}} * 368.25\right) =$

$178.75\ kN$

Shear failure is expected to be **inside** the shear reinforced zone.

B.2.6. Connection N-0.9-C8

B.2.6.1. Concrete properties

$f_c' = 43\ MPa$ $\phi_c = 1.0$ $\lambda = 1.0$

B.2.6.2. Properties of outer critical section

$l_1 = 285\ mm$

$l_2 = 476\ mm$

$l_3 = 476\ mm$

$l_4 = 270\ mm$

$l_x = 900\ mm$

$l_y = 1500\ mm$

$d_v = 160\ mm$

$b_o = 2 * (l_1 + l_2 + l_3) + l_4 = 2 * (285 + 476 + 476) + 270 = \mathbf{2744\ mm}$

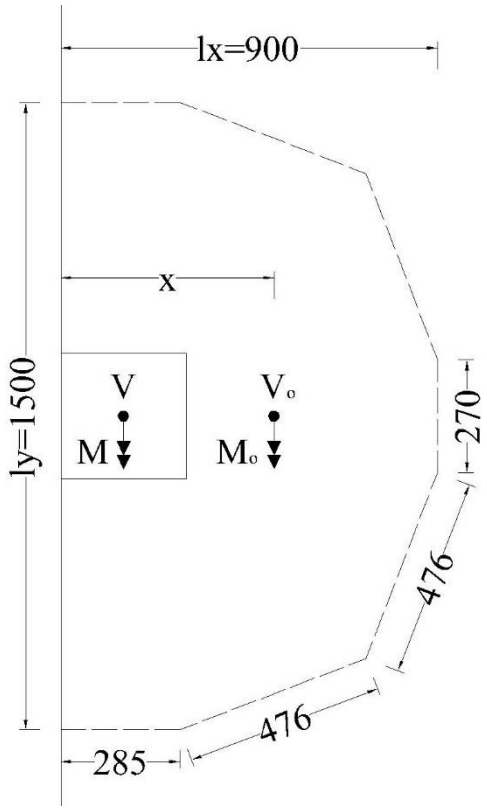

Figure B.5: Critical section outside the shear reinforced zone

To get distance X, we take the summation of the moments of the critical section segments about the free edge:

$2 * \left(285 * \frac{285}{2} + 476 * \frac{285+730}{2} + 476 * \frac{730+900}{2}\right) + 270 * 900 = 2744 * X$

$\therefore X = 577\ mm$

Calculating *J*:

$J = d \sum \frac{L}{3}\left(x_i^2 + x_i x_j + x_j^2\right)$

For segment 1: $x_i = -577\ mm$ $x_j = -292\ mm$

For segment 2: $x_i = -292\ mm$ $x_j = 153\ mm$

For segment 3: $x_i = 153\ mm$ $x_j = 323\ mm$

For segment 3: $x_i = 323\ mm$ $x_j = 323\ mm$

$\therefore J = \frac{160}{3} * \{2 * 285 * [(-577)^2 + (-577) * (-292) + (-292)^2] + 2 * 476 * [(-292)^2 + (-292) * (153) + (153)^2] + 2 * 476 * [(153)^2 + (153) * (323) + (323)^2] + 270 * [(323)^2 + (323) * (323) + (323)^2]\} = 3.458 * 10^{10}\ \text{mm}^4$

$\gamma_v = 1 - \frac{1}{1+\frac{2}{3}\sqrt{\frac{l_x}{l_y}}} = 1 - \frac{1}{1+\frac{2}{3}\sqrt{\frac{900}{1500}}} = 0.3405$

$\frac{M_o}{V} = \frac{M}{V} - \left(X - \frac{c}{2}\right)$

at $\frac{M}{V} = 0.4\ m$

$\frac{M_o}{V} = 0.4 - \left(0.577 - \frac{0.3}{2}\right) = -0.027\ m$

B.2.6.3. Capacity according to the modified CSA/A23.3-14

B.2.6.3.1. Shear strength at the inner critical section (d/2 from the column face)

B.2.6.3.1.1. Concrete contribution

$v_c = 0.041\lambda\phi_c\left(E_f\rho_f f_c'\right)^{\frac{1}{3}}$

$= 0.041 * 1.0 * 1.0 * (61085 * 0.0084 * 43)^{\frac{1}{3}} = 1.15\ \text{MPa}$

B.2.6.3.1.2. Corrugated bars contribution

$v_s = \frac{\phi_s A_v f_y}{b_o s} = \frac{\phi_s A_v f_{f_u}}{b_o s}$

$f_{f_u} = 0.005E_F = 0.005 * 52000 = 260\ MPa$

$\therefore\ v_s = \frac{1.0*(8*71.29)*260}{1220*120} = 1.01\ MPa$

B.2.6.3.1.3. Punching shear capacity

$v_r = v_c + v_{sF} = 1.15 + 1.01 = 2.16\ MPa$

$V = {v_r}\Big/\left(\frac{1}{b_O * d} + \frac{0.2884\gamma}{J} * e\right) = 2.16 * 10^{-3}\Big/\left(\frac{1}{1220*160} + \frac{0.38*0.2884*1000}{3377852377} * 118.4\right) = 240.95\ kN$

B.2.6.3.2. Shear strength at the outer critical section (3.75d from the column face)

<u>B.2.6.3.2.1. Punching shear capacity</u>

$v_r = v_c = 0.028\lambda\phi_c\left(E_f\rho_f f_c'\right)^{\frac{1}{3}}$

$= 0.028 * 1.0 * 1.0 * (61085 * 0.0084 * 43)^{\frac{1}{3}} = 0.785$ MPa

$V = {v_r}\Big/\left(\frac{1}{b_O * d} + \frac{0.2884\gamma}{J} * e\right) = 0.785 * 10^{-3}\Big/\left(\frac{1}{2744*160} + \frac{0.3405*0.027*1000}{3.458*10^{10}} * 577\right) = 322.9\ kN$

Shear failure is expected to be **<u>inside</u>** the shear reinforced zone

B.2.6.4. Capacity according to the modified ACI 318-11

B.2.6.4.1. Shear strength at the inner critical section (d/2 from the column face)

<u>B.2.6.4.1.1. Concrete contribution</u>

$E_c = 4700\sqrt{f_c'} = 4700 * \sqrt{43} = 30820\ MPa$

$n_f = \frac{E_f}{E_c} = \frac{61085}{30820} = 1.98$

$k = \sqrt{2\rho_f n_f + \left(\rho_f n_f\right)^2} - \rho_f n_f = \sqrt{2 * 0.0084 * 1.98 + (0.0084 * 1.98)^2} - 0.0084 * 1.98 =$

0.167

$c = kd = 0.167 * 160 = 26.72\ mm$

$V_c = \frac{3}{5}\lambda\sqrt{f_c'} b_o c$

$= \frac{3}{5} * 1.0 * \sqrt{43} * 1220 * 26.72 = 128257.2\ N$

$\therefore v_c = \frac{V_c}{b_o d} = \frac{128257.2}{1220*160} = 0.657\ MPa$

B.2.6.4.1.2. Corrugated bars contribution

$f_{f_u} = 0.004E_{f_{avg.}} = 0.004 * 52000 = 208\ MPa$

$v_s = \frac{A_v f_y}{b_o s} = \frac{A_v f_{fu}}{b_o s} = \frac{(8*71.29)*208}{1220*120} = 0.81$ MPa

B.2.6.4.1.3. Punching shear capacity

$v_n = v_c + v_{sF} = 0.657 + 0.81 = 1.467\ MPa$

$V = {}^{v_r}\Big/\left(\frac{1}{b_O*d} + \frac{0.2884\gamma}{J} * e\right) = 1.467 * 10^{-3}\Big/\left(\frac{1}{1220*160} + \frac{0.38*0.2884*1000}{3377852377} * 118.4\right) = 163.65\ kN$

B.2.6.4.2. Shear strength at the outer critical section (3.75d from the column face)

B.2.6.4.2.1. Punching shear capacity

$V_n = V_c = \frac{2}{5}\lambda\sqrt{f_c'}b_o c$

$= \frac{2}{5} * 1.0 * \sqrt{43} * 2740 * 26.72 = 192035.4\ N$

$\therefore v_n = v_c = \frac{V_c}{b_o d} = \frac{192035.4}{2740*160} = 0.438\ MPa$

$V = {}^{v_r}\Big/\left(\frac{1}{b_O*d} + \frac{0.2884\gamma}{J} * e\right) = 0.438 * 10^{-3}\Big/\left(\frac{1}{2744*160} + \frac{0.3405*0.027*1000}{3.458*10^{10}} * 577\right) = 180.2\ kN$

Shear failure is expected to be **inside** the shear reinforced zone.

APPENDIX C

FLEXURAL CAPACITY OF CONNECTIONS

C.1. YIELD LINE ANALYSIS

Figure C.1 shows the yield line pattern used to calculate the flexural capacities of the connections (El-Gendy and El-Salakawy 2016a). It consists of six plane segments and is defined by three parameters *x*, *y* and *z*.

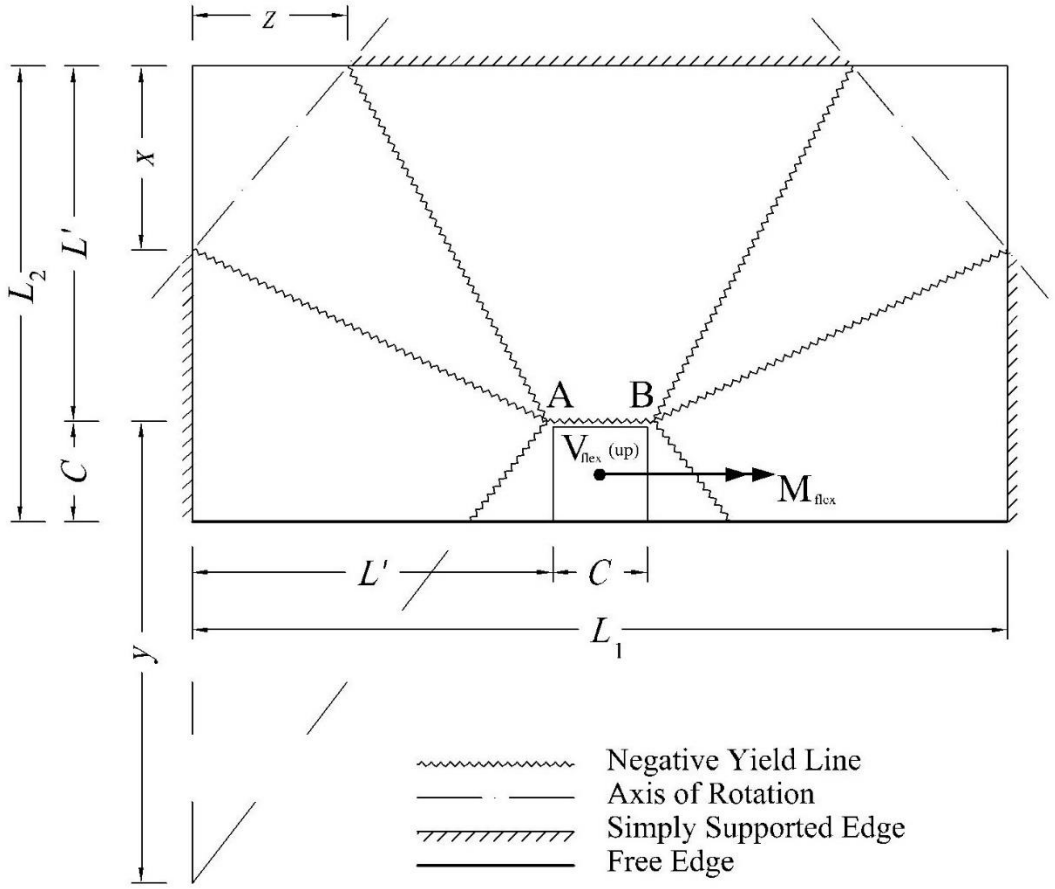

Figure C.1: Yield line pattern

The principal of virtual work (Park and Gamble 1980) is used in the analysis of the pattern. The line AB which has maximum deflection is given a unit displacement, δ, in the direction of the shear force, *V*. After that, Eqs. C.1 and C.2 are used to calculate the internal work done by the segments of the slab, *I*, and the external work done by the shear force and the unbalanced moment, *E*, respectively. The internal and external work are then equated (Eq. C.3) to calculate the flexural

capacity of the connection, V_{flex}. Since the flexural capacity is function of the three parameters *x*, *y* and *z*, Eqs. C.4, C.5 and C.6 are solved simultaneously to calculate the least possible value of V_{flex} (Table C.1).

$$I = 2m_{px}\,\delta\left[\frac{k(L_1 - 2z)}{2L'} + \frac{x^2 + kz^2}{L'z + (L' - z)x} + \frac{L_1 - x}{L'} + \frac{kC(2L' + y)}{2y^2}\right] \tag{C.1}$$

$$E = V_{\text{flex}}\,\delta\left(\frac{2y - C + 2\gamma}{2y}\right) \tag{C.2}$$

$$V_{\text{flex}} = \frac{4m_{px}y}{2y - C + 2\gamma}\left[\frac{k(L_1 - 2z)}{2L'} + \frac{x^2 + kz^2}{L'z + (L' - z)x} + \frac{L_1 - x}{L'} + \frac{kC(2L' + y)}{2y^2}\right] \tag{C.3}$$

$$\frac{\partial V_{\text{flex}}}{\partial x} = 0 \tag{C.4}$$

$$\frac{\partial V_{\text{flex}}}{\partial y} = 0 \tag{C.5}$$

$$\frac{\partial V_{\text{flex}}}{\partial z} = 0 \tag{C.6}$$

In the previous equations, m_{px} represents the equivalent plastic moment of resistance per unit width of the slab in the direction parallel to the free edge, γ represents the moment to shear ratio and *k* represents the ratio between the equivalent plastic moments of resistance of the slab in the directions parallel and perpendicular to the free edge, respectively.

Table C.1: Yield line analysis results

Connection	Pattern parameters (mm)			Flexural capacity, V_{flex} (kN)
	x	*y*	*z*	
H-0.9-XX	710	2,321	644	391
H-1.35-XX	712	2,331	643	465
H-1.8-XX	712	2,337	643	507
N-0.9-S8	714	2,347	642	300
N-0.9-C8	714	2,347	642	300
N-0.9-S6	714	2,346	642	303
N-0.9-C6	714	2,346	642	305

C.2. EQUIVALENT PLASTIC MOMENT, M_P, CALCULATIONS

The equivalent plastic moment is calculated using the following equation suggested by Gar et al. (2014):

$$M_p = 0.5M_n + 0.5\left(1 - \frac{I_{cr}}{2I_g}\right)\left(\frac{M_{cr}}{M_n}\right)M_{cr} \quad \text{(C.7)}$$

C.2.1. Connection H-0.9-XX

C.2.1.1. Perpendicular to the free edge, Mpy

$I_g = \frac{b*h^3}{12} = \frac{1000*200^3}{12} = 666.67 * 10^6\ mm^4$

$A_f = 1484.375\ mm^2 \quad \rho = 0.0087 \quad k = 0.141 \quad n = 1.33$

$I_{cr} = \frac{b*(kd)^3}{3} + n * A_f * (d - kd)^2$

$= \frac{1000*(0.141*170.25)^3}{3} + 1.33 * 1484.375 * (170.25 - 0.141 * 170.25)^2 = 46.83 * 10^6\ mm^4$

$M_{cr} = f_r * \frac{I_g}{y_t} = 5.4 * \frac{666.67*10^6}{100} * 10^{-6} = 36\ kN.m$

$$f_f = 0.5E_f\varepsilon_{c_u}\left[\left(1+\frac{4\alpha_1\beta_1\phi_c f_c'}{\rho_f\phi_f E_f\varepsilon_{c_u}}\right)^{1/2}-1\right]$$

$$= 0.5*54000*0.0035*\left[\left(1+\frac{4*0.7285*0.7675*1.0*81}{0.0087*1.0*54000*0.0035}\right)^{1/2}-1\right] = 901.89\ MPa$$

$$c = \frac{\phi_f A_f f_f}{\alpha_1\beta_1\phi_c f_c' b} = \frac{1.0*1484.375*901.89}{0.7285*0.7675*81*1000} = 29.55\ mm$$

$$M_n = \phi_f A_f f_f * \left(d-\frac{\beta_1 c}{2}\right) = 1.0*1484.375*901.89*\left(170.25-\frac{0.7675*29.55}{2}\right) =$$

$212.74\ kN.m$

$$M_{p_y} = 0.5M_n + 0.5\left(1-\frac{I_{cr}}{2I_g}\right)\left(\frac{M_{cr}}{M_n}\right)M_{cr} = 0.5*212.74+0.5\left(1-\frac{46.83}{2*666.67}\right)\left(\frac{36}{212.74}\right)36 =$$

$109.3\ kN.m$

C.2.1.2. Parallel to the free edge, Mpx

$A_f = 1228.45\ mm^2 \quad \rho = 0.0082 \quad k = 0.15 \quad n = 1.61$

$$I_{cr} = \frac{b*(kd)^3}{3} + n*A_f*(d-kd)^2 = \frac{1000*(0.15*149)^3}{3} + 1.61*1228.45*(149-0.15*$$

$149)^2 = 35.44*10^6\ mm^4$

$M_{cr} = 36\ kN.m$

$$f_f = 0.5E_f\varepsilon_{c_u}\left[\left(1+\frac{4\alpha_1\beta_1\phi_c f_c'}{\rho_f\phi_f E_f\varepsilon_{c_u}}\right)^{1/2}-1\right]$$

$$= 0.5*65374*0.0035*\left[\left(1+\frac{4*0.7285*0.7675*1.0*81}{0.0082*1.0*65374*0.0035}\right)^{1/2}-1\right] = 1015.56\ MPa$$

$$c = \frac{\phi_f A_f f_f}{\alpha_1\beta_1\phi_c f_c' b} = \frac{1.0*1228.45*1015.56}{0.7285*0.7675*81*1000} = 27.55\ mm$$

$$M_n = \phi_f A_f f_f * \left(d-\frac{\beta_1 c}{2}\right) = 1.0*1228.45*1015.56*\left(149-\frac{0.7675*27.55}{2}\right) = 172.7\ kN.m$$

$M_{p_x} = 0.5M_n + 0.5\left(1 - \frac{I_{cr}}{2I_g}\right)\left(\frac{M_{cr}}{M_n}\right)M_{cr} = 0.5 * 172.7 + 0.5\left(1 - \frac{35.44}{2*666.67}\right)\left(\frac{36}{172.7}\right)36 =$

$90\ kN.m$

$k = \frac{M_{p_y}}{M_{p_x}} = \frac{109.3}{90} = 1.214$